MATHEMATICAL MODELING OF LEAKAGE FLOW THROUGH LABYRINTH SEALS

Lourens Joubert, B.ENG

Dissertation submitted as partial fulfillment of the degree
Master of Engineering
In the
School of Mechanical and Materials Engineering,
Faculty of Engineering
at the
Potchefstroom University for Christian Higher Education

14 NOVEMBER 2003

Promoter: Dr. B. Botha
POTCHEFSTROOM
2003

ACKNOWLEDGEMENTS

I praise our Heavenly Father for providing me with the opportunities and ability to complete this work. Without strength that only He can provide, it would have been impossible to endure my long period of study.

To my parents, your strength, love and support both morally and financially have been priceless. To Thinus, my brother, thank you for your calmness and always seeing the lighter side of life.

Dr Barend Botha, my promoter, thank you for identifying this project. Your guidance and lessons have been invaluable. Without your intervention this would not have been possible. To Bennie du Toit, thanks for the use of you amazing math skills and time spent explaining them to me.

To Sarel Coetzee and the rest of the CFD department of the PBMR, thank you for the resources, time and hours of faultfinding you granted me in your busy schedule.

My fellow postgraduate students and friends, thank you for your help, jokes and lessons we learned from each other. I thank the University for the environment, resources and financial support they made available to help us further our studies.

To Yolanda, thank you for all your love, understanding and patience through very hard times. Thank you for always listening, your loving words and smiles gives me strength.

Lourens Joubert

ABSTRACT

Title: Mathematical modeling of leakage flow through labyrinth seals
Author: S.L. Joubert

Optimization of gas turbine systems has identified the need for simplified mathematical models to calculate the losses experienced within turbo machines. One such loss is that of the flow through labyrinth seals. As part of a larger study, this study concentrates on the development of such loss models to aid in the performance prediction of turbo machines. The aim of this study was therefore firstly to understand the nature of labyrinth leakage flows and secondly to investigate mathematical models to calculate or predict such leakages through most common geometries. Finally the ability of these models was evaluated by implementing the models into an "engineering tool" in Engineering Equation Solver (EES).

From a detailed literature survey, a few models for calculating and describing labyrinth seal leakages were identified. An "engineering tool" was subsequently developed by combining these models and the governing coefficients in the EES software. Although experimental validation would have been the optimum, a lack of such facilities together with a limited budget required alternative methods to be investigated. It was therefore decided to use Computational Fluid Dynamics (CFD) software such as Star-CD and Fluent. These software packages are accepted by the industry as a design standard and visualizing tool for validation. The results obtained compared favorably with that of the "engineering tool". It therefore proved that the suggested models offer good potential to be used for performance prediction of labyrinth seals.

UITTREKSEL

Titel: Wiskundige modelering van lekvloei deur labyrente seels

Outeur: S.L. Joubert

Termodinamiese simulasie van gas-turbine stelsels het die behoefte geïdentifiseer vir eenvoudige wiskundige modelle wat die verliese in die turbo masjiene meer akkuraat voorspel. Een so 'n verlies is die van lekvloei deur labyrinte seëls. As deel van 'n groter studie, konsentreer hierdie studie op die ontwikkeling van toepaslike verlies modelle wat kan bydra tot die simulasie van turbo masjien stelsels verrigting. Die doel van die studie was primêr om die aard van die lekvloei deur labyrinte seëls te verstaan, en om die wiskundige modelle daar te stel om die lekvloei deur die mees algemene geometrie te voorspel. Laastens moes die vermoë van die model om te help met die voorspelling van die lekvloei bevestig word deur die modelle te implementeer in 'n gereedskapstuk vir ingenieurs.

Deur middel van 'n gedetailleerde literatuurstudie is 'n paar modelle wat die lekvloei deur labyrente voorspel geïdentifiseer. 'n Gereedskapstuk vir ingenieurs is sodoende ontwikkel deur van die modelle te kombineer in die "Engineering Equation Solver" (EES) sagteware pakket. Alhoewel eksperimentele validasie die gewenste metode van validasie is, het 'n tekort aan 'n eksperimentele fasialiteit en 'n beperkte begroting dit verhoed. Daar is gevolglik besluit om die resultate met berekeningsvloei meganika-pakkette soos Star-CD en Fluent te valideer. Die sagteware pakkette word in die industrie aanvaar as 'n ontwerpstandaard en geniet hoë aansien as visualering sagteware. Die resultate wat verkry is vergelyk goed met dié van die gereedskapstuk. Dit is dus bewys dat die voorgestelde model goeie potensiaal toon om gebruik te word vir voorspellings van lekvloeie.

TABLE OF CONTENTS

LIST OF TABLES

LIST OF FIGURES

NOMENCLATURE

P	Pressure $[kPa]$
R	Gas constant $\left\lfloor J/kgK \right\rfloor$
γ	Ratio of constant specific heats
c_p	Constant pressure specific heat $\left\lfloor J/kgK \right\rfloor$
$\dot{m}$	Mass flow rate $\left\lfloor kg/s \right\rfloor$
h	Specific enthalpy $\left\lfloor J/kg \right\rfloor$
s	Specific entropy $\left\lfloor kJ/kgK \right\rfloor$
ρ	Gas density $\left\lfloor kg/m^3 \right\rfloor$
g	Gravitational acceleration $\left\lfloor m/s^2 \right\rfloor$
H	Tooth height $[m]$
S	Tooth pitch $[m]$
cl	Tooth clearance $[m]$
L	Tooth axial width $[m]$
V	Axial velocity $\left\lfloor m/s \right\rfloor$
A	Annular flow through area of constriction $\left\lfloor m^2 \right\rfloor$
T	Temperature $[K]$
n	Number of sealing points
C_d	Discharge coefficient
C_{ke}	Kinetic energy carry-over coefficient
M	Axial Mach number $[Mach]$

CHAPTER 1

INTRODUCTION

Chapter 1 states the origin and motivation of the study. The purpose for the research is clarified and supported. Further a proper outline of work to be done and aim of the study are discussed. Finally the impact of this research on the industry is also clarified.

1.1 Preface

With the fast and ever growing electricity demand it is essential that utility companies seek alternate ways in supplying greater amounts of power. It is necessary to design a power plant capable of being set up in less time and yielding higher efficiencies at the lowest possible capital cost. As power companies are financially driven, they seek to employ the most effective and profitable solutions to solve the electricity demand problems.

Due to the greater advancements in computer technology it is now possible to take all aspects affecting the efficiency of the cycle into account. This acts as a very powerful tool in the process of optimization. Designers can now increase efficiency and optimize cycles before starting construction. This greatly reduces capital costs for plant development as smaller power plants will be capable of providing the same or even more electricity than conventional systems. Fewer natural resources will be required to provide the necessary energy which will lead to greater financial gain of the company and reduced impact on the environment.

Turbo machines act as the hart of the power generation cycle, for this reason it is critical to maintain optimum efficiency in these machines. A slight increase in turbo efficiency could greatly enhance the market value and competitiveness of the process. Internal leakage flows within the machines is a major source of loss and should therefore be closely controlled and kept to a minimum. Traditionally labyrinth seals have been used within turbo machines to prevent and control some of these leakage flow rates.

This study concentrates on the better understanding and quantifying of leakages through labyrinth seals in turbo machinery. These seals are critical in optimization and control of turbo machinery and most rotordynamic equipment.

1.2 Introduction

Turbo machines have become synonymous with the power generation process as they are used in coal, nuclear and hydraulic power generation stations. Due to the high implementation and maintenance cost on these machines, optimization studies have become a very important step in the design process.

Higher efficiencies in power generating equipment mean that smaller machines and lower operating costs are needed to meet demands. One such area of ongoing optimization is the accurate prediction of leakage flow rates in the turbo machines, more specific the leakages through the various seals.

A small improvement in the efficiency, could lead to significant improvements in cycle efficiency leading to greater market support for the product. Improvements have been sought in various areas, but recent developments in computer technologies enable us to visualize the rather complex flow path through these machines. Computer packages enable the optimization even before machine construction starts.

Whether the situation is limited to a compressor, turbine, pump or any combination of these, there is always a need to control the flow in rotating machinery and prevent it from entering undesired areas and paths. Alternatively, it will sometimes be necessary to extract a predetermined amount of flow from the main flow path, in order to drive auxiliary systems, or for purposes such as blade cooling and rotor balancing. Extremely high rotational speeds and the sometimes marginal stability of these rotors prevent the designer from implementing positive contact seals. This problem is solved by implementing non-contact seal types. One example of such a seal is the labyrinth type. These seals use the pressure induced flow through the seal to provide a torturous flow path and, in doing so, increases flow resistance and therefore reduces the leakage. This study will focus on improved understanding of the functioning of the labyrinth seal.

1.3 Origin of the Study

This study was initiated through a simulation requirement identified during the design of the Pebble Bed Modular Reactor (PBMR (Pty.) Ltd.). The PBMR is a project currently being developed and dedicated to provide a cheaper and cleaner modular power plant that can be constructed in less time and dependent on fewer natural resources than the conventional coal power plants.

In order to optimize total efficiency, every possible aspect needs to be considered. With turbo machines being the heart of the cycle, the efficiency of these machines therefore play a major role in the overall cycle efficiency. Although the design and manufacturing of the turbo machines in the power conversion unit of the PBMR will be contracted out to reputable turbo machine manufacturers, the cycle simulation and control of the system will remain the responsibility of the PBMR personnel.

It is therefore important to predict leakage flow as accurately as possible to improve simulation accuracy and optimize cycle efficiency. This can therefore aid in ensuring optimum design conditions. The understanding of the leakage flow path through the labyrinth seals is just a minor part in the aim for higher efficiency, but nonetheless important. Preliminary design errors could cause auxiliary leakages to be too high, thus leading to reduced efficiency. If auxiliary leakages are too low, it could result in situations of improper cooling or unbalanced rotors. Accurate knowledge and understanding of seal leakage is therefore very important in simulating rotating machinery of the PBMR, allowance should therefore be made for the following situations:

- Estimating effect of seal leakage on performance
- Regulating leakage required for cooling or auxiliary purposes
- Determining balance thrust bearing load

The importance of accurately predicting leakage flow is increased through the use of helium as coolant. Its superior heat transfer ability and the fact that the fluid is chemically

as well as radioactively inert makes it an excellent choice for a closed loop Brayton cycle. However there are some disadvantages to using helium as coolant, the most relevant of these being:

- Friction welding of components at high temperatures is thought to be a notable problem.
- High leakage tendency due to the low molecular weight of helium.

When using helium, large amounts of leakages are present inside the cycle, some intentional, but in most instances it is unwanted and decreases cycle efficiency. It is therefore necessary to fully account for all leakages. The two fundamental problems associated with labyrinth seal values are:

- The accurate prediction of the leakage flow rate thought the seal. This leakage depends on a large number of parameters such as number of cavities, pressure ratio, temperature, geometry of the teeth and fluid being used.
- Predicting the effect of the seal on the rotor dynamics in terms of dynamic stiffness and damping coefficients.

Due to this existing shortcomings and requirements, a definite need was identified to better understand the leakages through labyrinth seals and to derive a model to predict this leakage flow. Traditional methods to account for labyrinth leakage flow are strongly based upon empirical results which limit flexibility and are frequently inaccurate.

1.4 Purpose of the study

The concept of limiting leakage flow by using an amount of annular constrictions is not a new idea. Several studies have been done on the different methods of accounting for these leakages and will be discussed in more detail throughout the next chapters.

Nonetheless, it is surprising to see that the research on the subject is rather incomplete and even contradictory. This lack of flexibility makes it difficult, if not impossible to accurately solve and compare labyrinth leakage values.

This research will attempt to better describe the flow path through some of the different labyrinth geometries. A mathematical model will be compiled that could describe the leakage flow through the seals and should as far as possible not be dependent upon empirical results.

1.5 Outline

Within this study we will first familiarize ourselves with the basic labyrinth seal theory and alternative non-contact seals. The general working within the labyrinth will be described and a method will be sought to predict these flow paths. It will be necessary to make certain assumptions to simplify calculations; these will be stated and discussed when used.

With this model and assumptions now available, it will be possible to program a computer function by using Engineering Equation Solver (EES) to simplify and speed up calculations. It will be necessary to validate results obtained. This will be done by comparing EES results with that found either in the literature or generated with the help of computational fluid dynamics (CFD) software. The CFD results will be generated by using either Star-CD or Fluent source code.

Due to the extended range of geometries available for the seals, the research will concentrate on the geometries found within the PBMR. These geometries could be narrowed down to two major groups namely straight and staggered labyrinth types. Variations of these types are commonly found elsewhere and it will be attempted to categorize them into some of the major groups.

1.6 Study Objectives

This study will investigate the mathematical modeling of flow through labyrinth seals. As part of this process, an investigation of the possibility of developing an engineering tool to predict leakage flow more accurately will also be studied.

1.7 Impact of Study

Primarily the study will create a better understanding of the fundamentals of labyrinth seals and the modeling of leakage values through such seals. It will also enable designers to predict the performance of the PBMR cycle more accurately.

1.8 Layout

In this Chapter some background is given on the origin and purpose of the study. The study objectives were set and the impact of these objectives have been discussed. In Chapter 2 the general theory and labyrinth terms are stated. This gives a helpful insight into the common labyrinth applications and defects that can be expected when using these seals in industrial applications.

Chapter 3 describes the process of compiling the mathematical model used to generate the engineering tool. The origin of the Saint Venant Wantzel equation is explained and some coefficients are given to account for certain phenomena occurring within the seals. In Chapter 4 the implementation and solving of the mathematical model is discussed. Some parametric studies on various seal geometries are done and the results are presented and discussed.

Validation and verification of the engineering tool is done in Chapter 5. This is done by comparing the results from the model to that available in literature and to some results generated with the help of CFD software. In Chapter 6 some conclusions are made on the effectiveness and limitations of the models. Some suggestions and recommendations are made for future research.

CHAPTER 2

LITERATURE STUDY

This chapter looks at the implementation of labyrinth seals in axial and centrifugal machines. Basic elements of labyrinth seals are identified and the functioning of a labyrinth seal is discussed. Different labyrinth geometries are studied and a convention is set for the identification of the various seals. The effects of shaft rotation on the leakages through the seals are also considered while labyrinth defects as well as leakage preventing and alternative non-contact sealing are discussed.

2.1 Introduction

Chapter 1 discusses the background and objectives of the study. It is clear that a need for a mathematical model or set of models have been identified to improve the simulation of labyrinth leakage flow. Before a model can be compiled some knowledge must be gained on the fundamentals and application of labyrinth seals. An extensive literature survey was done on the application and modeling of non-contact seals. Focus mainly fell on identifying labyrinth types and their basic geometries. This chapter discusses the implementation and fundamental terms surrounding labyrinth seals.

2.2 Implementation of Labyrinth Seals

Labyrinth seals are commonly found in most rotating machines such as turbines, pumps and compressors. The main objective of the labyrinth seals is to control the leakages from high-pressure areas to low-pressure areas.

Due to the pressure rise across successive compression stages in centrifugal and axial compressors, seals are required to prevent gas backflow from the discharge to the inlet end of the casing. The condition and effective performance of these seals directly influence the performance of the machinery. In large centrifugal compressors the leakages through the final compressor stage labyrinth could lead to a loss of between 14 and 16% of the total capacity of the flow (Benvenuti (1979)).

2.2.1 Centrifugal Machines

Implementation of the labyrinth seals in centrifugal machines could be explained by looking at Figure 2-1 as given by Childs (1986).

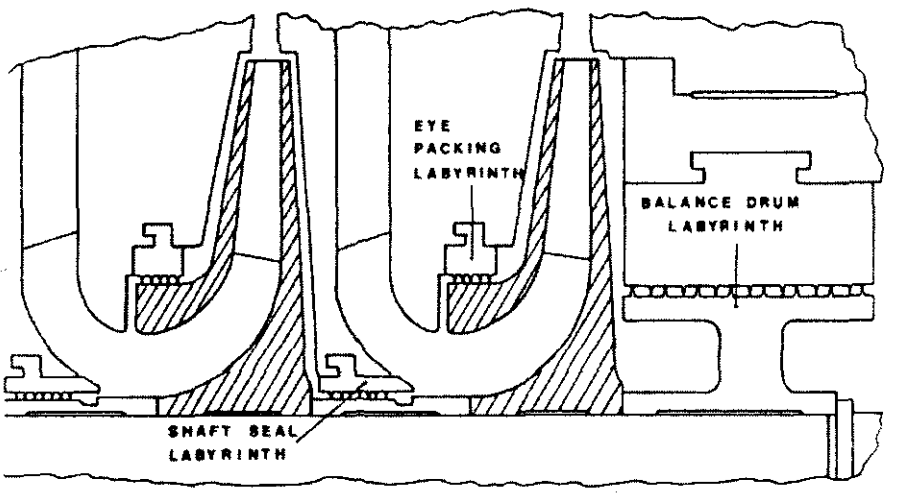

Figure 2-1: *Cross section of a centrifugal compressor*

The sketch shows a cross sectional diagram of a centrifugal compressor. The last two stages of the compressor are visible in the sketch. The labyrinth seals can clearly be seen at the different locations between the rotor and stator. The eye packing labyrinth limits return flow from down the front of the shrouded impeller. From the location of the shaft seal labyrinth it could be understood that it restricts leakage along the shaft towards the preceding stage. The leakage flow through the balance drum labyrinth is used to control and balance the pressure difference over the compressor producing or limiting the axial thrust.

2.2.2 Axial Machines

Labyrinth seals are as important for the proper functioning of axial machines as it is for centrifugal machines. The implementation of the seals in axial machines could be discussed by using Figure 2-2. The figure shows a cross section of the high pressure compressor of the PBMR. The ten axial stages and main flow path can be seen.

The labyrinths preventing the leakages through the front and rear end of the compressor rotor can be seen. Each compressor stage is fitted with single constriction labyrinths to prevent flow from bypassing compressor blades.

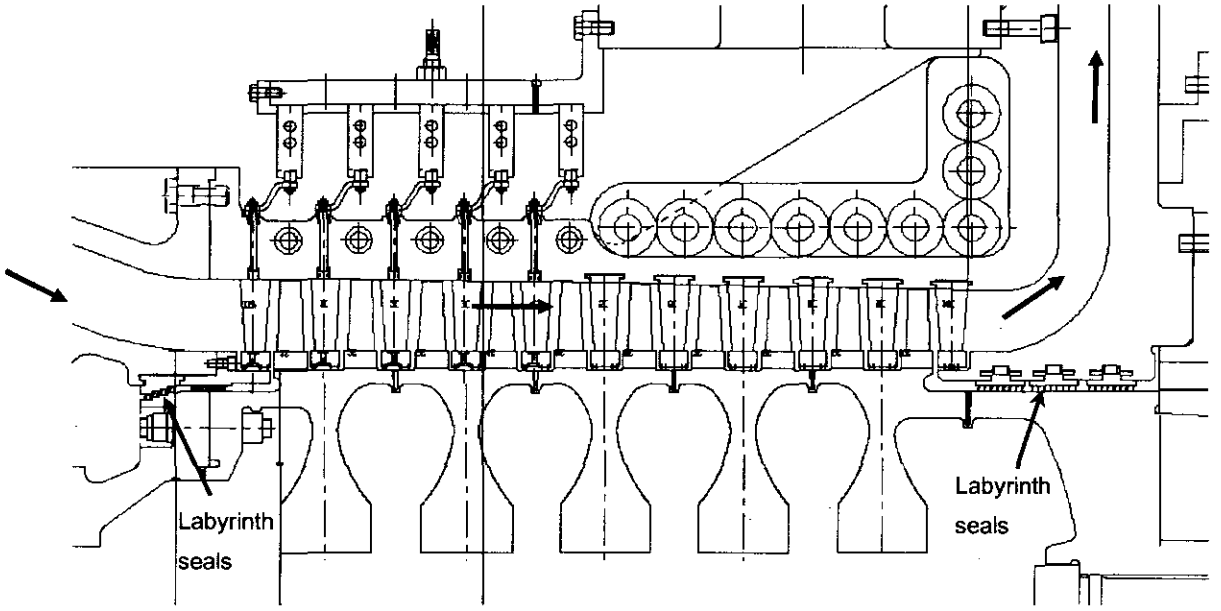

Figure 2-2: *Cross section of an axial compressor*

2.3 Labyrinth Seal Elements

Knowledge of the basic elements of labyrinths will be necessary before the working can be discussed. A labyrinth is defined as a complicated series of narrow corridors or streets through which it is difficult to find your way. This definition holds when describing mechanical labyrinth seals.

Labyrinth seal geometries are as diversified as their applications. Among these variations some common ground could be sought to define a seal as a labyrinth seal. As these seals are not in contact with the shaft and an amount of leakage always exist through them, they could not be defined as positive seals (Hanlon (2001)). All geometries try to provide the most complex flow path possible within the space available. This is accomplished by using a series of between 2 and 18 annular constrictions and chambers equivalent to a series of annular orifices (Eser (2001)).

Variations in the geometries of the teeth are common. Some of these non-straight configurations are discussed in more detail by other authors such as White (1999). A possible method to account for alternative non straight geometries will be discussed in later chapters.

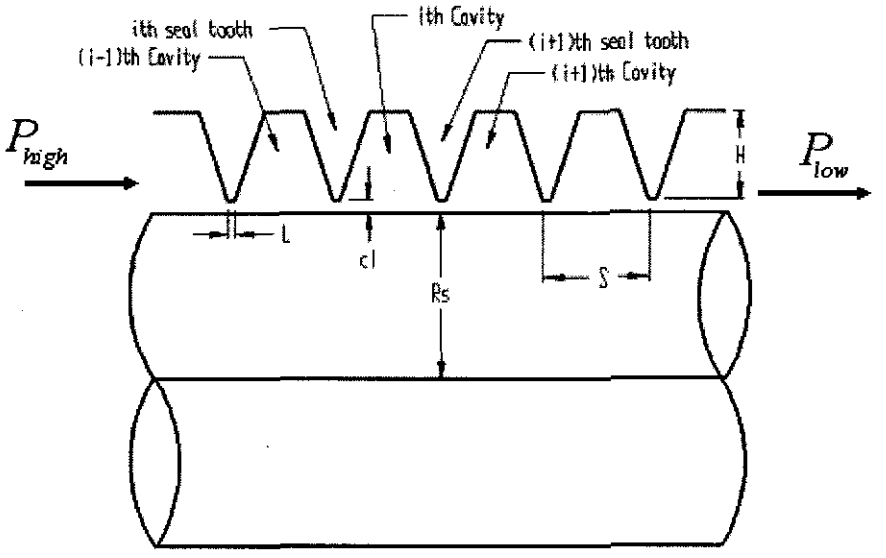

Figure 2-3: *Straight type labyrinth seal*

The figure defines the relevant terms as follow:

Table 2-1: *Labyrinth Terms*

R_s	Shaft Radius
H	Labyrinth Seal Tooth Height
L	Tooth tip Length
cl	Radial Clearance
S	Seal Pitch
Nt	Number of Teeth

Basic elements or parameters could be described using Figure 2-3. It uses a straight type labyrinth seal to identify different labyrinth parameters. A series 1 to Nt of so called teeth or constrictions can be seen. These teeth are alternated by $(Nt-1)$ cavities. The distance between seal teeth and the boundary layer are referred to as the clearance which is represented by cl. The aim is to keep this clearance value as small as possible. Seal height (H) and pitch (S) are the main parameters used to control cavity volume.

To create the most torturous flow path the designer is usually faced with the trade-off to install the largest number of cavities in the allowed space, while keeping cavity volume

as large as possible. In collaboration with these two parameters the most effective way of decreasing the leakage flow through all seals will be to minimize the leakage flow area. This does lead to some obvious problems, for instance less freedom of movement for rotating parts and tighter manufacturing tolerances.

2.4 Labyrinth Seal Operation

Using Figure 2-4 it would now be possible to describe the working of a labyrinth seal. Gas is forced to flow from a high pressure region through a constriction, whereby the gas speed will increase causing a pressure drop. In the cavity section of the labyrinth, the gas will be allowed to expand and whirl, causing the average gas speed to approach zero within each cavity. In each stage of the labyrinth, the pressure energy in the gas will, via the process of alternating gas speed and whirl, be converted to thermal energy. The result of the torturous flow path is that only a small amount of gas will leak through, allowing the seal to maintain a pressure difference between different sections.

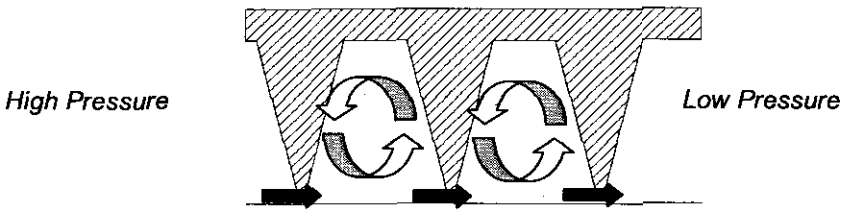

Figure 2-4: *Basic working of a labyrinth seal*

This process can be discussed in more detail with the aid of a Fanno line, an entropy-enthalpy relation locus for one dimensional compressible flow with no heat transfer. This will be done in the next chapter together with the explanation of the different governing equations.

2.5 Labyrinth Geometries

It will be impractical to account for all variations available in the different geometries and applications. Thus it was necessary to generalize the geometries available as no standards

could be found existing to govern these seals. There also seems to be no consensus among authors about the identification of labyrinth seals. Leyzerovich (1997) refers to a once through type and a classical type labyrinth, where Eser ((1995) and (2002)) refers to these seals as straight and stepped type labyrinths separately. Kearton (1952) and Egli (1935) also show differences in their reference to same geometrical type labyrinths. For this reason a basic agreement on the identification of the different labyrinth geometries will be made.

2.5.1 Straight Type Geometries

This is the simplest and most common of all labyrinth seals. This economical seal is commonly utilized between compressor stages and consists of a series of thin strips or fins. A close clearance is maintained between the casing and the tips of the fins (Hanlon (2001)).

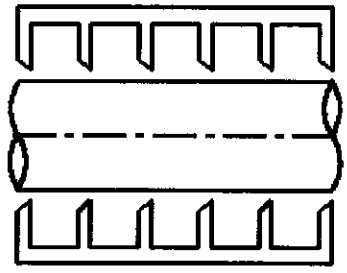

Figure 2-5: *Straight type labyrinth seals*

Different variations of teeth shape or angles can be found. An identifiable aspect of the straight type is that the flow forms a straight line of sight after flowing through the first cavity. The line of sight is formed due to the high velocity of the gas flowing through the seal; the gas does not fully expand within each chamber and passes by between the seal teeth and boundary layer. This effect adversely influences the seal performance and will be accounted for in the next chapter.

This characteristic is clearly shown in the next velocity vector diagram. From Figure 2-6 it can be seen that a jet of fluid with high velocity is present through the clearance gap. The geometry of the seal teeth and cavity volume of that shown in Figure 2-6 is notably different to previously mentioned geometries. But still due to the formation of a line of sight and a straight boundary layer it could be classified as a straight type labyrinth.

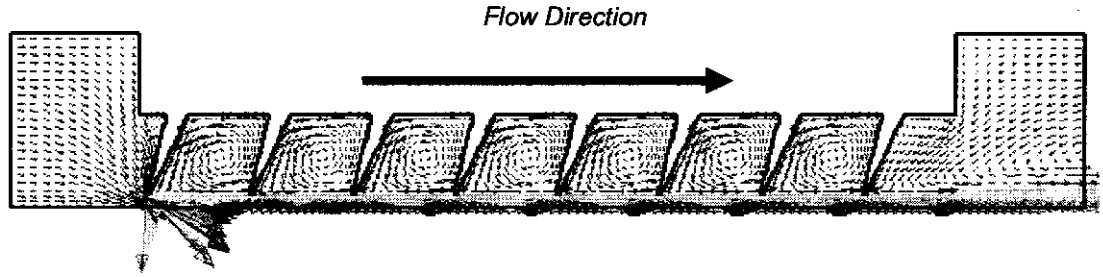

Figure 2-6: *Straight type labyrinth CFD velocity diagram*

2.5.2 Stepped and Staggered Type Labyrinths

Figure 2-7 shows the staggered and Figure 2-8 the stepped labyrinth types. The major difference between these and straight types is that the straight line of sight is not present or greatly diminished due to the more complex boundary layer.

The seal boundary layer could be described by $R_{boundary,i} = R_i \pm d$ for $i=1\ to\ (Nt-1)$ with R_i being the radius of the boundary layer and d noting the step height. The sign of d is positive or negative depending on whether the step is in the form of an indentation or step on the boundary layer. The amount of steps is usually given by $i = Nt-1$, but could be different in some cases.

The more complex flow path positively affects the seal performance as more of the kinetic energy is converted to thermal energy.

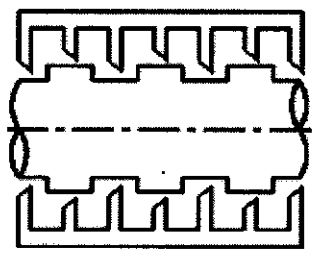

Figure 2-7: *Staggered Labyrinth Seal*

A negative aspect of the staggered configuration is that, due to more complex geometry, the movement of the rotor is severely limited in the axial direction. Unfortunately it will

mostly be necessary to remove the stator cover and splitting the seals during installation, an important factor to take into account during the design phase.

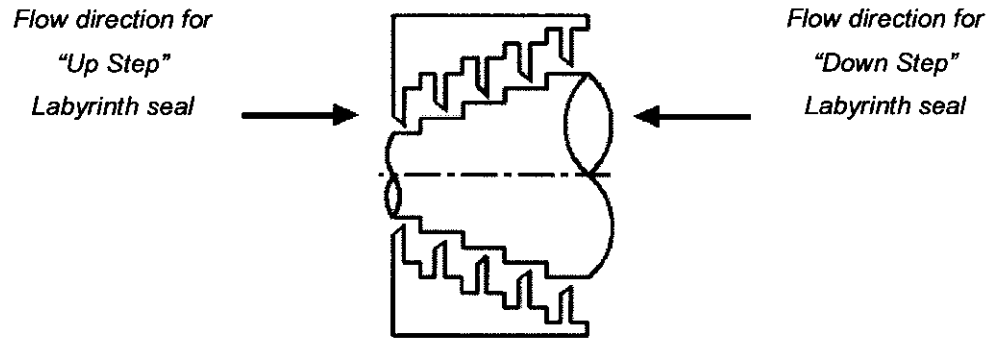

Figure 2-8: *Up and down stepped type labyrinth*

Figure 2-8 shows the up-the-step or down-the-step labyrinth, depending on the flow direction. The change in the boundary layer could be described by $R_i + d$ for up-the-step and $R_i - d$ for down-the-step with d again being the step height on the shaft. Research done by El-Gammal (1996) has shown a big difference between the up-the-step and down-the-step assessment. It was found that shaft rotation was beneficial for the sealing ability of up-the-step seals, while negatively influencing leakage through down-the-step configurations.

2.5.3 Interlocking Type Labyrinth Seals

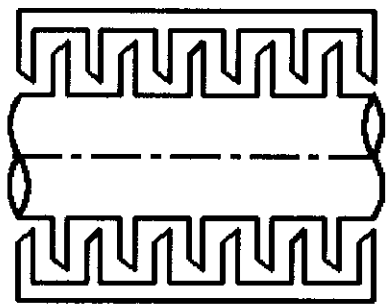

Figure 2-9: *Interlocking labyrinth seal*

The interlocking labyrinths could be compared to a stepped type applying the step as another tooth in the line of flow through the seal, this removes the straight line of sight and as such, increases the effectiveness of the seal above that of the straight type.

Unfortunately, due to the close tolerances between the rotating and stationary pars of the seal, it is very easily damaged with any movement in either radial or axial direction. Special thought also has to be given to the installation process, as previously stated.

2.5.4 Miscellaneous Geometries

As can be seen from Figure 2-10, variations in different geometries are as numerous as their applications. All these have some common elements as stated. Solving alternate geometries is a situation of accounting for the formation of a line of sight and the expansion of the gas in the cavities. Results on accounting for alternative non-straight geometries are discussed by White (1999).

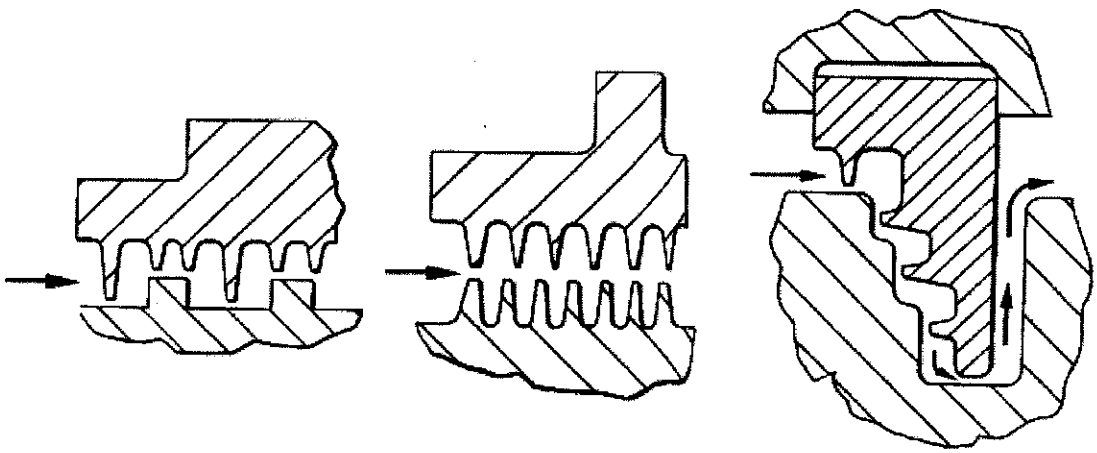

Figure 2-10: *Variations in labyrinth geometries*

2.6 Shaft Rotation Effect on Leakage Values

When determining the leakages through labyrinth seals in rotating machinery, a very important aspect to take into account is the effect of the shaft rotation. The effect of the shaft rotation upon the seal leakages and seal configurations will now be evaluated.

2.6.1 Seal Allocation

Some controversy exists around the effect of shaft rotation on the leakage of labyrinth seals. Some authors like Benvenuti (1979) and Witting (1983) claim that shaft rotation has no effect on the leakage value through the seals, while others believe it to have some

influence on sealing efficiency. El-Gammal (1996) did a study focusing on rotating and stationary labyrinth seals. He defined his results by showing vortice flow patterns within the seals. His study focused, among other on configurations which he referred to as grooved shaft and grooved casing seals. In the stated convention, a straight type seal with teeth located alternatively on the rotor or stator. He studied these configurations and published the following flow path results:

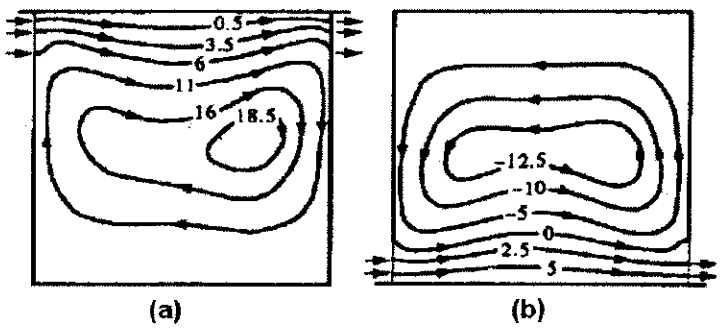

Figure 2-11: *Flow pattern for straight type seal on (a) grooved casing and (b) grooved shaft under stationary conditions*

Figure 2-11 shows the flow pattern in the casing cavity (a) and shaft cavity (b) under stationary shaft conditions, depicted by isometrical velocity lines. Although the flow rotation is in opposite directions within the cavity, the similarity between the different setups can be seen. By then adding rotation to the shaft for the same setup, the following results, as shown in Figure 2-12, was found.

Again relative similarities in the flow rotation can be seen between the casing (a) and shaft seal (b). By using these results it was possible for El-Gammal *et al* to prove that there is no significant distinction between seals located on the rotor or on the stator. As the study will focus on straight and staggered geometries, this will validate the statement that the theory developed within the next chapters will be applicable for seals located on the rotor or stator.

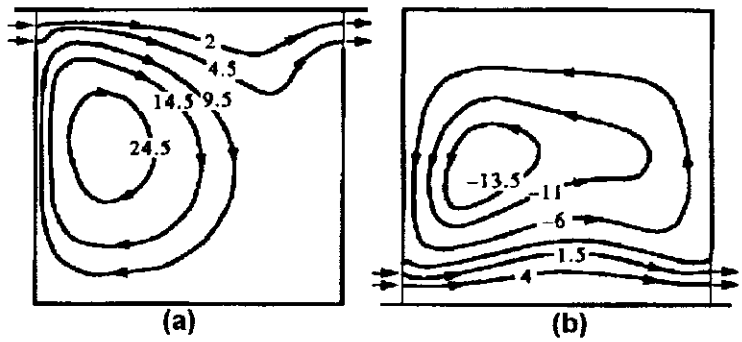

Figure 2-12: *Flow pattern for straight type seal on (a) grooved casing and (b) grooved shaft under rotating conditions*

2.6.2 Effect of Seal Rotation on Leakage Efficiency

Several authors do not even treat the problem of rotation and simply discard it as negligible. Benvenuti (1979), testing with a maximum peripheral speed of 60 m/s, found that the mass flow coefficient decreases slightly with increasing speed. He further found this to be greater for lower leakage rates. He also noted that the greatest difference in leakage due to shaft rotation occurs with very small tooth tip clearances and high rotational speeds. The difference in seal leakage due to shaft rotation under these extreme conditions never exceeded 7% variation from that measured for a stationary shaft.

The most complete work done on the subject was probably by El-Gammal. He generated the same flow path analysis for up and down stepped labyrinth types as discussed in the previous paragraph. Firstly his results obtained for leakage with no shaft rotation were as follows:

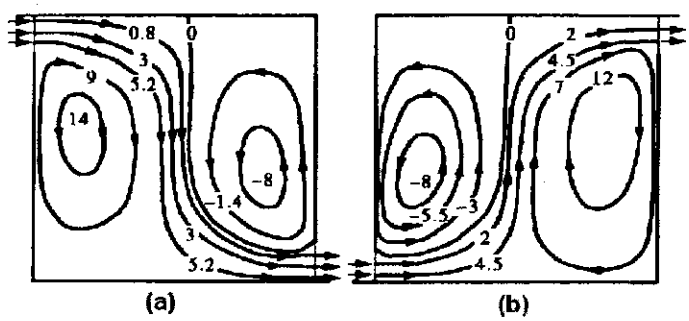

Figure 2-13: *Flow through down step (a) and up step (b) under stationary conditions*

He then proceeded to also discuss the analysis for rotating shaft conditions.

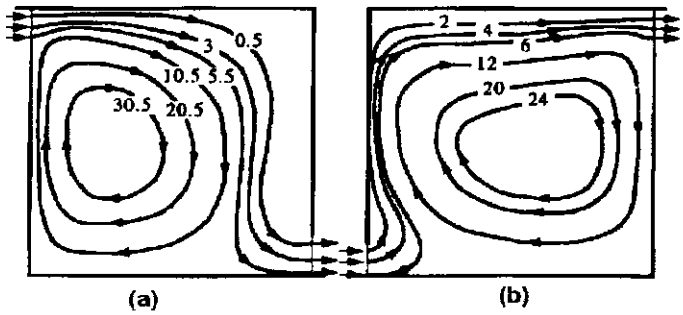

Figure 2-14: *Flow through down step (a) and up step (b) under rotating shaft conditions*

It was his conclusion that shaft rotation is beneficial to the sealing efficiency for up-the-step configuration and that it had an adverse effect on the sealing ability of a down-the-step setup.

He further also tested the straight type grooved shaft and grooved stator configurations with no leakage and only shaft rotation as shown in Figure 2-15.

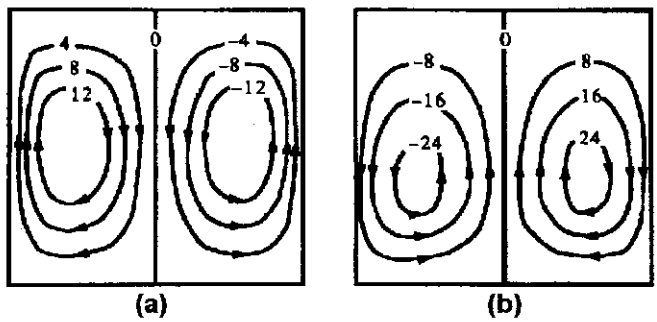

Figure 2-15: *Grooved shaft and grooved stator with no leakage and rotating shaft*

By using the results, as portrayed in Figure 2-11 to Figure 2-15, El-Gammal concluded that shaft rotation does have a minor effect on the sealing ability of stepped labyrinth seals. But he also added that shaft rotation had a negligible effect on the sealing capability of the straight type labyrinths, whether located on the rotating shaft or stationary boundary layer.

2.7 Leakage Control Configurations

In certain applications it may be required to totally isolate flow from certain areas. This is required when using dangerous or harmful gasses. Under such conditions it will be necessary to achieve a full isolation between areas and still not influence the rotordynamic stability of the machine. The seal application could be extended to achieve this by providing ports within the seals. To further improve the effectiveness, or as in the case of harmful or dangerous fluids, these ports would enable the implementation of injection or extraction systems within the labyrinths (Hanlon (2001)).

2.7.1 Injection Method

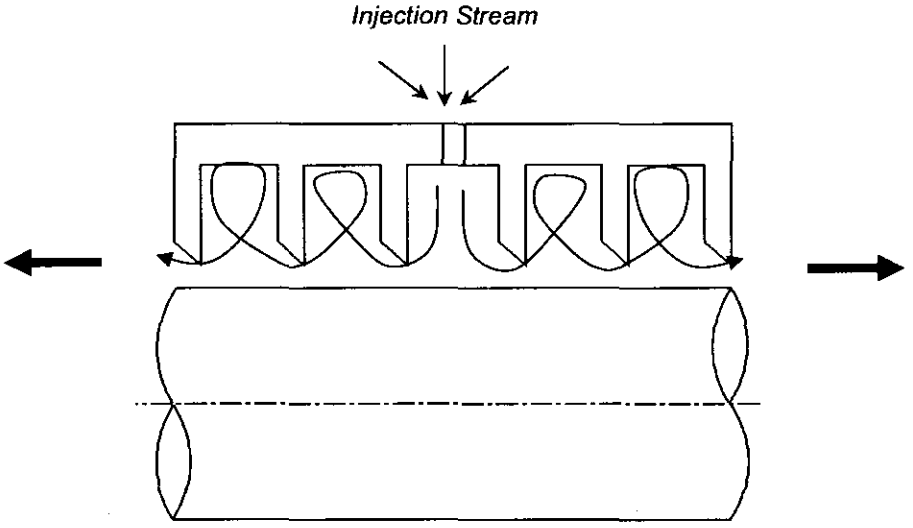

Figure 2-16: *Injection systems in labyrinth seals*

During the injection process, gas is injected into the seal through the port. The advantage of this injection method is to ensure that the leakage will always flow out of the labyrinth, thus ensuring that dangerous or harmful gasses be kept at bay. The injection gas is normally 20-35 kPa above the local gas pressure.

2.7.2 Extraction Method

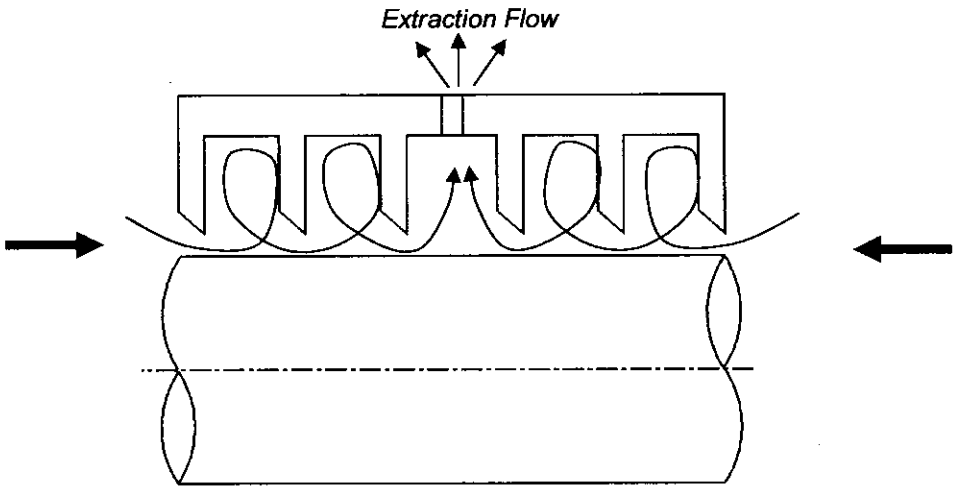

Figure 2-17: *Extraction systems in labyrinth seals*

The use of extraction flow from the labyrinth can be applied to prevent leakages between different stages inside a compressor or where contamination of 2 gas species can pose a problem. The extraction pressure could be anything from 350 – 700 kPa below the gas pressure. It is often used to prevent bearing lubricant from contaminating the main system fluid.

2.8 Labyrinth Defects

It is essential that some of the more frequent errors and defects surrounding labyrinth seals be discussed. In some instances these seals are working within a highly corrosive environment with exhaust gasses, steam or debris passing through the seals. This, together with undesirable mechanical occurrences such as seal rub, can cause severe damage to seals and render them useless.

2.8.1 Clogged up labyrinths

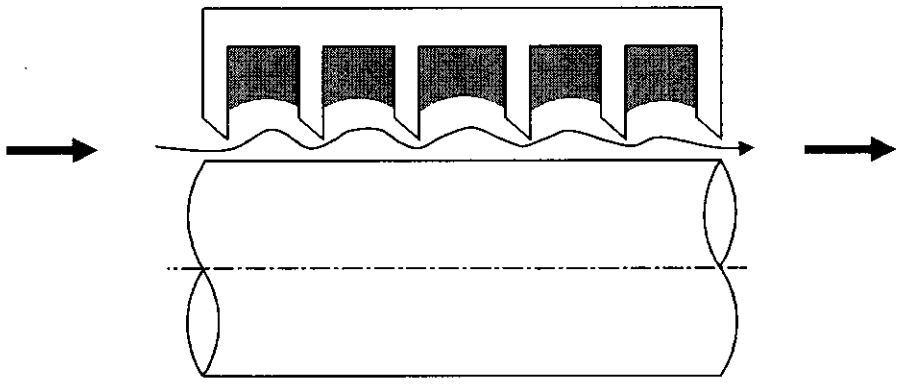

Figure 2-18: *Blocked labyrinth seal*

A major problem in labyrinth seals is that dirt tends to deposit in areas of low flow as shown in Figure 2-18. This occurs due to the presence of pollutants and impurities in the fluid. These then get trapped within the low velocity areas of the seal, effectively reducing cavity volume. The obstruction of the whirling motion increases the line of sight jet velocity and decreases the effectiveness of the seal. When this happens it would normally be necessary to remove and clean or replace the seal.

2.8.2 Labyrinth Tooth Damage

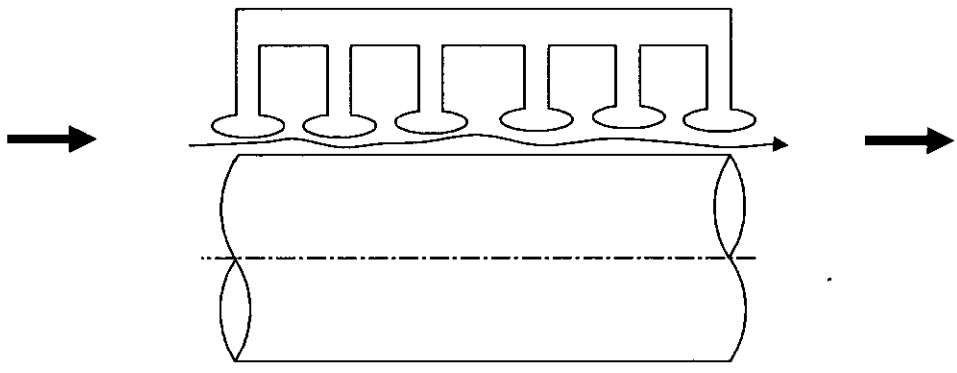

Figure 2-19: *Labyrinth tooth damage due to seal rub*

Figure 2-19 shows the effect of seal rub. This occurs with accidental contact between rotating and stationary parts of the seal. The deformed teeth increase leakage flow path area and obstruct the expansion into the cavity volume. Turbulence is therefore reduced

and the leakage flow increases. In some cases seal rub could occur in 180° of the seal radius, causing the leakage flow to be dramatically increased in one half of the seal radius and could negatively affect rotordynamics on marginally stable rotors.

Figure 2-20: *Labyrinth seal before and after rotor contact*

One effective way to prevent seal rub is the implementation of an electro-magnetically controlled labyrinth seal (ECLS). Such a system allows the clearance distance between the seal and the rotating components to be controlled, ensuring that the minimum clearance is maintained during normal working conditions. It can further allow a greater distance during startup or critical procedures, thus limiting the possibility of seal rub occurring. This level of control allows tighter sealing levels and improved seal performance.

2.8.3 Erosion Damage

Damage by particle erosion could put major limitations on the effective working and lifespan of labyrinth seals. Erosion is caused by hard particles such as sulphur, phosphor, silica or other elements passing through the seal. Figure 2-21 shows typical impact damage of these hard particles on a shaft labyrinth seal. It is quite clear that any seal teeth or cavities in this case are basically nonexistent and unable to function. A simple method to solve this is by installing flow deflectors. A method proven to reduce erosion by up to 80% (Mazur (2002)).

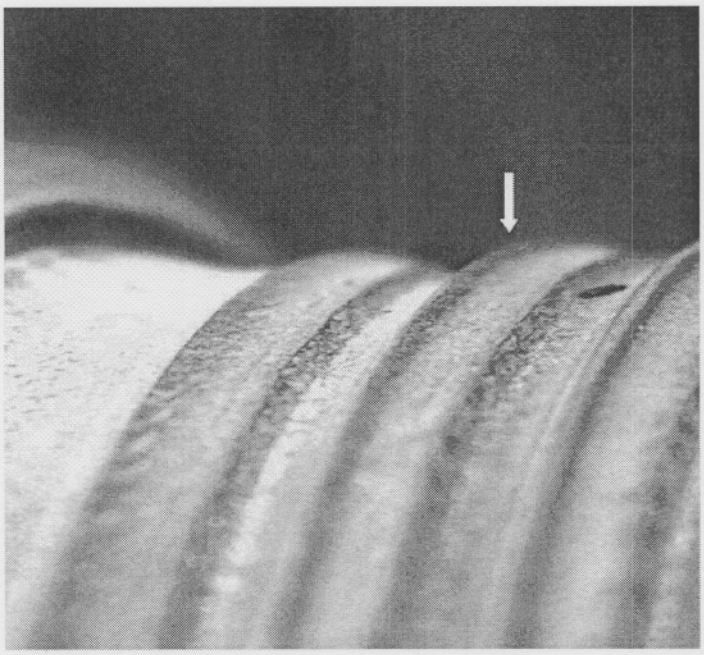

Figure 2-21: *Erosion damage to rotor labyrinth*

From all the information that has been given on some common labyrinth defects it can be seen that it necessary to keep the fluid flowing through these seals as clean as possible. When seals are installed in high erosion area or areas with a high amount of debris, special consideration should be given to replacement and maintenance of these seals.

2.9 Labyrinth Material Properties

Labyrinths are usually made of a light alloy material resistant to corrosion. The hardness level should always be lower than that of the shaft to prevent damaging the shaft in the case of accidental seal rub. The labyrinths are therefore usually made from annealed aluminum alloy with a Brinell hardness of 70 – 80. If the fluid in the cycle is not compatible with the aluminum alloy it could be replaced with stainless steel with 18% Cr and 8% Ni content (Hanlon (2001)).

The alternative is to make use of non-metallic labyrinth seals like carbon fiber composites or thermoplastic materials. These materials have the added benefits that they are extremely light, have high chemical resistance, high mechanical strength and a low

coefficient of expansion. Some propriety materials are also available offering outstanding wear and impact resistance as well as some that claim to be rub resistant.

2.10 Alternative Sealing

A number of other possible sealing methods within rotating machinery have been investigated. The most significant of these are discussed shortly.

2.10.1 Honeycomb Seals

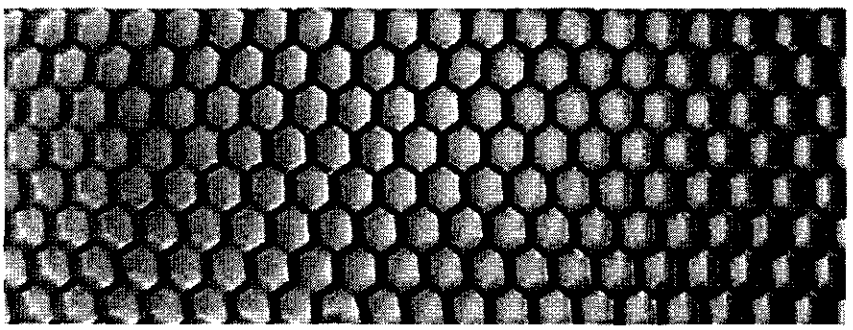

Figure 2-22: *Honeycomb material*

Honeycomb material as shown in Figure 2-22 is lined on the stator. This roughened stator reduces leakage and has the major advantage of reducing the circumferential velocity within the seal. An additional benefit of the lower circumferential velocity is that the destabilizing cross coupled stiffness coefficient is reduced. This seal type has been profitably used for balance drum applications in compressors and as a turbine interstage seal for the high-pressure oxygen turbo pump of the space shuttle main engine (Childs (1993)).

At operating speed, many teeth-on-rotor labyrinth blades can be designed to sufficiently grow due to centrifugal stresses that the blades cut into the stator and operate in an interference mode. By then aligning this so-called abrable seals to honeycomb material on the stator, it is possible to achieve a much greater sealing efficiency.

An extensive experimental investigation on honeycomb seals was conducted showing that the best sealing and rotordynamic performance for such seals with swirling incoming flows and followed by labyrinth seals are achieved for seals that are longer than 50 mm. For shorter seals (25mm), the rotordynamic stability is reduced (Chochua (2002)).

2.10.2 Brush Contact Seals

The biggest challenger for the labyrinth is the brush contact seal. Brush contact seals employ the same working principle as labyrinth seals, but with added advantages. As can be seen in Figure 2-23, brush seals consist of a dense pack of bristles sandwiched between a face plate and a backing plate. The bristles are orientated to the shaft in a lay angle generally 45° to 55° pointing in the direction of rotation. A primary attribute of the brush seal is the ability to accommodate transient shaft excursions and still return to small clearances (Steinetz (1994)).

The figure illustrates the brush packing in close contact with the shaft on a ceramic or chromium carbide rub running surface. The leakage flow experienced through a brush seal is substantially lower than that through normal labyrinths or honeycomb seal. Initial tests show leakages to be 10 to 20% of the normal labyrinth leakage values (Steinetz (1994)). The rotordynamic characteristics are also more favorable in comparison with other gas seal configurations (Childs (1993)).

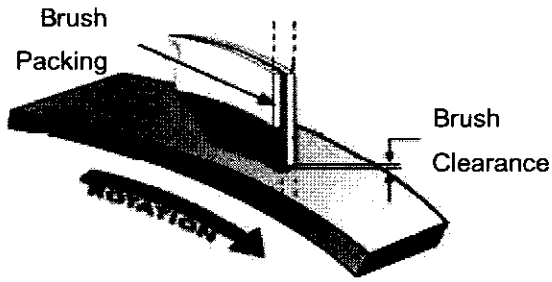

Figure 2-23: *Brush seal*

In a study led by Hendricks (1994) of the National Aeronautics and Space Administration, the relative performance comparison between labyrinths and dual brush

compressor discharge seals in an aircraft engine was examined. Direct comparisons between labyrinths and dual brush seals have been made.

The pressure drops measured over the dual brush seals were higher than that of their labyrinth counterparts and leakages were lower. The leakages experienced through labyrinth seals were 2.5 times greater than that through the brush seals.

Brush seal systems are efficient, stable, contact seals that are usually interchangeable with labyrinth shaft seals but require a smooth rub running interface and an interference fit upon installation. However, it would not be possible to upgrade labyrinth seals in an existing system with brush type seals without computing and accounting for all secondary airflow necessary for cooling and engine dynamics associated with the seal packing modifications.

Labyrinth seal systems where found to be very pressure dependent to function properly where the brush seals were only weakly dependent on the pressure. The brush seal in stead was found to be more dependent upon the packing factor of the bristles. The sealing ability of the brush seals will be dramatically decreased due to wear after about 500-1000 hours of use.

One might feel very tempted to believe that the option of brush seals is always the better option, but due to the need for regular service intervals, the application is mostly found on aircraft or spacecraft engines with shorter service intervals. In power plants such as the PBMR, however, implementing brush type seals it is not a feasible option. Using helium as coolant, friction welding is very likely to occur. Further more the much larger time span required between service intervals will limit performance efficiency.

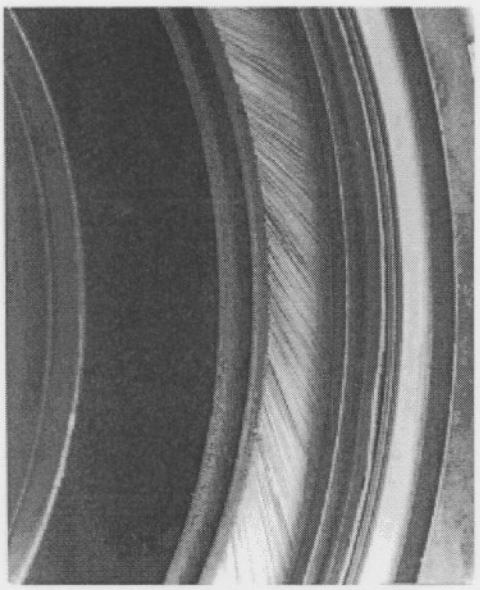

Figure 2-24: *Compressor discharge brush seal*

2.11 Rotordynamic Forces in Labyrinth seals

According to Childs (1993), many load dependent instability problems have been attributed to labyrinth seals. The rotordynamic coefficients of these seals are proportional to both the pressure ratio over the seal and the average fluid density within the seal.

The cross coupled stiffness coefficient arises primarily because of the circumferential velocity within the seal. From a rotordynamic viewpoint this is the central, most crucial fact related to labyrinth seals. It has been proven that, by placing swirl webs consisting of axial directed fins just upstream of the labyrinths to destroy inlet tangential velocity, the rotordynamic stability can be dramatically improved.

These destabilizing rotordynamic forces at work in the seals are small, but they are located at potentially sensitive areas. The cross coupled stiffness values can easily be the difference between stable and unstable operation. The importance of these coefficients requires it to be studied in lot more detail. However, it does not form part of the scope of this study and is therefore only mentioned here as a matter of interest.

4.1 Introduction

After deriving the model in Chapter 3, the next step is to implement it for calculating the labyrinth leakage flow. This chapter subsequently discusses the solving of the equation sets for choked and unchoked conditions for both straight and staggered geometries. For this purpose the proposed models were implemented into EES software to simplify calculations.

4.2 Flow through the complete labyrinth packing

In Chapter 3 the mass flow equation for leakage through a straight type seal was found to be

$$\dot{m}_i = C_{ke} C_d A_g \sqrt{\frac{2\gamma}{\gamma - 1} \frac{{p_{i-1}}^2}{RT_0} \left(\left(\frac{p_i}{p_{i-1}} \right)^{\frac{2}{\gamma}} - \left(\frac{p_i}{p_{i-1}} \right)^{\frac{\gamma+1}{\gamma}} \right)} \tag{4.1}$$

With the discharge coefficient defined by

$$C_d = \frac{\pi}{\pi - 7\left(\frac{P_{i-1}}{P_i} \right)^{\frac{\gamma-1}{\gamma}} + \left(\frac{P_{i-1}}{P_i} \right)^{\frac{2\gamma-2}{\gamma}} + 8} \tag{4.2}$$

The kinetic carry-over coefficient was found to be

$$C_{ke} = \frac{1}{\sqrt{1-\alpha}} \tag{4.3}$$

$$\alpha = \frac{8.52}{\frac{S-L}{cl} + 7.23} \tag{4.4}$$

By applying the equations to the appropriate amount of constrictions will lead to a matrix of equations. The solving of this equation set will now be discussed for unchoked and choked conditions.

2.12 Conclusion

This chapter discussed the basic implementation and working of labyrinth seals. Common elements of labyrinth seals were identified and a convention was set for distinguishing between different geometries. Further, the importance of shaft rotation on seal leakage was also investigated and some results from the literature are discussed. Common operational defects, found when working with labyrinth seals, were also identified. Some methods of limiting or controlling small leakages normally present in labyrinth seals under critical conditions where also discussed. Finally some alternative methods of sealing rotating machinery were described. With the basic elements and application of the seals now discussed, Chapter 3 will look at the governing physics and how to account for the leakage through the labyrinths.

CHAPTER 3

THEORY

Chapter 3 investigates the possibility of a method for predicting the leakage flow though the labyrinth seals. Some assumptions necessary for the solving of leakage values are identified. The working of a labyrinth is described using a temperature-entropy diagram and the Saint Venant-Wantzel equation for flow through a constrictor is derived. Flow through the seals is discussed for choked and unchoked conditions and coefficients are derived and studied to better account for some phenomena occurring within the seal boundaries.

3.1 Introduction

Chapter 3 describes the equations and physics governing the leakages through the major labyrinth geometries as discussed in Chapter 2. The major assumptions will be stated and justified in their use.

3.2 Assumptions

It will be necessary to make certain assumptions in order to simplify the prediction of leakage flow values through the labyrinth seals. The assumptions, as stated below, has also been accepted and implemented by among others Childs (1993), Eser (1995) and White (1999). These include:

- The rotation of the boundary layer or seal teeth does not significantly influence the axial leakage flow rate. (As discussed in Paragraph 2.6)
- Flow is adiabatic (No heat is added to or removed from the seal)
- Steady state flow is assumed
- The gas behaves according to relations of ideal gas laws.
- The rotor and seal teeth remain concentric, implicating rotor eccentricity of zero.
- Isentropic expansion of the fluid through the constriction is assumed.
- Pressure is uniformly distributed within each cavity

3.3 Flow of Gas through a Single Constriction

The nomenclature to be used for the straight labyrinth seal is as shown in Figure 2-3. The next section illustrates the basic physics involved in the operation of the labyrinth seal, by using the additional assumption that the flow is isothermal through the cavities. This assumption would be met if the flow is adiabatic and all the kinetic energy in each constriction is converted into thermal energy in the subsequent cavity.

3.3.1 Isothermal flow conditions

Using the mentioned assumptions, the problem of predicting the flow through a labyrinth seal can be reduced to one of determining the mass flow rate as a function of bulk cavity pressures $p_1, p_2, \ldots p_{n-1}, p_n$. Following the same methodology of Kearton (1952), Neumann (1964) and Eser (1995), the labyrinth seal is modeled as a series of annular orifices through which a pressure drop is established. To this end, consider the conservation of energy of a compressible gas in moving from cavity i-1 to constriction i, as can be seen in Figure 2-3:

$$\left(h_{i-1}\right)_{cavity} = \left(h_i + \frac{V_i^2}{2}\right)_{restriction} \tag{3.1}$$

Equation (3.1) results when assuming that the gas reaches static conditions in cavity i-1, after the throttling process in constriction i-1. This would be true if all the kinetic energy in constriction i-1 is converted to thermal energy in cavity i-1. Rewriting the equation in terms of the temperature results in:

$$\left(c_p T_{i-1}\right)_{cavity} = \left(c_p T_i + \frac{V_i^2}{2}\right)_{restriction} \tag{3.2}$$

Again assuming that the gas is retarded to zero axial velocity in cavity i results in Equation (3.2) when applying the energy equation for the gas in moving from constriction i to cavity i:

$$\left(c_p T_{i-1}\right)_{cavity} = \left(c_p T_i + \frac{V_i^2}{2}\right)_{restriction} = \left(c_p T_i\right)_{cavity} \tag{3.3}$$

From Equation (3.3) it is clear that the temperature of the gas, in moving from cavity i-1 to cavity i, remains constant. In other words, if all kinetic energy were converted into

thermal energy in the cavities, the flow would be isothermal. This scenario is displayed in Figure 3-1 on the temperature-entropy diagram:

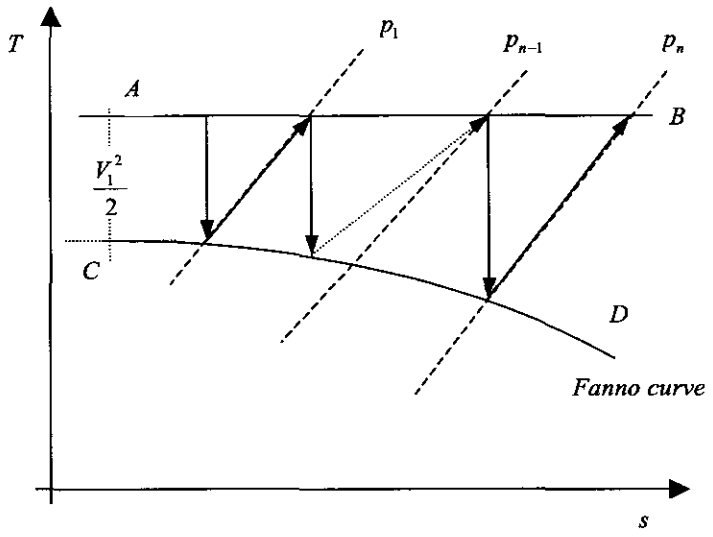

Figure 3-1: *The isothermal process on the temperature-entropy diagram*

Curve *AB* represents the constant temperature in the labyrinth cavities. The constant pressure curves $p_1,...,p_{n-1},p_n$ correspond to the pressures in the various cavities. From the state point on the temperature curve *AB* for the cavity, the gas expands isothermally through the constriction, reducing the static temperature component. An axial velocity is established through the constriction, determined by the vertical extent of the static temperature drop (*A-C*). Meanwhile, the gas pressure has dropped to the corresponding pressure in the subsequent cavity. In the cavity, this kinetic component is then converted into thermal energy at a constant pressure, increasing the entropy of the gas. The process is then repeated through the next constriction. Ultimately, the pressure and density decrease along the axial coordinate of the labyrinth, while the entropy increases.

The Fanno curve *CD* for this particular flow rate is also shown in the figure, and represents isentropic flow with friction, but zero heat transfer (Shames (1992)). The gas therefore expands isentropically to the point on the Fanno curve in moving form cavity *i-1* to constriction *i*. Notice that the constrictions at the rear of the labyrinth have a higher

axial velocity than the front constrictions. Due to the steady conditions, the mass flow rate through all constrictions should be equal. Since the density decreases along the axial coordinate of the labyrinth, the corresponding velocity component should increase, if the flow-through area remains unchanged. An increase in velocity results in higher values for kinetic energy per unit mass, and therefore the vertical extent of the isentropic process increases to the rear of the seal. This explains the shape of the Fanno curve.

3.3.2 Sonic Velocity in Last Constriction

Extending the Fanno curve in Figure 3-1 further will ultimately result in a point of maximum entropy for the given flow rate (Shames (1992)), as indicated in Figure 3-2:

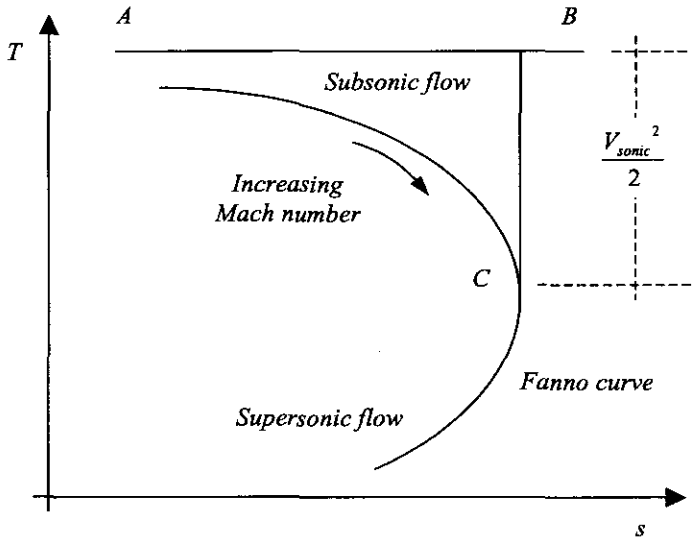

Figure 3-2: *Fanno curve plotted on the temperature entropy diagram*

The point C in the figure corresponds to the point of maximum entropy. The velocity V_{sonic} would then represent the velocity in the last constriction, equal to the sonic velocity of the gas. At these conditions, the last constriction would choke. This implies that, no matter how much the pressure drop over the seal is reduced further, a higher mass flow rate than that associated with the choked condition is impossible.

Knowing that the axial velocity and Mach number increase with axial coordinate, consider the equation relating the static pressure to the stagnation pressure for isentropic flow of a compressible gas:

$$\frac{p}{p_0} = \frac{1}{\left[1+\frac{\gamma-1}{2}M^2\right]^{\frac{\gamma}{\gamma-1}}} \tag{3.4}$$

From Figure 3-1 it is clear that the pressure in cavity i is equal to static pressure in constriction i. The static pressure in constriction i is calculated from the isentropic expansion process from cavity i-1 to constriction i. Therefore, the pressure in cavity i is related to the pressure in cavity i-1 as follows:

$$\frac{p_i}{p_{i-1}} = \frac{1}{\left[1+\frac{\gamma-1}{2}M_i^2\right]^{\frac{\gamma}{\gamma-1}}} \tag{3.5}$$

Equation (3.5) then predicts that the pressure drop through the constrictions increases with axial coordinate and therefore the last constrictor (n) will have the highest pressure drop. Also, the equation illustrates why the pressure drop through the last constriction equals that of the stagnation to static pressure for $M=1$, if the last restrictor is choked.

Although the pressure ratio over the last constriction equals that of the critical ratio for values of $M \geq 1$, the pressure drop $\frac{p_n}{p_{n-1}}$, where p_n represents the boundary outlet pressure, is not equal to the critical ratio. Therefore, if $M>1$, the pressure drop $\frac{p_n}{p_{n-1}} > \left(\frac{p_n}{p_{n-1}}\right)_{crit}$ and the additional pressure loss would be encountered outside the seal. Nevertheless, the critical ratio should be used for calculating the mass flow rate through the last constriction since the flow chokes at this pressure ratio.

3.4 Mass Flow Rate Calculation for Unchoked Conditions

By assuming that the last constrictor is not choked, and by using the energy equation of the gas flowing from cavity i-1 to constrictor i, it is possible to derive Equation (3.6) for the mass flow through a series of annular constrictions. Derivation of the equation is shown in Appendix A.

$$\dot{m}_i = A_g \sqrt{\frac{2\gamma}{\gamma - 1} \frac{{p_{i-1}}^2}{RT_0} \left(\left(\frac{p_i}{p_{i-1}} \right)^{\frac{2}{\gamma}} - \left(\frac{p_i}{p_{i-1}} \right)^{\frac{\gamma+1}{\gamma}} \right)} \tag{3.6}$$

Equation (3.6) is the well-known Saint Venant-Wantzel equation (Kearton (1952)) for isentropic flow through a constriction, which can be used as a basis for solving the leakage flow values through the labyrinth seals.

There is, however, some alternative effects occurring within the labyrinths that need to be taken into account. These are the discharge coefficient and kinetic energy carry-over coefficient. These will be discussed and taken into account in the leakage flow calculations in Paragraph 3.5 and Paragraph 3.6.

3.5 Discharge Coefficient

As is the case with any orifice, the high velocity of the fluid leads to the formation of the vena contracta in the restrictor passage and causes the effective flow-through area to be smaller than the geometrical flow area. As the theory used to solve labyrinth leakage values is related to orifice theory, this factor will have to be accounted for. This effect can be demonstrated in Figure 3-3 which shows the flow pattern through a normal orifice plate.

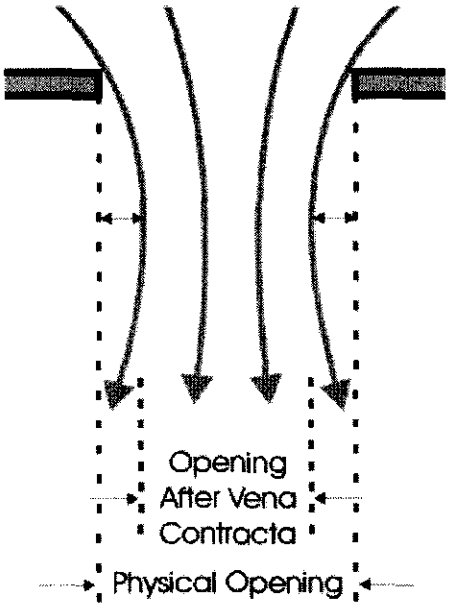

Figure 3-3: *Vena contracta reducing the flow through area*

Figure 3-3 shows the shape of the vena contracta in a normal orifice plate. However, in the case of the labyrinth seal the occurrence of the vena contracta could be shown as in Figure 3-4. Due to the presence of the rotor only half of the vena contracta is present between each sharp teeth edge and boundary layer. It can be seen from both Figure 3-3 and Figure 3-4 that the decreasing cavity flow area will improve seal performance.

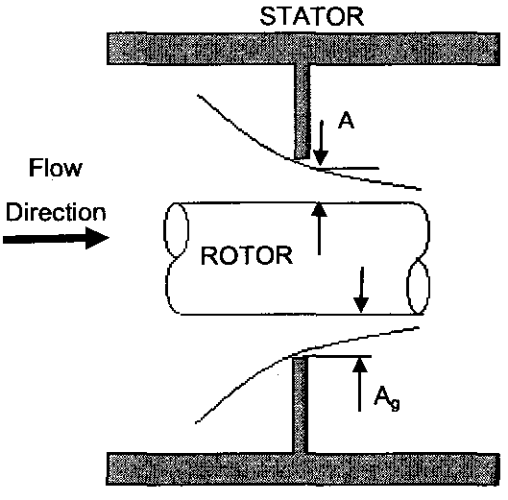

Figure 3-4: *Vena contracta as found within labyrinth seals*

This effect is accounted for by making use of the discharge coefficient, defined in Equation (3.7):

$$C_d = \frac{A}{A_g} \tag{3.7}$$

The discharge coefficient takes into account the change in geometrical area of the flow path through the labyrinth seal. The leakage flowrate through the labyrinth seal is then taken into account by modifying Equation (3.6) using the discharge coefficient:

$$\dot{m}_i = C_d A_g \sqrt{\frac{2\gamma}{\gamma - 1} \frac{p_{i-1}^2}{RT_0} \left(\left(\frac{p_i}{p_{i-1}} \right)^{\frac{2}{\gamma}} - \left(\frac{p_i}{p_{i-1}} \right)^{\frac{\gamma+1}{\gamma}} \right)} \tag{3.8}$$

Using Equation (3.8), a more accurate value for the mass flow rate through a restrictor can be obtained. Similar to other orifice models, the discharge coefficient is usually based on experimental data. Undoubtedly some propriety techniques exist to calculate these coefficients, but the discussion is limited to those found in literature.

3.5.1 Discharge coefficients determined from experiments by Snow

In the paper by Kearton (1952), Snow reported that experiments he had done on annular discharge coefficients is not dependent only on the pressure ratio, but also on the ratio of tooth axial width to clearance ratio $\left(\frac{L}{cl} \right)$. Using air as the working fluid, he constructed a graph for discharge coefficients for teeth similar in shape as that indicated on the graph (Figure 3-5). The user has the ability to obtain the required discharge coefficient from the graph and supplement into the leakage equation.

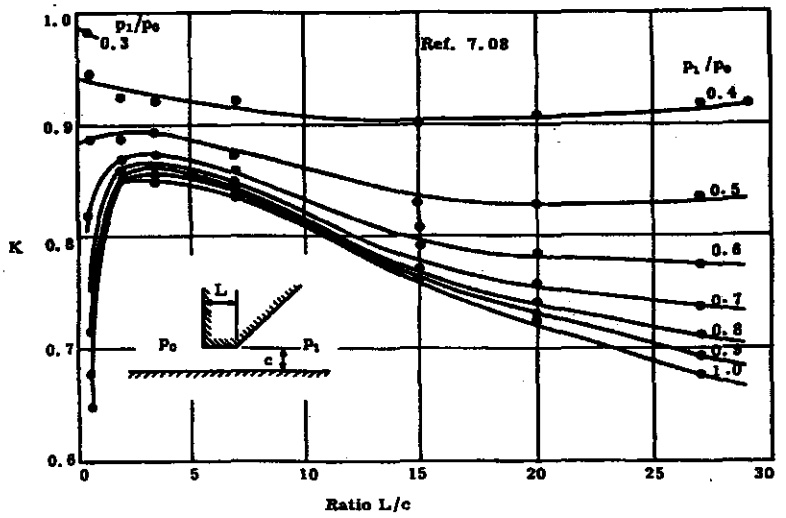

Figure 3-5: *Discharge coefficient as function of pressure ratio for air*

This method of accounting for discharge coefficients severely limits the flexibility, as all coefficient values are dependent on experimental results for air only and limited to those contained in the graph.

3.5.2 Discharge coefficients determined from experiments by Bell and Bergelin

Bell and Bergelin (1957) did a comprehensive study to determine discharge coefficients for oil and water in an annular shaped orifice. The data they generated, as shown in Figure 3-6, is dependent on the ratio $\left(\frac{L}{cl}\right)$ and the Reynolds number of the fluid. Although these tests were conducted using oil and water, Vermes (1961) found that the results could be used with good accuracy on air.

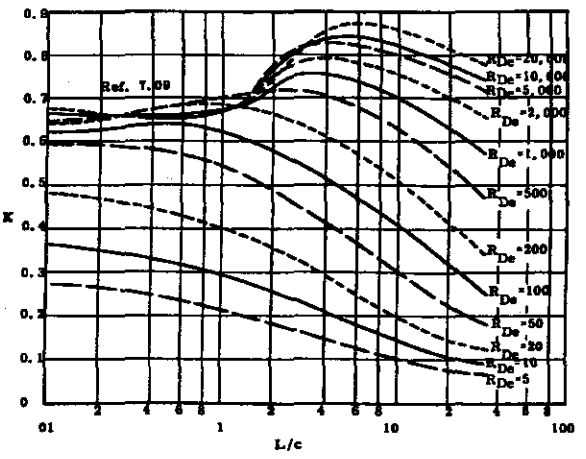

Figure 3-6: *Discharge coefficient as function of Reynolds number (oil and water)*

Once again the method is experimentally based and accuracy will have to be confirmed for other coolants.

3.5.3 Sharp edge single restrictor

Eser (1995) uses a formula derived by Chaplygin (Gurevich (1996)), which applies to a thin sharp edge single orifice plate. The formula is derived for case where the tooth tip length to clearance ratio approaches zero $\left(\frac{L}{cl} \to 0\right)$. This causes the value for the discharge coefficient to be dependent only on the pressure ratio and the ratio of specific heats. Eser (1995) states the following relations as derived by Chaplygin to determine the discharge coefficient:

$$C_d = \frac{\pi}{\pi + 2 - 5s_i + 2s_i^2} \tag{3.9}$$

$$s_i = \left(\frac{P_{i-1}}{P_i}\right)^{\frac{\gamma-1}{\gamma}} - 1 \tag{3.10}$$

By then substituting (3.10) into (3.9) it will be possible to simplify the discharge coefficient to the form:

$$C_d = \frac{\pi}{\pi - 7\left(\frac{P_{i-1}}{P_i}\right)^{\frac{\gamma-1}{\gamma}} + \left(\frac{P_{i-1}}{P_i}\right)^{\frac{2\gamma-2}{\gamma}} + 8} \tag{3.11}$$

Equation (3.11) now gives an effective coefficient to account for the discharge effect through the seals. As this is the only method dependent upon the relative gas constants it could be used to solve the discharge coefficient for either air or helium as fluid. Due to this flexibility and the fact that it is not dependent upon experimental results it will be used in the engineering tool to calculate the discharge coefficients in the solving of labyrinth leakage values.

3.6 Kinetic energy carry-over coefficient

In practice, the phenomena is encountered as a line of high velocity in labyrinth seals (Figure 2-6) where there is a significant amount of kinetic energy not converted into thermal energy, but carried over to the following restrictor. This is especially true for shorter pitched labyrinths as the smaller cavity section does not allow the gas to fully expand. Unlike the discharge coefficient, the effect of this occurrence adversely affects seal performance, meaning that increased leakage flows are present. This is accounted for by using a kinetic energy carry-over coefficient (C_{ke}), as shown in Equation (3.12).

$$\dot{m}_i = C_{ke} C_d A_g \sqrt{\frac{2\gamma}{\gamma - 1} \frac{p_{i-1}^{\,2}}{RT_0} \left(\left(\frac{p_i}{p_{i-1}}\right)^{\frac{2}{\gamma}} - \left(\frac{p_i}{p_{i-1}}\right)^{\frac{\gamma+1}{\gamma}} \right)} \tag{3.12}$$

The value for C_{ke} is always greater than one, therefore increasing the leakage flow rate. Normally the kinetic carry-over coefficient used is strongly dependent upon experimental values which limit model flexibility. Vermes (1961) approximated a model dependent upon the geometry of the seal. This results in a flexible model suitable for the purposes of the engineering tool and will be discussed in the next paragraph.

3.6.1 Vermes carry-over coefficient

Vermes (1961) approximated the flow in a labyrinth cavity as one half of a flat symmetrical jet originating from an infinitesimally narrow slot. The flow of a jet of this type is described by authors such as Schligting (1955). Vermes derived a parameter α termed the residual energy factor.

$$\alpha = \frac{8.52}{\frac{S-L}{cl} + 7.23} \tag{3.13}$$

As shown in Appendix B this residual energy factor can now be used to determine the kinetic energy carry-over by using Equation(3.14)

$$C_{ke} = \frac{1}{\sqrt{1-\alpha}} \tag{3.14}$$

This coefficient presents a reliable method of approximating the effect of the kinetic energy carry-over and will be implemented into the engineering tool.

3.7 Staggered type seal

All the assumptions used for the straight type seal in the beginning of the chapter will also apply to the staggered type seal. Thus the ideal leakage through the staggered seal could also be presented by Equation (3.6) as discussed in Paragraph 3.4. Similar to the straight type seal, the velocity through both the high and low constriction is given by Equation (3.15) with derivation as shown in Appendix A.

$$V_i = \sqrt{2\left(\frac{\gamma}{\gamma-1}R\right)T_{i-1}\left\{1-\left(\frac{p_i}{p_{i-1}}\right)^{\frac{\gamma-1}{\gamma}}\right\}} \tag{3.15}$$

Ideally, the mass flow rate through these two types of constrictions is thus given by Equation (3.6). The effect of the vena contracta is also present in the staggered type labyrinth, and the coefficient of discharge can be used unchanged from that for the straight through type for both high and low restrictors. However, the staggered type of seal performs better for limiting leak flow rates because the amount of kinetic energy carried over from one restrictor to the next is much less than in the case of the straight

through type. Assuming that the step depth of the seal is sufficiently large, it can be taken equal to zero. This assumption is similar to work done on staggered type of labyrinths by authors such as Egli (1935) and Kearton (1952). The mass flow rate through both a high and low constriction in a staggered type of labyrinth packing is therefore given by Equation (3.16):

$$\dot{m}_i = C_d A_g \sqrt{\frac{2\gamma}{\gamma - 1} \frac{p_{i-1}^{\,2}}{RT_0} \left(\left(\frac{p_i}{p_{i-1}} \right)^{\frac{2}{\gamma}} - \left(\frac{p_i}{p_{i-1}} \right)^{\frac{\gamma+1}{\gamma}} \right)} \tag{3.16}$$

3.8 Summary and conclusions

In this chapter a theory for calculating mass leak flow rate and pressure distribution through labyrinth seals was discussed. Two different models were presented, one for a straight through type of seal and the other applicable to the staggered type seal. The mass leak flow rate is calculated by considering the teeth of the seal to be annular shaped orifices, which throttles the flow.

This leakage flow equation formulated for ideal flow through the labyrinth does leave some phenomena unaccounted for. These are the occurrence of a vena contracta at the various constrictions, and the kinetic energy carry-over between different constrictions. These where taken into account by implementing a discharge coefficient and a kinetic energy carry-over coefficient. In Chapter 4 the physics derived in this chapter will be implemented and solved for some labyrinth geometries.

CHAPTER 4

MODEL IMPLEMENTATION AND RESULTS

The solving of a labyrinth packing for choked and unchoked conditions are discussed. EES models for straight and staggered configurations are also presented and used to solve various labyrinth geometries thereafter parametric studies are preformed over a range of pressure ratios to better illustrate the functioning of the seals. Finally results are presented for both straight and staggered configurations and sealing efficiency of the labyrinth types are compared.

4.2.1 Unchoked flow

Applying the resulting energy equation (Equation(4.1)) for all n-constrictions results in a system of n equations and $(3n+3)$ unknowns:

$$\dot{m} = C_{ke,1} C_{d,1} A_g \sqrt{\frac{2\gamma}{\gamma - 1} \frac{p_0^{\,2}}{RT_0} \left(\left(\frac{p_1}{p_0} \right)^{\frac{2}{\gamma}} - \left(\frac{p_1}{p_0} \right)^{\frac{\gamma+1}{\gamma}} \right)}$$

$$\dot{m} = C_{ke,2} C_{d,2} A_g \sqrt{\frac{2\gamma}{\gamma - 1} \frac{p_1^{\,2}}{RT_0} \left(\left(\frac{p_2}{p_1} \right)^{\frac{2}{\gamma}} - \left(\frac{p_2}{p_1} \right)^{\frac{\gamma+1}{\gamma}} \right)}$$

$$\vdots \qquad\qquad \vdots$$

$$\dot{m} = C_{ke,n-1} C_{d,n-1} A_g \sqrt{\frac{2\gamma}{\gamma - 1} \frac{p_{n-2}^{\,2}}{RT_0} \left(\left(\frac{p_{n-1}}{p_{n-2}} \right)^{\frac{2}{\gamma}} - \left(\frac{p_{n-1}}{p_{n-2}} \right)^{\frac{\gamma+1}{\gamma}} \right)}$$

$$\dot{m} = C_{ke,n} C_{d,n} A_g \sqrt{\frac{2\gamma}{\gamma - 1} \frac{p_{n-2}^{\,2}}{RT_0} \left(\left(\frac{p_{n-1}}{p_n} \right)^{\frac{2}{\gamma}} - \left(\frac{p_{n-1}}{p_n} \right)^{\frac{\gamma+1}{\gamma}} \right)}$$

In addition to the above n equations, there should be $2n$ additional equations or data to determine C_d and C_{ke} for each constriction. The unknown variables are the pressures $p_0, p_1, \ldots, p_{n-1}, p_n$, the n discharge coefficients, the n kinetic energy carry-over coefficients, the mass flow rate $\dot{m}$ and the inlet temperature T_0. The needed boundary input data is that of the pressures p_0 and p_n as well as the inlet temperature T_0. In other words, a closed system of $(3n+3)$ equations and $(3n+3)$ unknowns is formed and can be iteratively solved. The solution will yield the mass flow rate and pressure distribution through the labyrinth seal.

4.2.2 Choked flow

In the case of a choked seal, Equation (4.1) is still applicable to all the constrictions, including the last. This time, however, the pressure ratio over the last constriction does

not have to be determined from the calculation, but is known and equal to $\left(\frac{p_n}{p_{n-1}}\right)_{crit}$. Therefore, the given outlet boundary pressure p_n drops away and is replaced by the given pressure ratio over the last constriction. Again, a closed system of $(3n+3)$ equations and $(3n+3)$ unknowns is formed, which can be iteratively solved.

Equations for calculating the discharge coefficient is no longer valid at the last constriction, this is due to the fact that the coefficient is dependent upon $\left(\frac{p_{i-1}}{p_i}\right)$. This is solved by using the critical pressure ratio over the choking constriction to calculate the discharge coefficient, causing it to remain constant.

Prior to solving the flow through the labyrinth seal, it will be unknown whether or not the last constriction is choked. However, this can be easily determined. The methodology followed is to first solve the system of equations pertaining to choked conditions. If the last constriction is indeed choked, then it should be true that the inequality $\left(\frac{p_n}{p_{n-1}}\right)_{crit} > \frac{p_n}{p_{n-1}}$ holds. If not, then the seal is not choked and the unchoked system of equations should be used for determining the mass flow rate.

4.3 Straight Type EES Model

The resulting EES model is shown in Appendix C.1. The geometry used in this model is based on that used by Eser (1995). It uses a two constriction straight type labyrinth with small tip width. The geometry of seal is as shown in Figure 4-1.

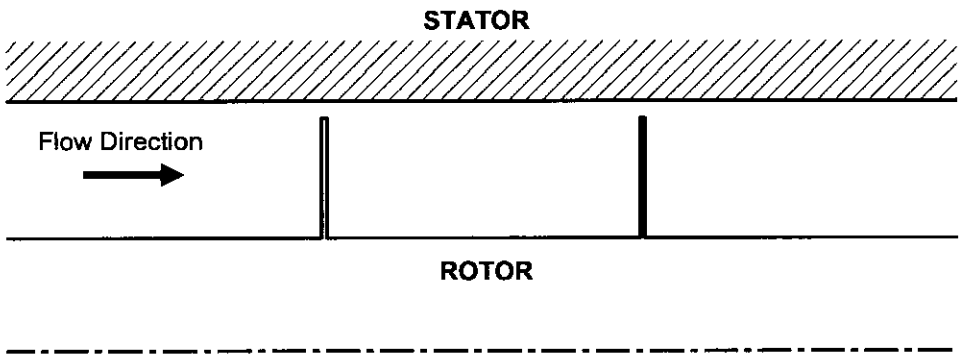

Figure 4-1: *Eser straight type geometry*

The geometrical values and operating conditions of the seal are defined in Table 4-1.

Table 4-1: *Eser straight type geometry and operating conditions*

Eser Geometry and operating conditions					
Fluid	Air		No of Teeth	2	
Inlet Pressure	241.3	*kPa*	Shaft Radius	101.6	*mm*
Outlet Pressure	206.8	*kPa*	Clearance	0.16	*mm*
Inlet Temperature	298.2	*K*	Tooth Pitch	12.91	*mm*
Shaft Speed	1800	*rpm*	Tooth Height	5.03	*mm*
Inlet swirl velocity	16.8	*m/s*	Tooth Tip Width	0.2	*mm*

By supplementing the above mentioned data into the straight type EES model, the results, as shown in Table 4-2, were obtained. It is now possible to determine the leakage flow rate through the seal and the pressure distribution between the different cavities.

Table 4-2: *EES Model results for Eser (1995) straight type geometry*

Model Results For Straight Type Eser (1995) Operating Conditions						
P_{in}	P_{out}	P_{in}/P_{out}	Leakage kg/s	P_1	P_2	P_3
241	206.8	0.86	0.02032	241	224.555	206.8

4.4 Straight Type Parametric Studies

As the results displayed in Table 4-2 is only applicable to a single pressure ratio, it is difficult to fully understand the functioning of the seal. For that reason a decision was made to keep inlet pressure to the seal constant while altering the pressure ratio by changing the outlet pressure. By using this method it is possible to illustrate the seal working over the full range of applicable pressure ratios. This was achieved by making use of a parametric study in EES, which allows the user to specify a variable for a number of iterations between two set values.

4.4.1 Two Constriction Parametric Study

By keeping the seal geometry as specified in Table 4-1 and keeping seal inlet pressure constant at 300 kPa, it is possible to vary the pressure ratio by varying the outlet pressure from 300 kPa to 60 kPa. The results of this parametric study for the two constriction straight labyrinth are shown in Appendix D.1. The leakage flow can now be presented as a function of the pressure ratio over the seal as seen in Figure 4-2.

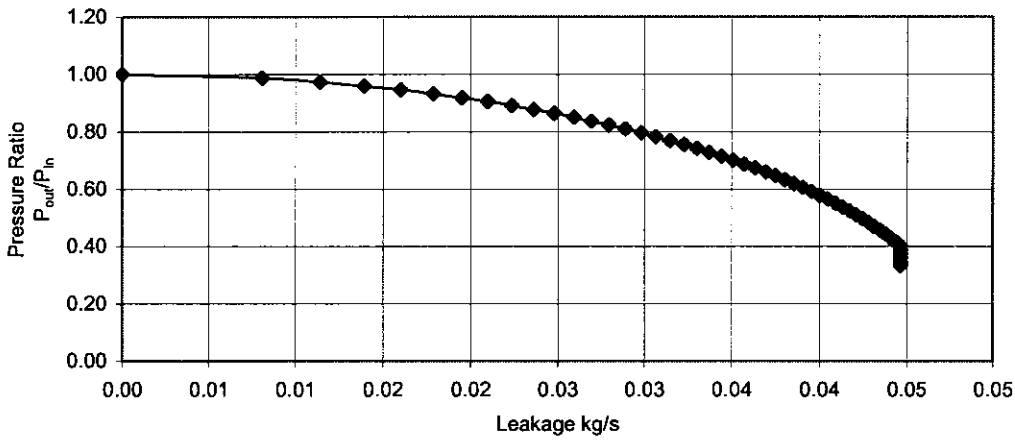

Figure 4-2: *Leakage flow through Eser (1995) 2 teeth straight type labyrinth*

From the graph it can be seen that, when there is no pressure difference over the seal, leakages will amount to zero. As the pressure difference is increased, there will be an increase in leakage mass flow rate. As density decreases through the consecutive cavities it causes the velocity in the last cavities to be the higher. When the leakage through the

seal increases, the velocity through the constrictions will also increase. This will be the case until the velocity through the last constriction reaches sonic velocity and the seal chokes. This effect is clearly visible as the leakage flow rate approaches a limit and reaches a maximum leakage value at a pressure ratio of 0.4.

This effect is one of the great advantages of labyrinth seals; no matter how much the pressure difference over the seal is further increased, the leakage flow rate will not exceed the maximum value. By making use of this labyrinth characteristic, greater control can be achieved over seal leakage values.

4.4.2 Altering Constriction Numbers

Altering the number of constrictions within the labyrinth will surely have an effect upon the leakage through the seal. In the previous Paragraph a parametric study was done for two constrictions. More parametric studies were done for 4, 6, 8 and 10 constrictions. The same tooth geometry and pitch distance was used as in Table 4-1, only more constrictions were added. Pressure ratios were altered by using the same method as before. The leakage flow results were solved using parametric studies and are shown in Appendix D.2. The leakage flow data is represented in Figure 4-3

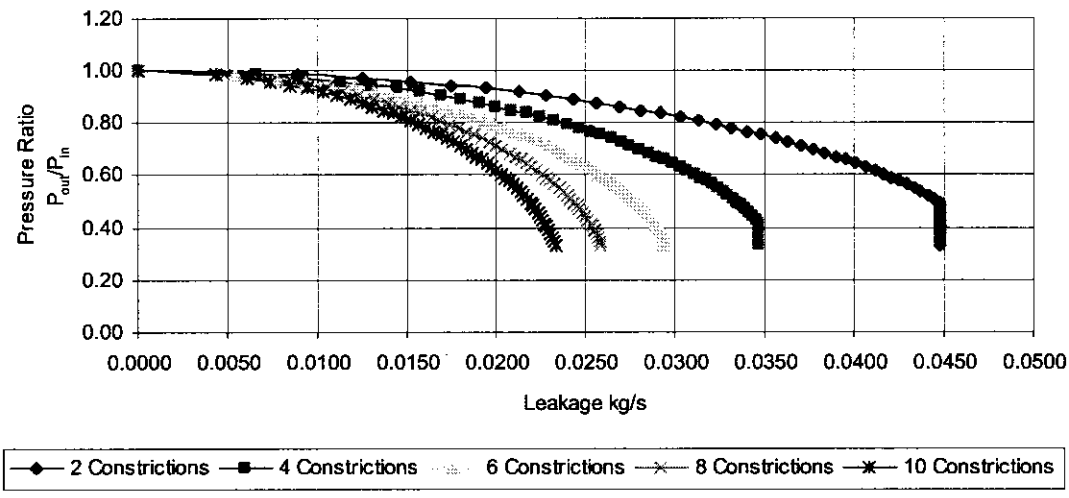

Figure 4-3: *Leakage Flow through different constriction numbers*

From the graph it can be seen that the leakage is significantly reduced throughout the whole range of pressure ratios with the addition of more constrictions. With more

constrictions, choking will take place at a lower mass flow rate. This can be of great use to a designer applying the seal in such a manner that it will operate in its choking region.

4.4.3 Pressure distribution through constrictions

As the change in pressure through the seal is not an instantaneous event, it is necessary to evaluate the pressure distribution through the cavities. Results for a 5 constriction straight labyrinth displayed in Appendix D.3 have been used to visually present the pressure distribution through the seal as a function of the pressure ratio as shown in Figure 4-4.

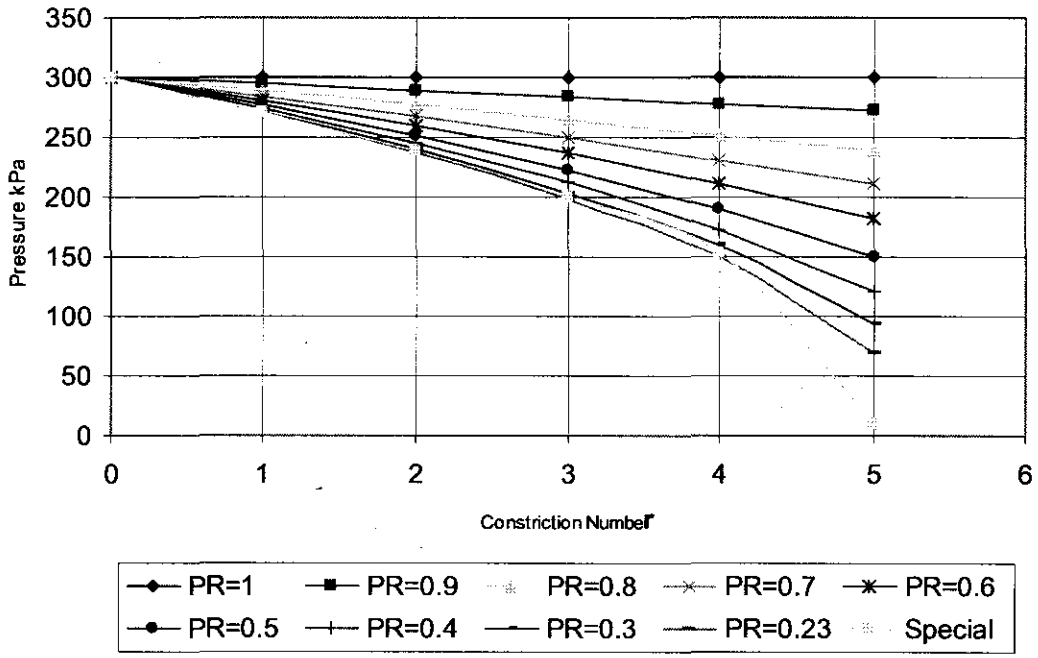

Figure 4-4: *Pressure distribution through constrictions*

It can be seen that, as the pressure ratio is increased, the gradient of pressure loss through the seal increases. With a outlet pressure of 79 kPa the flow through the seal is already choked, meaning the data series for PR=0.23 is for choked conditions. If the outlet pressure is further reduced to 10 kPa, as was done in the special data series, it can be seen that the pressure within the last constriction has stayed constant, but the outlet pressure is at the specified pressure. This is due to the fact that the seal is choked and the further expansion of the fluid has taken place outside the last cavity as was discussed in Paragraph 3.3.2.

4.4.4 Discharge Coefficient

Discharge coefficients for the 5 constriction staggered seal are displayed in Figure 4-5. (Series data given in Appendix D.4)

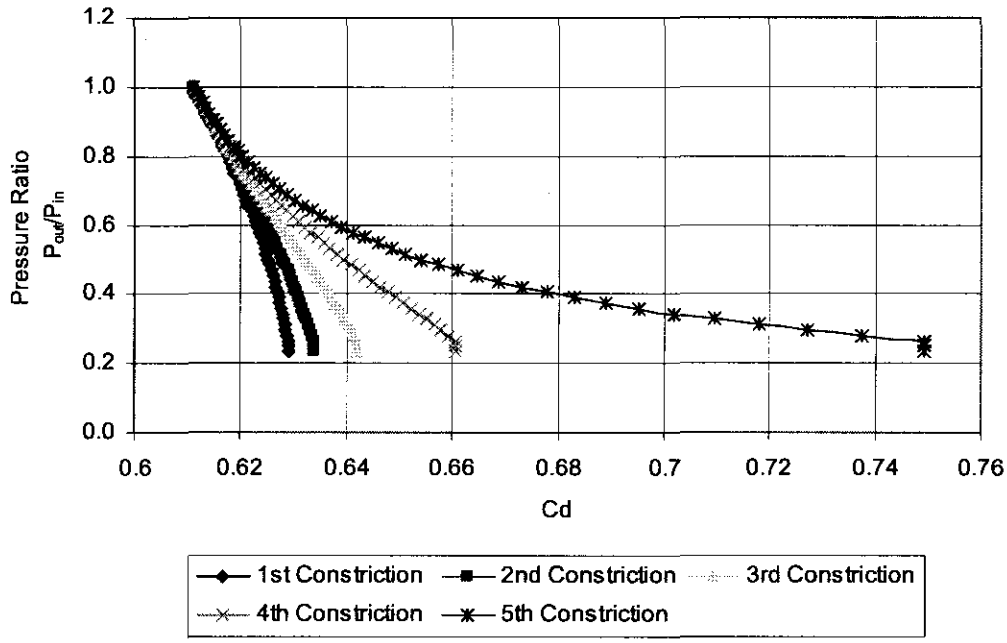

Figure 4-5*: Discharge coefficients for straight type seal*

From the plotted results it can be seen that the discharge coefficient rises as the pressure difference over the seal is increased. Due to the rise in velocity through the consecutive constrictions, the effect of the vena contracta increases and geometrical flow area decreases. A large increase in the coefficient in the last constriction can be seen as the seal approaches choked conditions, this is due to the higher pressure ratio developed over the last constriction. As the pressure difference over the seal is further increased, the fluid reaches sonic velocity in the last constriction and the seal chokes. The discharge coefficient and mass flow becomes constant where the seal is working under sonic conditions.

4.5 Staggered Type EES Model

Leakage through staggered labyrinths is also governed by the Saint Venant Wantzel Equation as derived in Appendix A. According to Egli (1935), if the step is of sufficient height, the kinetic energy carry-over amounts to zero. It can now be stated as in Paragraph 3.7 that leakage through a staggered labyrinth is governed by Equation (4.5).

$$\dot{m}_i = C_d A_g \sqrt{\frac{2\gamma}{\gamma - 1}\frac{p_{i-1}^{\,2}}{RT_0}\left(\left(\frac{p_i}{p_{i-1}}\right)^{\frac{2}{\gamma}} - \left(\frac{p_i}{p_{i-1}}\right)^{\frac{\gamma+1}{\gamma}}\right)} \tag{4.5}$$

With the discharge coefficient remaining the same as in Equation (4.3). Similar as in the solving of the straight type, a system of $(3n+3)$ equations and $(3n+3)$ variables is formed when the boundary values are added. The system of equations could then be iteratively solved. The same methodology is used solving the staggered model for unchoked and choked conditions as was discussed in Paragraph 4.2. The EES model for solving leakages through staggered labyrinths is shown in Appendix C.2.

4.6 Staggered Type Parametric Studies

A number of parametric studies were solved for staggered labyrinths to better illustrate the working of the seals through the range of pressure ratios.

4.6.1 Five constriction staggered seal

The geometry of the staggered seal to be solved is as shown in Figure 4-6 with geometrical values and operating conditions as defined in **Table 4-3**. Pressure ratio was altered by varying seal outlet pressure between 300 kPa and 70 kPa.

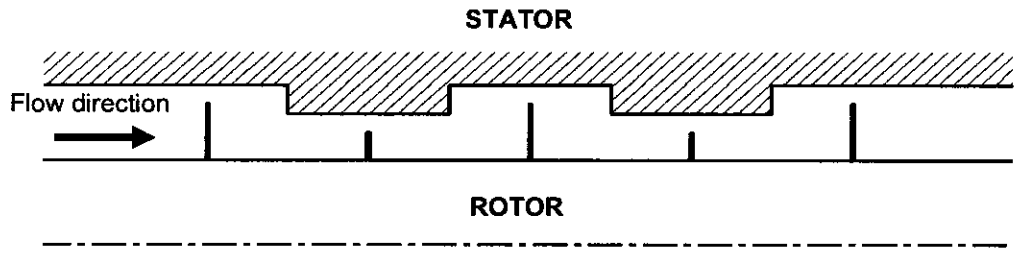

Figure 4-6: *Five Constriction Staggered Type Labyrinth*

Table 4-3: ***Five Constriction Staggered Type labyrinth***

Geometrical Values and Operating Conditions					
Fluid	Air		No of Teeth	5	
Inlet Temperature	298.2	*K*	Shaft Radius	101.6	*mm*
Tooth Height	5.03 / 2.5	*mm*	Clearance	0.16	*mm*
Tooth Tip Width	0.2	*mm*	Tooth Pitch	12.91	*mm*

Model results are displayed in Appendix E.1. Parametric results for seal leakage as a function of the pressure ratio can be graphically presented as shown in **Figure 4-7.**

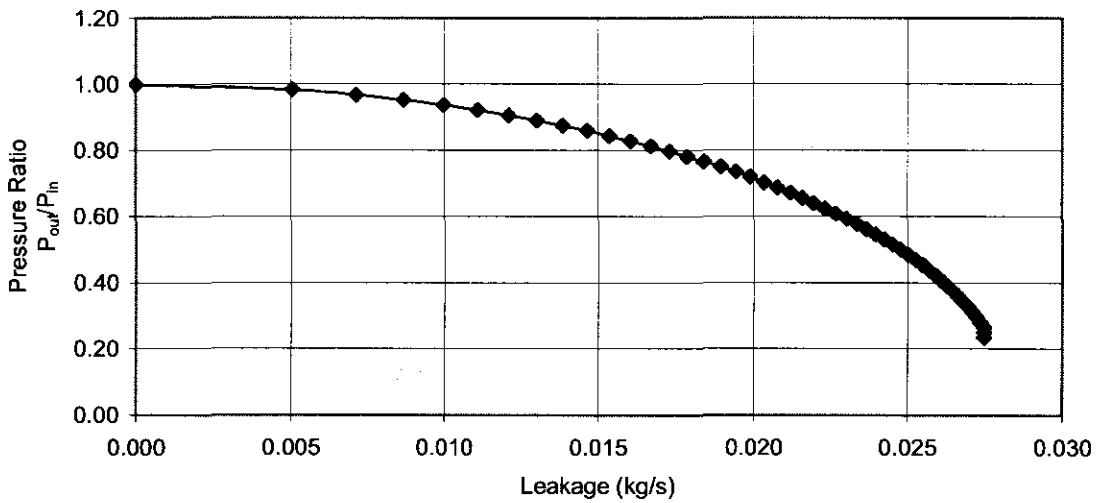

Figure 4-7*: Leakage through five constriction staggered labyrinth*

Similar to the flow through the straight type, no leakage occurs without any pressure difference. Leakage is increased as pressure difference increases up to a maximum leakage value where the flow through the seal is choked. Therefore it can be said that the staggered labyrinth has similar advantages to that of the straight type.

4.6.2 Pressure distribution through constrictions

By plotting cavity pressures for each cavity through the range of pressure ratios of the five constriction staggered geometry results in the graph as shown in Figure 4-8. It can be seen that the pressure distribution in the cavities of the staggered geometry is similar to that of the straight labyrinth. If the outlet pressure of the seal is further lowered after the

seal is choked the pressure in the last cavity will stay constant and any further pressure loss will occur outside the seal.

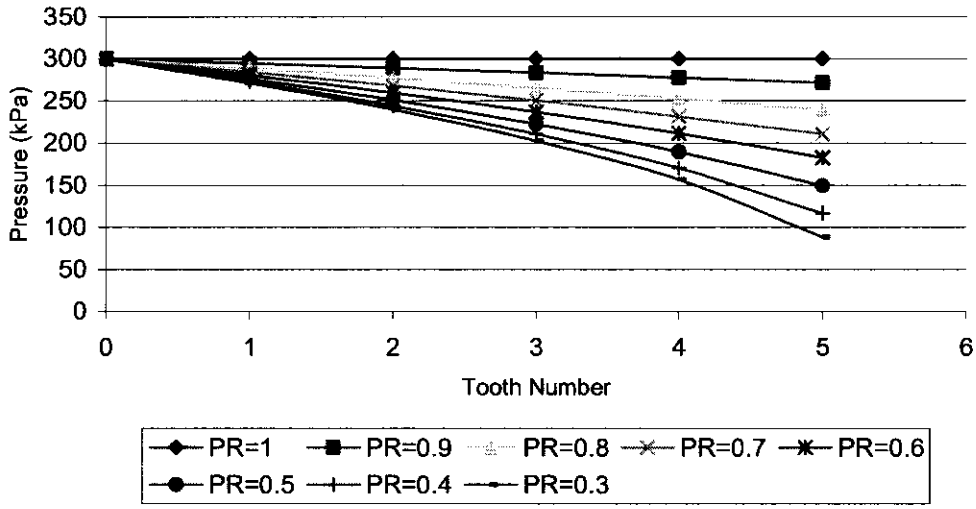

Figure 4-8: *Pressure distribution between cavities of five tooth staggered seal*

4.7 Straight and Staggered Labyrinth Comparison

Clear similarities can be seen between the leakage flow curves of the straight and staggered labyrinths. Difference in the effectiveness of the seals is best illustrated by comparing the leakage flow curves. The geometry of the staggered labyrinth seal used for the comparison is similar to that defined in **Table 4-3**. The straight labyrinth constriction geometry was chosen the same as in Table 4-1 with five constrictions. This will allow for a comprehensive comparison between the different seal geometries. Data for straight labyrinth seals can be found in Appendix D.3 and staggered seal data in Appendix E.1

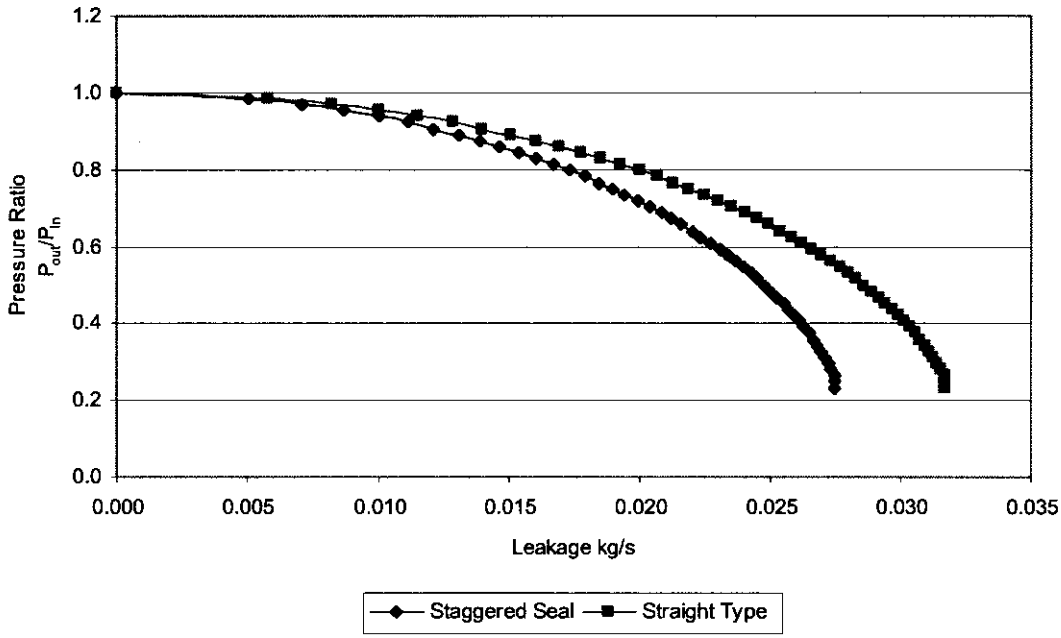

Figure 4-9: *Straight staggered seal comparison*

Figure 4-9 shows the leakage flow curve for the staggered and straight type geometries. The similarities in the functioning of the seals are clearly visible. Due to the more complex flow path, an improvement in the sealing efficiency of the staggered type can be observed. Choking occurs at a reduced leakage flowrate within the staggered seal. This means that a staggered seal with same manufacturing and working tolerances as a comparable straight type seal will have a greater sealing ability.

4.8 Conclusion

Proposed models resulting from Chapter 3 has been discussed and implemented into EES to provide a useful engineering tool for solving various straight and staggered labyrinth configurations. The resulting models for leakages through labyrinths have been used to approximate leakages.

Straight labyrinths have been solved for different constriction numbers using the model. The result was portrayed and discussed to better understand the working of the seal. Some staggered labyrinth results were also generated and discussed. A comparison was

made between the functioning of straight and staggered type labyrinths. It was found that the leakage through the staggered geometry was 26% lower than through an equivalent straight type. It will now be necessary to evaluate the results from the EES models. Chapter 5 will compare EES results with that found in literature and results generated with the use of CFD software.

CHAPTER 5

VALIDATION AND VERIFICATION

Leakage flow results generated with EES models discussed in Chapter 4 are compared to data available from the literature. Models are compared against CFD analyses done by PBMR to determine the effect of tip clearance size on the leakage flow through the seal. Alternatively models equivalent to that solved in Paragraph 4.4 and 4.6 will be solved with the use of CFD software. These results will be compared to the results obtained for the five constriction straight and staggered labyrinths discussed in Chapter 4.

5.1 Introduction

In previous chapters of this study the theory governing leakage flow through labyrinth seals and the implementation of possible models into EES have been discussed. This chapter will compare the results from the EES models to that found in the literature and against CFD results. Due to a lack of experimental facilities and a limited budget an experimental validation could not be done.

5.2 Validation and Verification

Before verification and validation is attempted, it is necessary that the definition and implementation of these terms be clarified.

5.2.1 Verification

Verification can be described as the process of ensuring that the controlling physical equations have been correctly translated into computer code, or as in the case of manual calculations, correctly incorporated into the calculation procedures. This is done by physically checking each equation that is implemented into each program manually. This was done thoroughly for each equation of each program.

5.2.2 Validation

Validation can be defined as the evidence demonstrating that the code or calculation method is fit for its purpose. This will be done by comparing results generated with the engineering tool to those found in the literature and generated by the use of CFD software. Unfortunately, very few benchmarks have been published, and those that are available do not include seal geometry or operating conditions. One complete labyrinth benchmark for straight labyrinths was published by Eser (1995), this will firstly be compared to generated results in Paragraph 5.3.

Further validation was done by comparing results from the engineering tool to that generated with CFD software. The straight labyrinth model is compared to two sets of CFD results, the first comparison model is that with the ECLS employed within the PBMR and secondly the engineering tool was validated by comparing it to a simple geometry CFD model. These two benchmarks are discussed in Paragraphs 5.4 and 5.5.

No available results were found in literature to benchmark staggered models, so it was necessary to do so with CFD techniques. In Paragraph 5.6 the staggered model results are evaluated against the results obtained with a staggered CFD simulation.

5.3 Straight Labyrinth Type Compared to Eser (1995)

Eser (1995) published a benchmark for a two constriction straight type labyrinth seal. He discusses two sets of results in his publication, the first was obtained by theoretical calculations and the other was measured with the use of an experimental setup. These results are shown in Table 5-1. The geometry of the two constriction labyrinth used for the benchmark is similar to that described in Table 4-1.

Table 5-1: *Eser Straight Labyrinth Results*

Results				
	Eser Theoretical		Eser Experimental	
Leakage	0.02072	*kg/m^2 s*	0.02	*kg/m^2 s*
P_0	241	*kPa*	241	*kPa*
P_1	224.592	*kPa*	222.5	*kPa*
P_2	207	*kPa*	207	*kPa*

Results generated by using the engineering tool for the same geometry and pressure ratio can now be compared to that published by Eser.

Table 5-2: *Two Constriction Labyrinth EES results*

Engineering Tool Results For Straight Type Eser (1995) Operating Conditions						
P_{in}	P_{out}	P_{in}/P_{out}	Leakage kg/s	P_1	P_2	P_3
241	206.8	0.86	0.02032	241	224.555	206.8

By comparing these three sets of results in Table 5-3 it can be seen that there is a maximum of 1.9% difference between the theoretical leakage flow values of Eser and the proposed model. The engineering tool shows only a 1.6% variation when predicting the experimental leakage flow through the seal.

Table 5-3: *Two Constriction Labyrinth Comparison*

	Benchmark Leakage [kg/s]	Engineering Tool Leakage [kg/s]	% Variation
Eser	0.02072	0.02032	1.9
Experimental	0.02	0.02032	-1.6

It can be stated that the EES code compares favorably when benchmarked to the results published by Eser (1995). This can be seen as an indication that the model is fairly correct. Unfortunately the results where only obtained for a single pressure ratio over the seal. It will therefore be necessary to further validate the engineering tool to ensure that it remains consistent over a range of different seal values.

5.4 ECLS Comparison

A CFD simulation of the twenty constriction electro-magnetically controlled labyrinth seal (ECLS) in the PBMR has been solved by Venter (2000). The ECLS can be described as a twenty constriction straight type labyrinth with varying tip clearance. The objective of the analysis was to better understand the effect of tooth tip clearance on the leakage flow through the seal. Therefore the CFD analysis was done for five different tip clearance distances, calculating the leakage flow at each. These leakage flow results can now be used as a source of validation and to highlight the flexibility of the engineering tool.

5.4.1 ECLS Geometry

It will be possible to control the leakage flow through the ECLS by altering the radial distance between the seal and the rotor. For this all the geometrical values will stay constant except for the tooth tip clearance. The seal geometry and operating conditions for the ECLS are given in Table 5-4.

Table 5-4: *ECLS Geometry and operating conditions*

Geometry			
Number of teeth	20	Height of Seal Strip	5 mm
Inner Radius	575 mm	Tooth-tip width	0.5 mm
Pitch of Seal Strip	4.5 mm		
Operating Conditions			
Inlet Temperature	373 K	Fluid	Helium
Inlet Pressure	4200 kPa	Specific Heat	5192.6 J/kg K
Outlet Pressure	2600 K	Viscosity	2.333×10^{-5} kg/m s
Shaft Rotational Speed	3000 rpm	Turbulence Model	k-ε high Re number
Wall temperature	Adiabatic		

5.4.2 CFD Model

Star-CD (version 3.1), a world renowned CFD software package with a high degree of credibility, was used to solve the models. The CFD model consisted of a 5° wedge with cyclic boundary conditions. This enables the solving of a small section of the seal in comparison to solving the whole 360° seal model, thus significantly saving computational effort. No-slip wall conditions were applied on the surfaces. A velocity equal to the rotational speed of the shaft was applied to the wall boundaries of the straight boundary layer in the simulation. A cross section of the numerical mesh is shown in Figure 5-1 with the complete mesh resulting in 20 000 cells. Pressure contours and velocity vector results of the model are shown in Appendix F.

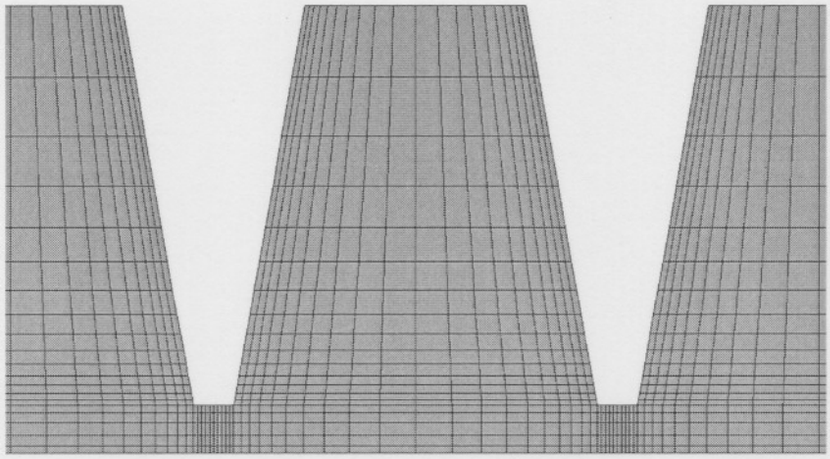

Figure 5-1*: ECLS Mesh*

5.4.3 ECLS Results

Figure 5-2 shows the total pressure plot for the flow through the ECLS, the decrease in pressure as the fluid expands through the seal can be seen. By looking at the steady pressure gradient over the last constriction it can be seen that the seal is not operating under choked conditions.

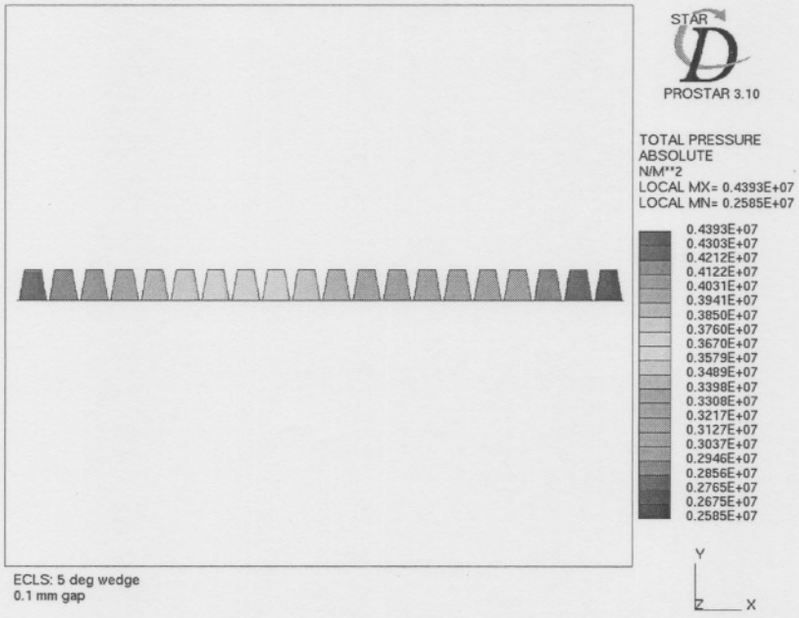

Figure 5-2*: Pressure distribution through ECLS*

The leakage flow simulations were solved for five different tip clearances. By using the engineering tool for straight labyrinths it will be possible to generate equivalent results to that obtained by Venter (2000) with CFD simulations. The leakage results for both the mathematical and the CFD models are shown in Table 5-5.

Table 5-5: *ECLS Results for Various Clearance Sizes*

Clearance Size (mm)	CFD Leakage flow (kg/s)	Engineering Tool Leakage Flow (kg/s)	% Difference
0.1	0.28	0.2490	11.07
0.4	1.77	1.6420	7.23
0.6	3.168	2.9600	6.57
0.8	4.932	4.4680	9.41
1	6.88	6.0920	11.45

The results shown in Table 5-5 can be graphically compared as in Figure 5-3. From the graph it can clearly be seen that the leakage through the seal increases as the tip clearance increases.

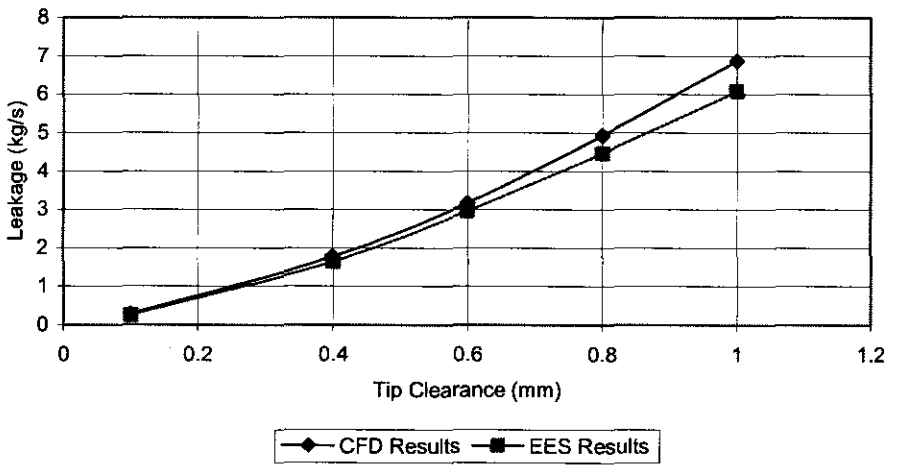

Figure 5-3: *Leakage results for various tip clearance sizes*

This effect can best be explained by studying the velocity vector charts generated with the CFD simulation. Figure 5-4 shows the velocity vectors of the fluid flowing through the seal with a gap size of 0.1mm. By looking at the vectors in the cavity between the two

constrictions, the whirling and expansion of the gas can be seen. Two other effects can be observed when looking at the velocity vectors, an area of low or zero velocity exists in the middle of the cavity section and a line of very high velocity is clearly visible on the boundary layer. These two effects support the statement made in Paragraph 2.4 on the throttling motion of the gas as it flows through the labyrinth.

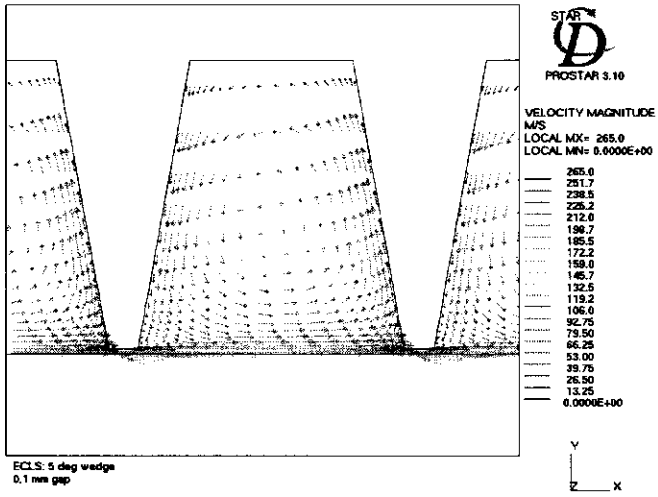

Figure 5-4: *Velocity vectors for 0.1mm gap size*

When the clearance size is increased to 1.0 mm as shown in Figure 5-5 the drastic increase in the line-of-sight can be seen. This phenomenon severely influences the sealing efficiency of the labyrinth.

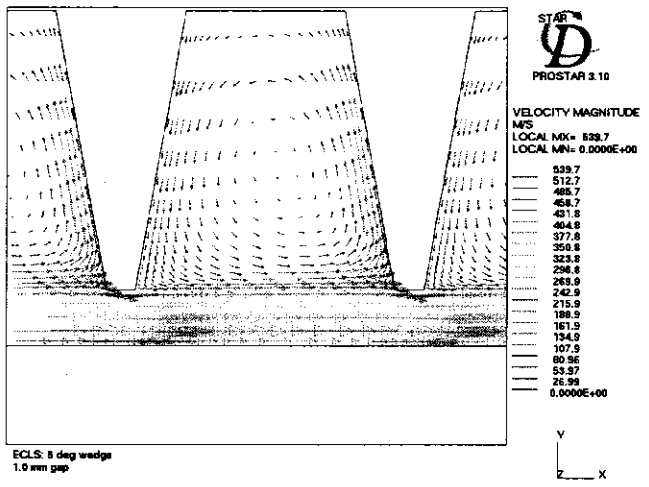

Figure 5-5: *Velocity vectors for 1.0 mm gap size*

A maximum variation of 11.45% between CFD and engineering tool leakage flow values where observed. This can be attributed to a number of factors. The geometry of the seal as seen in Figure 5-1 differs from the ideal labyrinth geometry as shown in Figure 4-1. The cavity volume in the actual ECLS labyrinth is smaller than that accounted for by the ideal labyrinth calculations. Apart from that the CFD analysis also accounted for shaft rotation, this effect is very small as discussed in Paragraph 2.6, but it does, however, influence the leakage results.

5.5 Straight Labyrinth Validation

Up to this point the straight labyrinth model has been compared to Eser's single pressure ratio benchmark and to the CFD simulations done for the ECLS of the PBMR. The main validation will be to compare the performance of the engineering tool in calculating the leakage flow over a range of pressure ratios.

For this aspect of the validation the leakage flow through a five constriction straight type labyrinth similar to the one discussed in Paragraph 4.7 will be solved with the help of CFD simulations. The seal geometry and operating conditions is as specified in Table 5-6 with the outlet pressure varying from 300 kPa to 50 kPa.

Table 5-6: *Five constriction straight type geometry and operating conditions*

Geometrical Values and Operating Conditions					
Fluid	Air		No of Teeth	5	
Inlet Temperature	298.2	*K*	Shaft Radius	101.6	*mm*
Tooth Height	5.03 / 2.5	*mm*	Clearance	0.16	*mm*
Tooth Tip Width	0.2	*mm*	Tooth Pitch	12.91	*mm*
Inlet Pressure	300	*kPa*			

This seal geometry was chosen as the cavity volume will be closer to that of an ideal labyrinth. CFD results for the pressure contour plots and velocity vector charts are displayed in Appendix G.1.

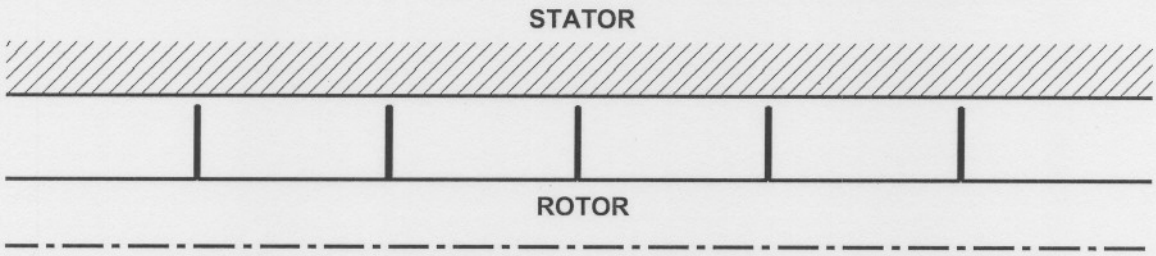

Figure 5-6: *Five Constriction Straight Labyrinth*

5.5.1 Straight Labyrinth Results

By observing the pressure distribution plots through the seal for pressure ratios 0.667 (Figure 5-7) and 0.167 (Figure 5-8), the difference between choked and unchoked conditions can be illustrated. Figure 5-7 shows the pressure plots for unchoked conditions. This can be seen by observing the steady pressure gradient over the last constriction.

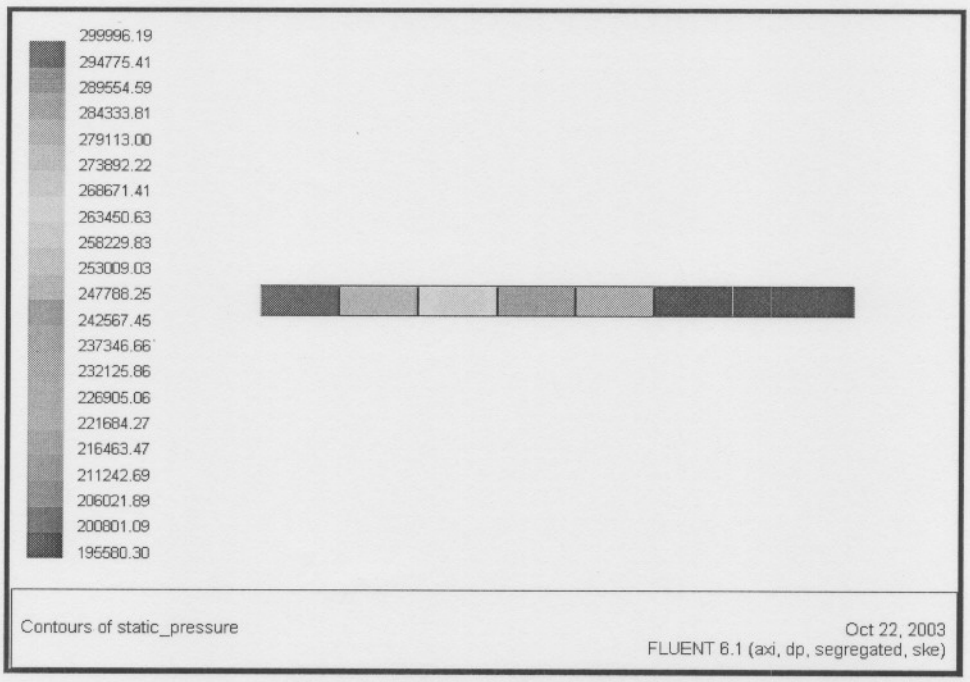

Figure 5-7: *Pressure distribution for straight type labyrinth – Not choked Pr=0.667*

When observing the pressure distribution for the labyrinth operating under choked conditions as shown in Figure 5-8 the higher pressure gradient over the last constriction can be seen. This happens due to the fact that when the seal is choked, the maximum pressure loss through the seal has been established, causing any additional pressure loss to occur outside the seal.

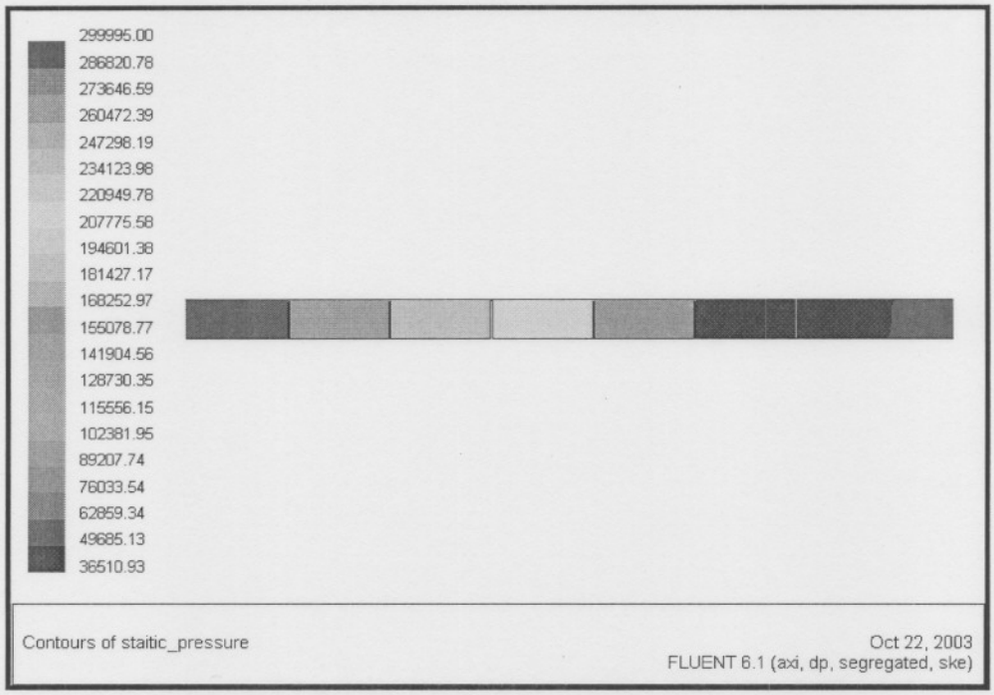

Figure 5-8: *Pressure distribution for straight labyrinth - Choked*

The leakage flow results for the engineering tool and CFD simulations are displayed in Table 5-7 and graphically presented in Figure 5-9. The results show a good correlation between the leakage values. With the seal operating under choked conditions, a 4% variation exists between calculated results and that obtained with CFD simulations.

This variation can be attributed to the fact that the geometry was not ideal. In the derivation of the discharge coefficient in Paragraph 3.5.2, the assumption was made that tooth tip length to clearance ratio will approach zero $\left(\frac{L}{cl} \to 0\right)$. As this is not the case in an actual labyrinth, it does affect leakage flow calculations.

Table 5-7: *CFD and EES Comparison for Straight Type Labyrinth*

Total pressure			CFD Leakage Flow	Engineering Tool Leakage Flow	% Error
Inlet [Pa]	Outlet [Pa]	p_r	[kg/s]	[kg/s]	
300000	199661.213	0.6655	0.027	0.02544	5.77
300000	189621.170	0.6321	0.028	0.02639	5.75
300000	179574.980	0.5986	0.029	0.02726	6.00
300000	169525.780	0.5651	0.030	0.02804	6.53
300000	158847.890	0.5295	0.030	0.02879	4.03
300000	149409.873	0.4980	0.031	0.02939	5.19
300000	139354.200	0.4645	0.032	0.02995	6.41
300000	129286.320	0.4310	0.032	0.03045	4.84
300000	119211.260	0.3974	0.032	0.03088	3.50
300000	99024.153	0.3301	0.033	0.03167	4.03
300000	88922.928	0.2964	0.033	0.03166	4.06
300000	78821.241	0.2627	0.033	0.03171	3.90
300000	68722.427	0.2291	0.033	0.03171	3.90
300000	58637.883	0.1955	0.033	0.03171	3.90
300000	48577.669	0.1619	0.033	0.03171	3.90

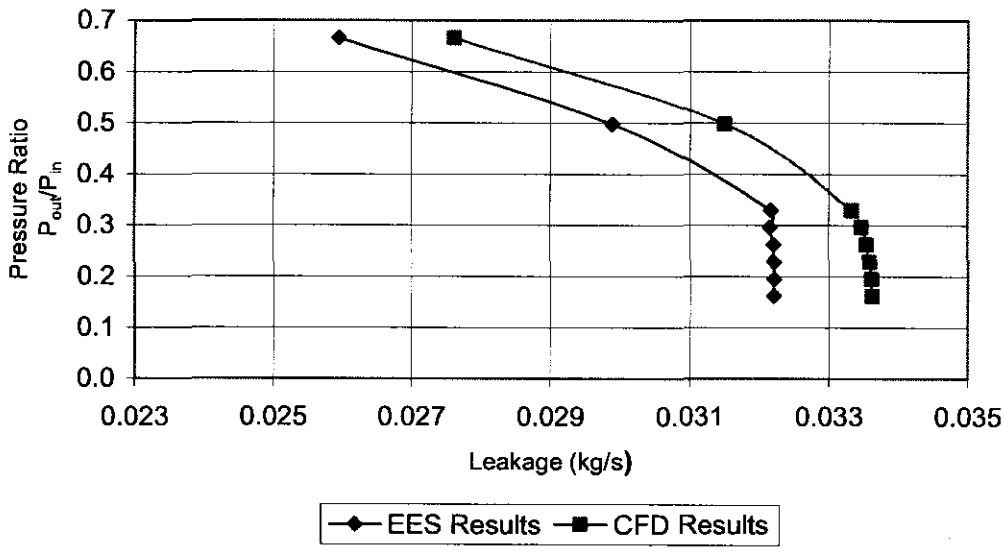

Figure 5-9: *CFD and EES Comparison for Straight Type Labyrinth*

5.6 Staggered Labyrinth Validation

The straight labyrinth model has been validated with three result sets. Unfortunately, no data was found in the literature that can be used to benchmark the staggered leakage flow models. For this reason a CFD simulation was used to generate leakage flow results over a range of pressure ratios. Although the validation of the staggered labyrinths is more limited than that of the straight labyrinth, the CFD comparison will be an adequate indication of the model performance.

The staggered type labyrinth as discussed in Paragraph 4.6.1 was solved with the use of the Fluent v6.1.18 software package. Seal geometry and operating conditions is similar to the five constriction staggered arrangement discussed in Table 4-3. The inlet pressure remained constant at 300 kPa while altering the outlet pressure between 300 kPa and 50 kPa. Leakage flow results as well as pressure and vector plots obtained with the Fluent software are displayed in Appendix G.2.

5.6.1 Staggered Labyrinth Results

By looking at Figure 5-10 the velocity vector chart of flow through a staggered labyrinth can be seen. When observing the high velocity jet that originates through the clearance gap, it can be seen that it differs from that seen in the straight type labyrinth. The step in the boundary layer prevents the formation of a line-of-site and in doing so greatly enhance the efficiency of the seal. This supports the statement by Egli (1935) that in the calculation of staggered leakage flow values the kinetic energy carry-over can be neglected. Leakage flow results obtained with Fluent software are compared to that of the engineering tool in Table 5-8.

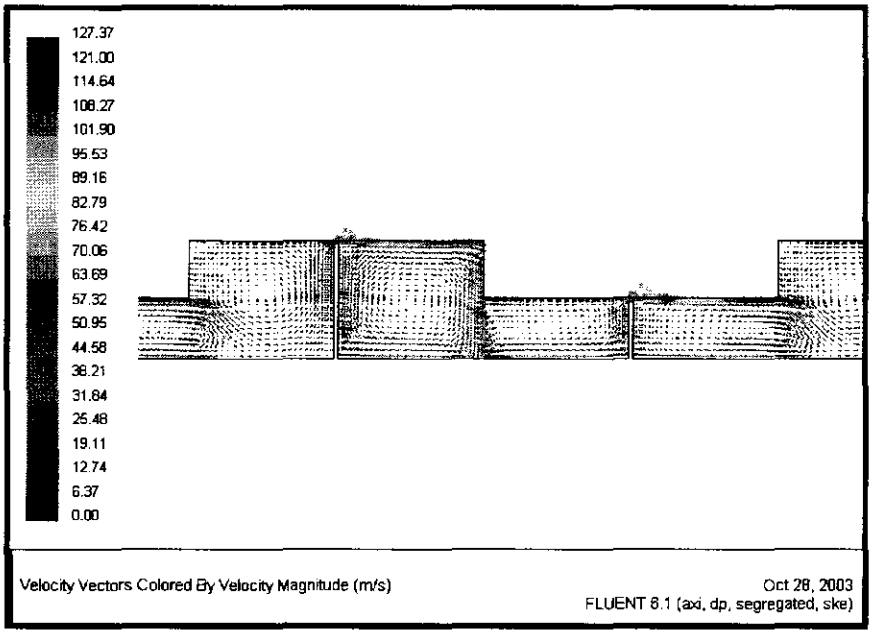

Figure 5-10: *Velocity vector chart for staggered labyrinth*

Table 5-8: *CFD and EES comparison for staggered labyrinth seals.*

Total pressure			CFD Leakage Flow	Engineering Tool Leakage Flow	% Error
Inlet [Pa]	Outlet [Pa]	p_r	[kg/s]	[kg/s]	
300000	199673.33	0.666	0.025	0.02203	11.63
300000	189628.89	0.632	0.026	0.02286	11.47
300000	179581.72	0.599	0.027	0.02361	11.33
300000	169531.47	0.565	0.027	0.02429	11.19
300000	159477.58	0.532	0.028	0.0249	11.07
300000	149419.48	0.498	0.029	0.02545	10.94
300000	139356.47	0.465	0.029	0.02595	10.79
300000	129287.48	0.431	0.030	0.02638	10.68
300000	119211.41	0.397	0.030	0.02675	10.57
300000	99032.47	0.330	0.030	0.02728	10.45
300000	88927.25	0.296	0.031	0.02743	10.44
300000	78829.57	0.263	0.031	0.02747	10.57
300000	68763.06	0.229	0.031	0.02747	10.70
300000	58757.49	0.196	0.031	0.02747	10.76
300000	48820.53	0.163	0.031	0.02747	10.80

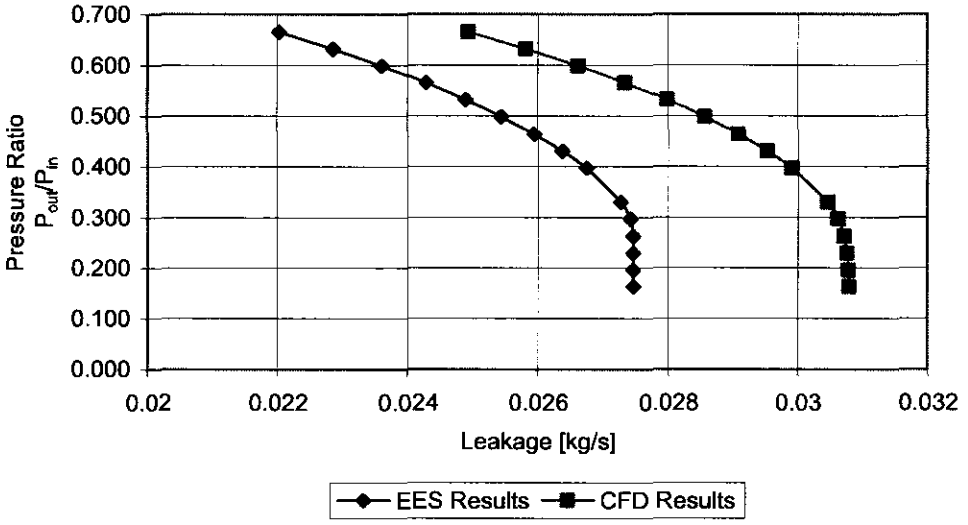

Figure 5-11: *CFD and EES comparison for staggered type labyrinth*

Figure 5-11 graphically shows the comparison between the two models. A good correlation between the result sets can be seen as a 10.7% difference exists between the two sets when the seal is working under choked conditions. The difference in leakage prediction is larger than that found when modeling the straight type labyrinths. This can be attributed to a number of factors. The influence of the tooth tip width on the discharge coefficient will account for some loss in accuracy in the same way as discussed with straight labyrinths.

Another possible problem could arise from the kinetic energy carry-over coefficient. The assumption of Egli (1935) was used that, in the case of staggered labyrinth seals, the steps in the boundary layer would prevent the transfer of any kinetic energy between the different stages. When the velocity vector chart in Figure 5-10 is observed, it can be seen that most of the velocity line is destroyed by the boundary layer and it does seem like Egli is correct, but there is a possibility that some of the high velocity is transferred to the following cavity sections. The effect of these two phenomena could be large enough to influence the leakage flow through the seal.

5.7 Conclusion

This chapter compares the results of the engineering tool with that obtained by CFD analyses. Some assumptions and terms mentioned in previous chapters has been visualized and discussed with the help of the CFD results. From the results given it can be seen that the two models compare relatively well. The leakage flow results are fairly close to each other, therefore suggesting that the models are correct. The differences that do exist between the correlations can mostly be attributed to the discharge coefficient. This coefficient is based on the assumption that the tooth tip length to clearance ratio will approach zero. Although this value is normally very small in most labyrinths, it does contribute to some loss in accuracy. This effect can be clarified by verifying the answers with experimental results. Although Star-CD and Fluent are trusted and reliable software packages, the possibility of discrepancies in either the software or the engineering tool, will make experimental data the only way to verify results.

CHAPTER 6

CONCLUSIONS AND FUTURE WORK

In Chapter 6 conclusions on the applicability of the derived engineering tool are made and some of the shortcomings are identified. Finally recommendations are made for future work and the improvement of the models.

6.1 Introduction

In this chapter a summary will be provided of the most important results that were discussed in the previous chapters. From these results, certain conclusions will be made, leading to recommendations for further research.

6.2 Summary

In Chapter 1 some background information was given on why the study was regarded as important. The objectives of the study were given, emphasizing the importance of thorough understanding of the leakage flow through labyrinth seals. In Chapter 2 a detailed literature survey was conducted discussing the implementation and functioning of labyrinth seals. A convention was set to identify the different labyrinth geometries and some of the common defects occurring in labyrinths have been considered.

The mathematical theory governing the leakage through the seals has been discussed in Chapter 3. Assumptions necessary to solve the leakage values have been stated and some phenomena occurring in the labyrinth seals have been accounted for with the discharge and kinetic energy carry-over coefficients.

In Chapter 4 the implementation and solving of the model for choked and unchoked conditions have been discussed. Parametric studies have been done on selected geometries to explain the functioning of the seal over a range of pressure ratios.

The engineering tool was validated and verified in Chapter 5. This was done by comparing engineering tool results to either that found in the literature or to results generated with CFD simulations.

6.3 Conclusions

In this study the potential to develop an engineering tool for estimating the leakage rates through labyrinth seals was investigated. With the seal geometry, inlet and outlet pressure and the gas temperature given, the models presented can calculate the gas flow rate through the seal and pressure distribution within the cavities.

With the model it is possible to study the effect of various seal parameters. From the parametric studies that were preformed some of the effects of the seal geometry can be illustrated. It was found that by increasing the number of constrictions or increasing the complexity of the flow path the leakage flow could be reduced. The simplest method of controlling the seal leakage was illustrated to be by limiting the leakage flow area.

If the pressure difference over the seals were large enough, the seal would operate under choked conditions. This means the fluid has reached sonic velocity in the last constriction and that the maximum amount of leakage flow is passing through the seal. Even if the pressure difference over the seal is increased, leakage flow will remain constant. This effect can be very useful to a designer trying to gain maximum seal performance.

Computational fluid dynamics was used to visualize the flow through the seals and act as a source of validation for the model. Some degree of error was found on comparing the EES results to CFD or literature data. Results obtained with the CFD software were within 10% of that estimated by the EES models. These errors can be attributed to certain factors at work in the relevant models. The discharge and kinetic energy carry-over coefficients seem to be the greatest source of error in the labyrinth models. With the "engineering tool" programmed in EES, the model seems to be flexible and with acceptable accuracy to be combined into a larger flow network software package.

6.4 Shortcomings and Recommendations for Future Work

Very little experimental data is available from the literature, and with the given data not including the seal geometries and operating conditions, full validation with other sources was not possible. It is thus suggested that further studies include the building of an experimental setup to improve the engineering tool where necessary.

In the models discussed by Eser (1995), White (1999) and other authors the tooth height is never taken into account as it is always assumed that enough volume exists to allow for full expansion of the gas within each chamber. Taking the constriction height into account could greatly improve optimizing capability of the model. The discharge coefficient uses the assumption that tip clearance to width ratio approaches zero. As this is not the case in actual labyrinths, it needs to be taken into consideration for deriving a more accurate coefficient model.

When observing the velocity vector charts for both the straight and staggered labyrinths in Appendix G, a clear line of higher velocity is visible in the straight seal. In the straight labyrinth this was accounted for by using the kinetic energy carry-over coefficient, but in the staggered geometry it was discarded as recommended by Egli (1935). From the higher error margin between the staggered model and CFD result values, it might be necessary to refine the kinetic carry-over coefficient to also account for staggered labyrinths.

During the study straight type labyrinths have been thoroughly validated while staggered labyrinths have only been compared to one set of CFD results. By comparing the staggered model results with more result sets it will be possible to prove its accuracy and flexibility as well. Some other factors that can be taken into consideration to provide a more complete model will be:

- Allowing for eccentric shaft rotation
- Calculation of the rotordynamic forces at work in the labyrinth seals.
- Calculation of leakage flows under transient conditions.
- Accounting for heat transfer through the seal.

REFERENCES

Bell K.J. & Bereglin O.P. (1957). **Flow through annular orifices.** *Transactions of the ASME,* Vol 79, pp593-601.

Benvenuti E., Ruggeri G. and Tomasini E.P. (1979). **Analytical and experimental development of labyrinth seals for process centrifugal compressors.** *ASME, NY, pp. 298-285*

Brownell J.B.; Millward J.A.; Parker R.J. (1989). **Nonintrusive investigations into life-size labyrinth seal flow fields.** *Journal of engineering for gas turbines and power, April, Vol. 111, pp.335-342.*

Childs D.W. (1993) **Turbo Machinery Rotordynamics Phenomena, Modeling & Analysis.** *John Wiley and Sons, Inc., pp 290-304.*

Childs D.W. & Scharrer J.K. (1986). **An Iwatsubo-based solution for labyrinth seals: Comparison to experimental results.** *Journal of engineering for gas turbines and power, April, Vol. 108, pp.325-331.*

Chochua G., Shyy W., Moore J., (2002), **Computational modeling for honeycomb-stator gas annular seal,** *International Journal of Heat and Mass Transfer, Vol. 45, pp 1894 -1863.*

Egli A. (1935). **The leakage of steam through labyrinth seals.** *Transactions of the ASME, Vol 57, pp115-122.*

El-Gammal H.A.; Awad T.H. ; Saber E. (1996). **Leakage from labyrinth seals under rotating and stationary conditions.** *Tribology International, Vol. 29, No.4, pp.291-297.*

Erwin F. & Idelchick I.E.(1989); **Flow resistance: A guide for engineers.** *Hemisphere publishing corporation, ISBN 0-89116-435-9.*

Eser D. (2002). **Rotordynamic coefficients in stepped labyrinth seals.** *Computer methods in applied mechanics and engineering, Vol. 191, pp.3127-3135.*

Eser D. & Kazakia J.Y. (1995). ***Air flow in cavities of labyrinth seals.*** *International journal of engineering science, Vol. 33, No. 15, pp. 2309-2326.*

Hanlon P.C, (2001) **Compressor Handbook**, *McGraw-Hill Professional; 1st edition, ISBN 0070260052*

Hendricks R.C. *et al*; (1994). **Relative performance comparison between baseline labyrinth and dual-brush compressor discharge seals in a T-700 engine test.** *39th International gas turbine and aeroengine congress and exposition, Netherlands, June 13-16.*

Kearton W.J. & Keh T.H. (1952). **Leakage of air through labyrinth glands of staggered type.** *Proceedings of the institute of mechanical engineers, Series A, Vol 116, pp. 180-195.*

Mazur Z. *et al* (2002). **Numerical analysis of erosion of the rotor labyrinth seal in a geothermal turbine.** *Geothermics, Vol. 31, pp.563-577.*

Leyzerovich A. (1997), **Large power steam turbine: Vol. 1 Design**, *Pennwell Publishing, ISBN: 0878147179*

Neumann K (1964). **Zur frage der verwendung von durchblickdichtungen im dampfturbinenbau.** *Maschinentechnik, Vol. 13.*

Mazur Z *et al* (2002), **Numerical analysis of erosion of the rotor labyrinth seal in geothermal turbine,** *Geothermics, Vol. 31.*

Perry J.A. (1949). **Critical flow through sharp edged orifices.** *Transactions of the ASME, Vol. 71, pp.757-764.*

Schlichting H. (1955). **Boundary layer theory.** *Pergamon Press, New York, London, Paris.*

Shames I. H. (1992). **Mechanics of fluids.** *McGraw-Hill, Singapore.*
ISBN 0-07-112815-8

Sierra F. *et al*, (2000). **Analysis of design modification to labyrinth seal of last stage blade in a geothermal turbine.** *2000 International joint power generation conference, Miami Beach, Florida, July 23-26.*

Steinetz B.M., Hendricks R.C. (1994), **Engine seal technology requirements to meet NASA's advanced subsonic technology program goals.** *30th Joint Propulsion Conference, Indianapolis, Indiana, June 27-29.*

Venter P.J., van Staden M.P., (2000) **CFD simulation of ECLS.** *Internal PBMR document no. 003447-34.*

Vermes G. (1961). **A fluid mechanics approach to the labyrinth seal leakage problem.** *Journal of engineering for power, April, pp. 161-169.*

White F.M. (1999). **Heat transfer and fluid flow.** *Genium Publishing Corporation, New York, ISBN: 0931690021*

Witting S.L.K., Dorr I. and Kim S. (1983), **Scaling effects on leakage losses in labyrinth seals**, *J. Eng. Power, April, Vol. 105, pp. 305-309*

Yucel Y. & Kazakia J.Y. (2001). **Analytical techniques for axisymmetric flow in gas labyrinth seals.** *Journal of engineering for gas turbines and power, January, Vol. 123, pp.255-257.*

Zabriskie W. & Sternlicht B. (1959). **Labyrinth-seal leakage analysis.** *Journal of basic engineering, September Vol. 81, pp.332-340.*

APPENDIX A

Saint Venant Wantzel Equation

In this section the derivation of the Saint Venant Wantzel Equation for Isentropic flow through a constriction is shown. The equation is used in Chapter 3 and 4 to solve the leakage flow through straight and staggered labyrinth seals.

Introduction

This Appendix shows the derivation of the Saint Venant Wantzel equation for isentropic flow through a constriction. This equation is used in Chapter 3 and 4 as the basis for the calculation of the leakage flow through both the straight and staggered labyrinth seals.

Saint Venant Wantzel Equation

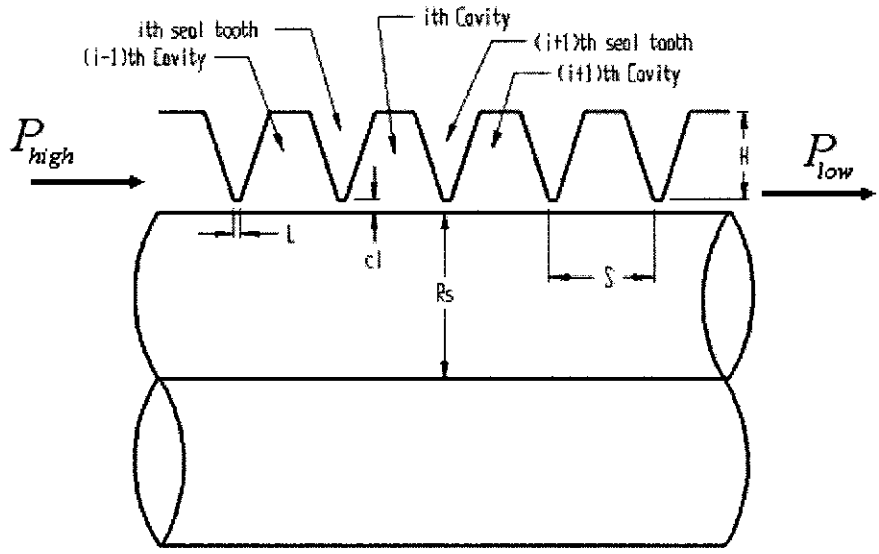

Figure A.1: *Labyrinth geometry*

Figure A.1 shows the geometry of a straight type labyrinth with leakage flow in the direction as indicated. By assuming the flow through the last constriction has not reached sonic velocity it can be said that the seal is not choked. Then the energy equation for the gas flowing from Cavity i-1 to Constrictor i results in:

$$c_p T_{i-1} = c_p T_i + \frac{V_i^2}{2} \tag{A.1}$$

Therefore, the velocity can be calculated according to:

$$V_i = \sqrt{2\left(c_p T_{i-1} - c_p T_i\right)} \tag{A.2}$$

$$V_i = \sqrt{2c_p T_{i-1}\left(1-\frac{T_i}{T_{i-1}}\right)} \tag{A.3}$$

The isentropic property relation $\frac{T_i}{T_{i-1}} = \left(\frac{p_i}{p_{i-1}}\right)^{\frac{\gamma-1}{\gamma}}$ can then be used to replace the temperature ratio found in Equation (A.3). Since the static pressure in Constriction i equals the stagnation pressure in Cavity i (Figure 3-1), the ratio $\frac{p_i}{p_{i-1}}$ designates the upstream pressure of Constriction i divided by the downstream pressure of Constriction i. Substituting this into Equation (A.3) results in

$$V_i = \sqrt{2c_p T_{i-1}\left(1-\left(\frac{P_i}{P_{i-1}}\right)^{\frac{\gamma-1}{\gamma}}\right)} \tag{A.4}$$

By then replacing c_p with $\frac{\gamma}{\gamma-1}R$, Equation (A.3) can be rewritten as:

$$V_i = \sqrt{2\left(\frac{\gamma}{\gamma-1}R\right)T_{i-1}\left(1-\left(\frac{p_i}{p_{i-1}}\right)^{\frac{\gamma-1}{\gamma}}\right)} \tag{A.5}$$

The mass flow rate through Constriction i is calculated from the annular flow area and velocity with:

$$\dot{m} = \rho_i V_i A_g \tag{A.6}$$

Therefore, the mass flow rate through Constriction i is given by:

$$\dot{m}_i = A_g \sqrt{2\left(\frac{\gamma}{\gamma-1}R\right)\rho_i^{\,2} T_{i-1}\left(1-\left(\frac{p_i}{p_{i-1}}\right)^{\frac{\gamma-1}{\gamma}}\right)} \tag{A.7}$$

Using the ideal gas law, this equation can be manipulated as follows:

$$\dot{m}_i = A_g \sqrt{2\frac{\gamma}{\gamma-1}\rho_{i-1}p_{i-1}\left(\frac{\rho_i}{\rho_{i-1}}\right)^2\left(1-\left(\frac{p_i}{p_{i-1}}\right)^{\frac{\gamma-1}{\gamma}}\right)} \tag{A.8}$$

Substituting isentropic relation $\frac{\rho_i}{\rho_{i-1}} = \left(\frac{p_i}{p_{i-1}}\right)^{\frac{1}{\gamma}}$ into Equation (A.8) and again using the ideal gas law, the leakage mass flow can be formulated as follows:

$$\dot{m}_i = A_g \sqrt{\frac{2\gamma}{\gamma-1}\frac{p_{i-1}^{\,2}}{RT_0}\left(\left(\frac{p_i}{p_{i-1}}\right)^{\frac{2}{\gamma}}-\left(\frac{p_i}{p_{i-1}}\right)^{\frac{\gamma+1}{\gamma}}\right)} \tag{A.9}$$

Equation (A.9) is the well-known Saint Venant-Wantzel equation (Kearton (1952)) for isentropic flow through a constriction. Because the temperature remains unchanged through the cavities of the seal, the temperature T_0 is used to designate the inlet temperature to the seal.

Conclusion

This section has shown the derivation for the Saint Venant Wantzel equation. Equation A.9 is used in Chapter 3 when compiling the leakage flow models for both straight and staggered labyrinths and is implemented into the engineering tool in Chapter 4.

APPENDIX B

Vermes Velocity Carry Over

Appendix B shows the derivation of the Vermes carry-over coefficient. This coefficient is used in Chapter 3 to account for the line of sight occurring in straight type labyrinth seals.

Introduction

In this section the derivation of the velocity carry-over coefficient is illustrated. The derivation of the coefficient was done by Vermes (1961) while researching a fluid mechanics approach to the labyrinth seal leakage problem. The residual energy factor α is implemented into the coefficient in Paragraph 3.6.1.

Velocity Carry-Over Coefficient

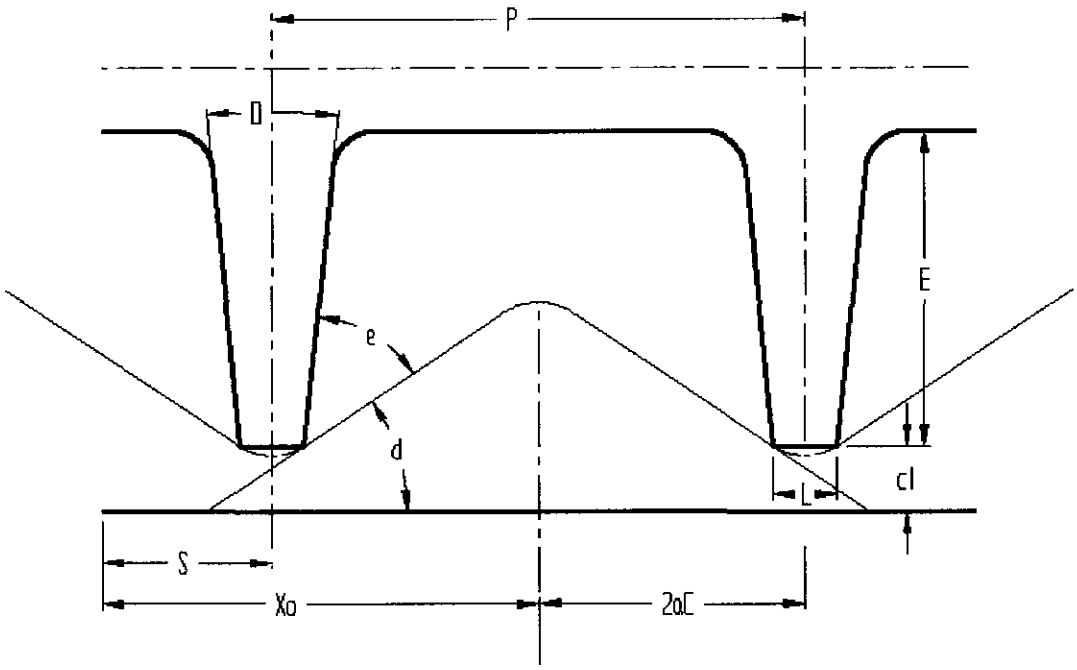

***Figure B.1**: Straight labyrinth seal adapted from Vermes (1961)*

Vermes (1961) approximated the flow in a labyrinth cavity as one half of a flat symmetrical jet originating from an infinitesimally narrow slot. The flow of a jet of this type is described by authors such as Schligting (1955). Vermes defined a parameter α termed the residual kinetic energy factor, defined by Equation (B.1)

$$\alpha = \frac{\bar{V}_{x0}^{\,2}}{V^2} \tag{B.1}$$

Where $\bar{V}_{x0}$ is the average axial velocity in the cavity before acceleration to the next constriction begins. V represents the velocity in the constriction. Vermes then derived a formula for α which is repeated in Equation (B.2):

$$\alpha = \frac{8.52}{\frac{S-L}{cl} + 7.23} \tag{B.2}$$

In order to illustrate how the α parameter is related to the kinetic energy carry-over coefficient, consider the energy equation between the point $x0$ (where the acceleration starts) and the subsequent constriction:

$$\left(c_p T_{i-1} + \frac{\bar{V}_{x0,i-1}^{\ 2}}{2} \right)_{cavity(i-1)} = \left(c_p T_i + \frac{V_i^2}{2} \right)_{restriction(i)} \tag{B.3}$$

Using the definition of α, this equation can be written as:

$$\left(c_p T_{i-1} \right)_{cavity(i-1)} + \alpha \left(\frac{V_{i-1}^{\ 2}}{2} \right)_{restriction(i-1)} = \left(c_p T_i + \frac{V_i^2}{2} \right)_{restriction(i)} \tag{B.4}$$

where V_{i-1} represents the velocity in the $(i\text{-}1)^{st}$ constriction. If it is further assumed that the velocity between two consecutive constrictions is nearly equal, then Equation (B.4) can be rewritten as follows:

$$c_p T_{i-1} = c_p T_i + (1-\alpha)\frac{V_i^2}{2} \tag{B.5}$$

Further manipulation results in:

$$V_i = \frac{1}{\sqrt{1-\alpha}}\sqrt{2c_p T_{i-1}\left(1-\frac{T_i}{T_{i-1}}\right)} \tag{B.6}$$

Therefore, the mass flow rate is given per Equation (B.7):

$$\dot{m}_i = \frac{1}{\sqrt{1-\alpha}} C_d A_g \sqrt{\frac{2\gamma}{\gamma-1}\frac{p_{i-1}^{\ 2}}{RT_0}\left(\left(\frac{p_i}{p_{i-1}}\right)^{\frac{2}{\gamma}} - \left(\frac{p_i}{p_{i-1}}\right)^{\frac{\gamma+1}{\gamma}}\right)} \tag{B.7}$$

Illustrating that the kinetic energy carry-over coefficient is given as:

$$C_{ke} = \frac{1}{\sqrt{1-\alpha}} \tag{B.8}$$

Conclusion

This section showed the origin of the kinetic energy carry-over coefficient. This factor is used in Chapter 3 and 4 in the straight labyrinth model. The coefficient accounts for loss in sealing efficiency due to the line of high velocity that originates when fluid flows through the seal.

APPENDIX C

EES Models

Appendix C shows the EES models for both straight and staggered labyrinth seals as discussed in Chapter 4.

Contents

C.1 Straight Labyrinth Model

Appendix C.1 shows the EES program code used to solve the Straight labyrinth geometry. The code shown was used to solve two constriction Eser (1995) discussed in Chapter 4.

C.2 Staggered Labyrinth Model

Appendix C.2 shows EES program code used in solving the leakage flow results through a staggered labyrinth. Code shown was used to solve geometry as defined in Table 4.3.

C.1 Straight Type Labyrinth Model

"Flow model for an ideal straight-through labyrinth seal. The seal may or may not choke in the last restriction
Chaplygin's formula is used for the contraction coefficient
The kinetic energy carry-over coefficient is determined from the paper by Eser and Kazakia

Assumptions
1) Steady state
2) Isentropic flow
4) No heat transfer across labyrinth boundary

Geometry
The geometry as used in 'Air flow in cavities of labyrinth seals' by Eser (1995)"

```
"=================================================================="

FUNCTION FuncSonic (p_last,p_2_last,PR_choked)
        IF ((p_last/p_2_last)<PR_choked) THEN
                FuncSonic=1
        ELSE
                FuncSonic=0
        ENDIF
END


MODULE SealPressureData (p_u,p_c,Sonic:p_e)
        p_e=Sonic*p_c+(1-Sonic)*p_u
END

"=================================================================="

"Number of teeth"
n=2

"Boundary values"
p[0]=300000  "Pa"          " Inlet Pressure "
p[n]= 206800  "Pa"         "Outlet Pressure"
T_stag=298.2 "K"           "Temperature"

"Constants"
R=287
gamma=1.4

"Seal geometry"
L=0.01291   "m"            "Pitch"
cl=0.00016  "m"            "Clearance"
R_i=0.1016  "m"            "Shaft Radius"

R_o=R_i+cl
A=PI*(R_o^2-R_i^2)         "m^2"

"=================================================================="
```

```
"Leakage Flow Area"
DUPLICATE k=1,n
        A_g[k]=A
END

"Number the sealing points"
DUPLICATE k=0,n
        Number[k]=k
END

"Seal pressure difference"
PR=p[n]/p[0]

"----------CHOKED FLOW----------"
"Define boundary pressures"

p_c[0]=p[0]
p_c[n]=p[n]

PR_choked=1/((1+(gamma-1)/2)^(gamma/(gamma-1)))

"Choked Leakage Flow Equation For Each Constriction"
DUPLICATE k=1,n-1
        m_dot_choked^2=(C_KE*C[k]*A_g[k])^2*(2*gamma)/(gamma-1)*p_c[k-
1]^2/(R*T_stag)*((p_c[k]/p_c[k-1])^(2/gamma)-(p_c[k]/p_c[k-1])^((gamma+1)/gamma))
END

m_dot_choked^2=(C_KE*C[n]*A_g[n])^2*(2*gamma)/(gamma-1)*p_c[n-
1]^2/(R*T_stag)*((PR_choked)^(2/gamma)-(PR_choked)^((gamma+1)/gamma))

"=========================================================================="

"----------UNCHOKED FLOW----------"
"Define boundary pressures"
p_u[0]=p[0]
p_u[n]=p[n]

" Unchoked Leakage Flow Equation For Each Constriction"
DUPLICATE k=1,n
        m_dot_unchoked^2=(C_KE*C[k]*A_g[k])^2*(2*gamma)/(gamma-1)*p_u[k-
1]^2/(R*T_stag)*((p_u[k]/p_u[k-1])^(2/gamma)-(p_u[k]/p_u[k-1])^((gamma+1)/gamma))

END

"=========================================================================="

"Estimate Discharge Coefficients"
"First (n-1) restrictions"

"Discharge Coefficient For Unchoked Conditions"
DUPLICATE k=1,(n)
        S[k]=(p[k-1]/p[k])^(1-1/gamma)-1
        C[k]=PI/(PI+2-5*S[k]+2*S[k]^2)
        "Assume constant discharge coefficient"
        {C[k]=0.65}
END
```

```
"=============================================================================="

"Estimate the kinetic energy carry-over coefficient"
J=1-(1+16.6*cl/L)^(-2)
C_KE=sqrt(n/((1-J)*n+J))

"=============================================================================="

"Test for subsonic/supersonic conditions"
Sonic=FuncSonic (p[n],p[n-1],PR_choked)

"=============================================================================="

"Calculate mass flow rate"
m_dot=Sonic*m_dot_choked+(1-Sonic)*m_dot_unchoked

"=============================================================================="

"Calculate pressure distribution"
DUPLICATE k=1,n-1
        CALL SealPressureData (p_u[k],p_c[k],Sonic:p[k])
END

"=============================================================================="

"Calculate pressure ratios for individual restrictions"
DUPLICATE k=1,n
        PR_Restriction[k]=p[k]/p[k-1]
END

" Seal Leakage in lb_m/kgsec^2"
w=(m_dot/A)*(1/0.4535924)*(1/10.76391) "w=lb_m/kgsec^2"

"=============================================================================="
```

C.2 Staggered Type Labyrinth Model

"Flow model for an ideal Staggered labyrinth seal. The seal may or may not choke in the last restriction
Chaplygin's formula is used for the contraction coefficient
The kinetic energy carry-over coefficient is neglected due to staggered boundary layer

Assumptions
1) Steady state
2) Isentropic flow
4) No heat transfer across labyrinth boundary

Geometry
The geometry used in this model has been modified from Eser (1995) literature. The model presents a 5 tooth staggered geometry with similar teeth dimensions"

```
"=================================================================="

FUNCTION FuncSonic (p_last,p_2_last,PR_choked)
        IF ((p_last/p_2_last)<PR_choked) THEN
                FuncSonic=1
        ELSE
                FuncSonic=0
        ENDIF
END


MODULE SealPressureData (p_u,p_c,Sonic:p_e)
        p_e=Sonic*p_c+(1-Sonic)*p_u
END

"=================================================================="

"Number of teeth"
n=5

"Boundary values"
p[0]=300000 "Pa"          " Inlet Pressure "
{p[n]= 206800  "Pa"       "Outlet Pressure"}
T_stag=298.2"K"           "Temperature"

"Constants"
R=287
gamma=1.4

"Seal geometry"
L=0.01291 "m"                   "Pitch"
cl=0.00016 "m"                  "Clearance"
R_i=0.1016 "m"                  "Shaft Radius"

R_o=R_i+cl
A=PI*(R_o^2-R_i^2) "m^2"

"=================================================================="
```

```
DUPLICATE k=1,n
        A_g[k]=A
END

"Number the sealing points"
DUPLICATE k=0,n
        Number[k]=k
END

"Seal pressure difference"
PR=p[n]/p[0]

"=========================================================================="

"------------CHOKED FLOW-----------"
"Define boundary pressures"
p_c[0]=p[0]
p_c[n]=p[n]

PR_choked=1/((1+(gamma-1)/2)^(gamma/(gamma-1)))

DUPLICATE k=1,n-1
        m_dot_choked^2=(C[k]*A_g[k])^2*(2*gamma)/(gamma-1)*p_c[k-
1]^2/(R*T_stag)*((p_c[k]/p_c[k-1])^(2/gamma)-(p_c[k]/p_c[k-1])^((gamma+1)/gamma))
END

m_dot_choked^2=(C[n]*A_g[n])^2*(2*gamma)/(gamma-1)*p_c[n-
1]^2/(R*T_stag)*((PR_choked)^(2/gamma)-(PR_choked)^((gamma+1)/gamma))

"=========================================================================="

"------------UNCHOKED FLOW-----------"
"Define boundary pressures"
p_u[0]=p[0]
p_u[n]=p[n]

DUPLICATE k=1,n
        m_dot_unchoked^2=(C[k]*A_g[k])^2*(2*gamma)/(gamma-1)*p_u[k-
1]^2/(R*T_stag)*((p_u[k]/p_u[k-1])^(2/gamma)-(p_u[k]/p_u[k-1])^((gamma+1)/gamma))

END
"=========================================================================="
"                          DISCHARGE COEFFICIENTS                          "
"=========================================================================="
"Discharge Coefficient For Unchoked Conditions"

DUPLICATE k=1,(n)
        S[k]=(p[k-1]/p[k])^(1-1/gamma)-1
        C[k]=PI/(PI+2-5*S[k]+2*S[k]^2)

        "Assume constant discharge coefficient"
        {C[k]=0.64}
END
```

```
"Kinetic energy carry-over coefficient neglected"
"=============================================================================="
"Test for subsonic/supersonic conditions"
Sonic=FuncSonic (p[n],p[n-1],PR_choked)
"=============================================================================="

"Calculate mass flow rate"
m_dot=Sonic*m_dot_choked+(1-Sonic)*m_dot_unchoked

"=============================================================================="
"Calculate pressure distribution"

DUPLICATE k=1,n-1
        CALL SealPressureData (p_u[k],p_c[k],Sonic:p[k])
END
"=============================================================================="

"Calculate pressure ratios for individual restrictions"
DUPLICATE k=1,n
        PR_Restriction[k]=p[k]/p[k-1]
END
"=============================================================================="
"Seal Leakage in lb_m/kgsec^2"
w=(m_dot/A)*(1/0.4535924)*(1/10.76391) "w=lb_m/kgsec^2"
"=============================================================================="
```

APPENDIX D

Straight Labyrinth Model Results

EES model results for various straight type geometries are shown in this section. The results are discussed and graphically presented in Chapter 4. Highlighted table sections indicate the seal is functioning under choked conditions.

Contents

D.1 Straight Type Model – Two Constriction Eser (1995) Geometry

EES results are displayed for parametric study done on labyrinth geometry given in Table 4.1. Appendix D.1 shows seal leakage results and pressure distribution through the seal. Discharge coefficients in the two constrictions are also given. Parametric results are graphically presented and discussed in Paragraph 4.4.1.

D.2 Straight Type Model – Various Constriction Numbers

Appendix D.2 displays parametric study results for leakage flows through various constriction numbers. The geometries are as displayed in Table 4.1 with given amount of restrictions. Results are discussed and graphically presented in Paragraph 4.4.2.

D.3 Five Constriction Straight Type

Appendix D.3 displays parametric study results for a five constriction labyrinth seal. These results have been compared with leakage flow results through a staggered labyrinth. Results compared with that of the straight type CFD results in Chapter 5.

D.1 Straight Type Model – 2 Teeth Eser (1995) Geometry

	Results	Eser (1995) Geometry as discussed in Paragraph 4.4.1								
	Notes:	Straight Type EES Code								
#	P_{in} kPa	P_{out} kPa	PR	Leakage kg/s	P_0 kPa	P_1 kPa	P_2 kPa	C_{d1}	C_{d2}	Choke
1	300.00	300.00	1.00	0.000005	300.00	300.00	300.00	0.611	0.611	0
2	300.00	295.92	0.99	0.008104	300.00	297.97	295.92	0.6122	0.6122	0
3	300.00	291.84	0.97	0.011420	300.00	295.95	291.84	0.6133	0.6134	0
4	300.00	287.76	0.96	0.013940	300.00	293.94	287.76	0.6145	0.6147	0
5	300.00	283.67	0.95	0.016040	300.00	291.95	283.67	0.6157	0.6159	0
6	300.00	279.59	0.93	0.017870	300.00	289.98	279.59	0.6168	0.6173	0
7	300.00	275.51	0.92	0.019500	300.00	288.02	275.51	0.618	0.6187	0
8	300.00	271.43	0.90	0.020990	300.00	286.07	271.43	0.6192	0.6201	0
9	300.00	267.35	0.89	0.022350	300.00	284.14	267.35	0.6204	0.6216	0
10	300.00	263.27	0.88	0.023620	300.00	282.23	263.27	0.6216	0.6231	0
11	300.00	259.18	0.86	0.024810	300.00	280.34	259.18	0.6228	0.6247	0
12	300.00	255.10	0.85	0.025920	300.00	278.46	255.10	0.624	0.6263	0
13	300.00	251.02	0.84	0.026970	300.00	276.60	251.02	0.6252	0.628	0
14	300.00	246.94	0.82	0.027960	300.00	274.76	246.94	0.6263	0.6297	0
15	300.00	242.86	0.81	0.028910	300.00	272.94	242.86	0.6275	0.6316	0
16	300.00	238.78	0.80	0.029810	300.00	271.13	238.78	0.6287	0.6335	0
17	300.00	234.69	0.78	0.030660	300.00	269.35	234.69	0.6299	0.6354	0
18	300.00	230.61	0.77	0.031480	300.00	267.59	230.61	0.6311	0.6375	0
19	300.00	226.53	0.76	0.032260	300.00	265.84	226.53	0.6323	0.6396	0
20	300.00	222.45	0.74	0.033010	300.00	264.12	222.45	0.6335	0.6418	0
21	300.00	218.37	0.73	0.033730	300.00	262.42	218.37	0.6347	0.644	0
22	300.00	214.29	0.71	0.034420	300.00	260.74	214.29	0.6359	0.6464	0
23	300.00	210.20	0.70	0.035090	300.00	259.08	210.20	0.6371	0.6489	0
24	300.00	206.12	0.69	0.035720	300.00	257.44	206.12	0.6383	0.6515	0
25	300.00	202.04	0.67	0.036340	300.00	255.83	202.04	0.6394	0.6542	0
26	300.00	197.96	0.66	0.036930	300.00	254.25	197.96	0.6406	0.657	0
27	300.00	193.88	0.65	0.037490	300.00	252.68	193.88	0.6418	0.6599	0
28	300.00	189.80	0.63	0.038040	300.00	251.15	189.80	0.6429	0.6629	0

29	300.00	185.71	0.62	0.038570	300.00	249.64	185.71	0.6441	0.6661	0
30	300.00	181.63	0.61	0.039070	300.00	248.16	181.63	0.6452	0.6695	0
31	300.00	177.55	0.59	0.039560	300.00	246.70	177.55	0.6463	0.673	0
32	300.00	173.47	0.58	0.040030	300.00	245.27	173.47	0.6474	0.6766	0
33	300.00	169.39	0.56	0.040480	300.00	243.88	169.39	0.6485	0.6804	0
34	300.00	165.31	0.55	0.040910	300.00	242.51	165.31	0.6496	0.6845	0
35	300.00	161.22	0.54	0.041330	300.00	241.17	161.22	0.6507	0.6887	0
36	300.00	157.14	0.52	0.041730	300.00	239.87	157.14	0.6517	0.6931	0
37	300.00	153.06	0.51	0.042110	300.00	238.59	153.06	0.6528	0.6978	0
38	300.00	148.98	0.50	0.042480	300.00	237.35	148.98	0.6538	0.7027	0
39	300.00	144.90	0.48	0.042840	300.00	236.15	144.90	0.6548	0.7079	0
40	300.00	140.82	0.47	0.043170	300.00	234.98	140.82	0.6558	0.7134	0
41	300.00	136.74	0.46	0.043500	300.00	233.85	136.74	0.6567	0.7192	0
42	300.00	132.65	0.44	0.043800	300.00	232.76	132.65	0.6577	0.7254	0
43	300.00	128.57	0.43	0.044100	300.00	231.70	128.57	0.6586	0.7319	0
44	300.00	124.49	0.42	0.044380	300.00	230.69	124.49	0.6594	0.7388	0
45	300.00	120.41	0.40	0.044640	300.00	229.71	120.41	0.6603	0.7462	1
46	300.00	116.33	0.39	0.044640	300.00	229.71	116.33	0.6603	0.7462	1
47	300.00	112.25	0.37	0.044640	300.00	229.71	112.25	0.6603	0.7462	1
48	300.00	108.16	0.36	0.044640	300.00	229.71	108.16	0.6603	0.7462	1
49	300.00	104.08	0.35	0.044640	300.00	229.71	104.08	0.6603	0.7462	1
50	300.00	100.00	0.33	0.044640	300.00	229.71	100.00	0.6603	0.7462	1

D.2 Straight Type Model - Various Constriction Numbers

	Results	Various Constriction Numbers as discussed in Paragraph 4.4.2						
	Notes:	Straight Type EES Code for 2,4,6 Constrictions						
#	P_{in} kPa	P_{out} kPa	PR	Leakage 2 teeth kg/s	Leakage 4 Teeth kg/s	Leakage 6 Teeth kg/s	Leakage 8 Teeth kg/s	Leakage 10 Teeth kg/s
1	300.00	300.00	1.0000	0.0000	0.0000	0.0000	0.0000	0.0000
2	300.00	295.10	0.9864	0.0089	0.0066	0.0055	0.0048	0.0043
3	300.00	290.20	0.9728	0.0125	0.0093	0.0077	0.0067	0.0061
4	300.00	285.31	0.9592	0.0152	0.0113	0.0094	0.0082	0.0074
5	300.00	280.41	0.9456	0.0175	0.0130	0.0108	0.0094	0.0085
6	300.00	275.51	0.9320	0.0195	0.0145	0.0120	0.0105	0.0095
7	300.00	270.61	0.9184	0.0213	0.0158	0.0131	0.0115	0.0103
8	300.00	265.71	0.9048	0.0229	0.0170	0.0141	0.0123	0.0111
9	300.00	260.82	0.8912	0.0243	0.0181	0.0150	0.0131	0.0118
10	300.00	255.92	0.8776	0.0257	0.0191	0.0159	0.0139	0.0125
11	300.00	251.02	0.8639	0.0270	0.0200	0.0166	0.0145	0.0131
12	300.00	246.12	0.8503	0.0282	0.0209	0.0174	0.0152	0.0137
13	300.00	241.22	0.8367	0.0293	0.0217	0.0181	0.0158	0.0142
14	300.00	236.33	0.8231	0.0303	0.0225	0.0187	0.0164	0.0147
15	300.00	231.43	0.8095	0.0313	0.0233	0.0193	0.0169	0.0152
16	300.00	226.53	0.7959	0.0323	0.0240	0.0199	0.0174	0.0157
17	300.00	221.63	0.7823	0.0332	0.0246	0.0205	0.0179	0.0161
18	300.00	216.74	0.7687	0.0340	0.0253	0.0210	0.0184	0.0165
19	300.00	211.84	0.7551	0.0348	0.0259	0.0215	0.0188	0.0169
20	300.00	206.94	0.7415	0.0356	0.0265	0.0220	0.0192	0.0173
21	300.00	202.04	0.7279	0.0363	0.0270	0.0225	0.0196	0.0177
22	300.00	197.14	0.7143	0.0370	0.0276	0.0229	0.0200	0.0180
23	300.00	192.25	0.7007	0.0377	0.0281	0.0233	0.0204	0.0183
24	300.00	187.35	0.6871	0.0384	0.0285	0.0237	0.0207	0.0187
25	300.00	182.45	0.6735	0.0390	0.0290	0.0241	0.0211	0.0190
26	300.00	177.55	0.6599	0.0396	0.0295	0.0245	0.0214	0.0192
27	300.00	172.65	0.6463	0.0401	0.0299	0.0248	0.0217	0.0195
28	300.00	167.76	0.6327	0.0407	0.0303	0.0252	0.0220	0.0198

29	300.00	162.86	0.6190	0.0412	0.0307	0.0255	0.0223	0.0201
30	300.00	157.96	0.6054	0.0417	0.0310	0.0258	0.0226	0.0203
31	300.00	153.06	0.5918	0.0421	0.0314	0.0261	0.0228	0.0205
32	300.00	148.16	0.5782	0.0426	0.0317	0.0264	0.0231	0.0208
33	300.00	143.27	0.5646	0.0430	0.0321	0.0267	0.0233	0.0210
34	300.00	138.37	0.5510	0.0434	0.0324	0.0269	0.0235	0.0212
35	300.00	133.47	0.5374	0.0437	0.0327	0.0272	0.0238	0.0214
36	300.00	128.57	0.5238	0.0441	0.0330	0.0274	0.0240	0.0216
37	300.00	123.67	0.5102	0.0444	0.0332	0.0276	0.0242	0.0217
38	300.00	118.78	0.4966	0.0448	0.0335	0.0279	0.0244	0.0219
39	300.00	113.88	0.4830	0.0448	0.0337	0.0281	0.0245	0.0221
40	300.00	108.98	0.4694	0.0448	0.0339	0.0283	0.0247	0.0222
41	300.00	104.08	0.4558	0.0448	0.0341	0.0284	0.0249	0.0224
42	300.00	99.18	0.4422	0.0448	0.0343	0.0286	0.0250	0.0225
43	300.00	94.29	0.4286	0.0448	0.0345	0.0288	0.0252	0.0226
44	300.00	89.39	0.4150	0.0448	0.0347	0.0289	0.0253	0.0228
45	300.00	84.49	0.4014	0.0448	0.0347	0.0291	0.0254	0.0229
46	300.00	79.59	0.3878	0.0448	0.0347	0.0292	0.0255	0.0230
47	300.00	74.69	0.3741	0.0448	0.0347	0.0293	0.0256	0.0231
48	300.00	69.80	0.3605	0.0448	0.0347	0.0293	0.0257	0.0232
49	300.00	64.90	0.3469	0.0448	0.0347	0.0293	0.0258	0.0233
50	300.00	60.00	0.3333	0.0448	0.0347	0.0293	0.0258	0.0233

D.3 Five Constriction Straight Type

	Results	5 Constriction Straight Type Results as discussed in Paragraph 4.7									
	Notes:	Straight Type EES Code									
#	P_{in} kPa	P_{out} kPa	PR	Leakage kg/s	P_0 kPa	P_1 kPa	P_2 kPa	P_3 kPa	P_4 kPa	P_5 kPa	Choke
1	300.00	300.00	1.0000	0.00000	300.0	300.0	300.0	300.0	300.0	300.0	0
2	300.00	295.31	0.9844	0.00583	300.0	299.1	298.1	297.2	296.3	295.3	0
3	300.00	290.61	0.9687	0.00821	300.0	298.1	296.3	294.4	292.5	290.6	0
4	300.00	285.92	0.9531	0.01001	300.0	297.2	294.4	291.6	288.8	285.9	0
5	300.00	281.22	0.9374	0.01151	300.0	296.3	292.6	288.9	285.1	281.2	0
6	300.00	276.53	0.9218	0.01282	300.0	295.5	290.8	286.2	281.4	276.5	0
7	300.00	271.84	0.9061	0.01399	300.0	294.6	289.1	283.4	277.7	271.8	0
8	300.00	267.14	0.8905	0.01504	300.0	293.7	287.3	280.7	274.0	267.1	0
9	300.00	262.45	0.8748	0.01602	300.0	292.9	285.6	278.1	270.4	262.4	0
10	300.00	257.76	0.8592	0.01692	300.0	292.0	283.9	275.4	266.7	257.8	0
11	300.00	253.06	0.8435	0.01775	300.0	291.2	282.2	272.8	263.1	253.1	0
12	300.00	248.37	0.8279	0.01854	300.0	290.4	280.5	270.2	259.5	248.4	0
13	300.00	243.67	0.8122	0.01928	300.0	289.6	278.8	267.6	255.9	243.7	0
14	300.00	238.98	0.7966	0.01998	300.0	288.8	277.2	265.1	252.4	239.0	0
15	300.00	234.29	0.7810	0.02064	300.0	288.1	275.6	262.6	248.8	234.3	0
16	300.00	229.59	0.7653	0.02127	300.0	287.3	274.0	260.1	245.3	229.6	0
17	300.00	224.90	0.7497	0.02187	300.0	286.6	272.5	257.6	241.8	224.9	0
18	300.00	220.20	0.7340	0.02244	300.0	285.8	270.9	255.1	238.3	220.2	0
19	300.00	215.51	0.7184	0.02299	300.0	285.1	269.4	252.7	234.9	215.5	0
20	300.00	210.82	0.7027	0.02351	300.0	284.4	267.9	250.3	231.4	210.8	0
21	300.00	206.12	0.6871	0.02401	300.0	283.7	266.5	248.0	228.0	206.1	0
22	300.00	201.43	0.6714	0.02449	300.0	283.1	265.0	245.7	224.6	201.4	0
23	300.00	196.74	0.6558	0.02494	300.0	282.4	263.6	243.4	221.3	196.7	0
24	300.00	192.04	0.6401	0.02538	300.0	281.8	262.2	241.1	218.0	192.0	0
25	300.00	187.35	0.6245	0.02580	300.0	281.1	260.9	238.9	214.7	187.3	0
26	300.00	182.65	0.6088	0.02620	300.0	280.5	259.5	236.7	211.4	182.7	0
27	300.00	177.96	0.5932	0.02659	300.0	279.9	258.2	234.6	208.2	178.0	0
28	300.00	173.27	0.5776	0.02696	300.0	279.3	257.0	232.5	205.0	173.3	0
29	300.00	168.57	0.5619	0.02732	300.0	278.7	255.7	230.4	201.9	168.6	0
30	300.00	163.88	0.5463	0.02766	300.0	278.2	254.5	228.4	198.8	163.9	0

31	300.00	159.18	0.5306	0.02798	300.0	277.6	253.3	226.4	195.7	159.2	0
32	300.00	154.49	0.5150	0.02830	300.0	277.1	252.2	224.4	192.7	154.5	0
33	300.00	149.80	0.4993	0.02860	300.0	276.6	251.0	222.5	189.7	149.8	0
34	300.00	145.10	0.4837	0.02889	300.0	276.1	250.0	220.7	186.8	145.1	0
35	300.00	140.41	0.4680	0.02916	300.0	275.6	248.9	218.9	184.0	140.4	0
36	300.00	135.71	0.4524	0.02942	300.0	275.2	247.9	217.1	181.1	135.7	0
37	300.00	131.02	0.4367	0.02968	300.0	274.7	246.9	215.4	178.4	131.0	0
38	300.00	126.33	0.4211	0.02992	300.0	274.3	245.9	213.8	175.7	126.3	0
39	300.00	121.63	0.4054	0.03014	300.0	273.9	245.0	212.1	173.1	121.6	0
40	300.00	116.94	0.3898	0.03036	300.0	273.5	244.1	210.6	170.5	116.9	0
41	300.00	112.25	0.3741	0.03057	300.0	273.1	243.2	209.1	168.1	112.2	0
42	300.00	107.55	0.3585	0.03076	300.0	272.7	242.4	207.7	165.7	107.6	0
43	300.00	102.86	0.3429	0.03095	300.0	272.4	241.6	206.3	163.3	102.9	0
44	300.00	98.16	0.3272	0.03112	300.0	272.1	240.9	205.0	161.1	98.2	0
45	300.00	93.47	0.3116	0.03128	300.0	271.8	240.2	203.8	159.0	93.5	0
46	300.00	88.78	0.2959	0.03143	300.0	271.5	239.5	202.6	157.0	88.8	0
47	300.00	84.08	0.2803	0.03158	300.0	271.2	238.9	201.5	155.1	84.1	0
48	300.00	79.39	0.2646	0.03171	300.0	270.9	238.3	200.5	153.2	79.4	1
49	300.00	74.69	0.2490	0.03171	300.0	270.7	237.7	199.4	151.3	74.7	1
50	300.00	70.00	0.2333	0.03171	300.0	270.4	237.1	198.2	149.3	70.0	1

D.4 Discharge Coefficients for Five Constriction Straight Labyrinth

	Results	5 Constriction Straight Type Discharge Coefficients as discussed in Paragraph 4.4.4					
	Notes:	Straight Type EES Code					
#	PR	C_{d1}	C_{d2}	C_{d3}	C_{d4}	C_{d5}	Choke
1	1.000	0.611	0.611	0.611	0.611	0.611	0
2	0.984	0.6115	0.6115	0.6116	0.6116	0.6116	0
3	0.969	0.6121	0.6121	0.6121	0.6121	0.6121	0
4	0.953	0.6126	0.6126	0.6127	0.6127	0.6127	0
5	0.937	0.6131	0.6132	0.6132	0.6133	0.6133	0
6	0.922	0.6136	0.6137	0.6138	0.6139	0.614	0
7	0.906	0.6141	0.6142	0.6144	0.6145	0.6147	0
8	0.891	0.6146	0.6148	0.615	0.6152	0.6154	0
9	0.875	0.6151	0.6153	0.6156	0.6158	0.6161	0
10	0.859	0.6156	0.6159	0.6162	0.6165	0.6169	0
11	0.844	0.6161	0.6164	0.6168	0.6172	0.6177	0
12	0.828	0.6166	0.617	0.6174	0.618	0.6186	0
13	0.812	0.6171	0.6175	0.6181	0.6187	0.6195	0
14	0.797	0.6175	0.6181	0.6187	0.6195	0.6204	0
15	0.781	0.618	0.6186	0.6194	0.6203	0.6214	0
16	0.765	0.6185	0.6192	0.62	0.6211	0.6225	0
17	0.750	0.6189	0.6197	0.6207	0.622	0.6236	0
18	0.734	0.6194	0.6203	0.6214	0.6228	0.6248	0
19	0.718	0.6198	0.6208	0.6221	0.6237	0.626	0
20	0.703	0.6202	0.6213	0.6228	0.6247	0.6273	0
21	0.687	0.6206	0.6219	0.6235	0.6256	0.6287	0
22	0.671	0.6211	0.6224	0.6242	0.6266	0.6302	0
23	0.656	0.6215	0.6229	0.6249	0.6276	0.6317	0
24	0.640	0.6219	0.6235	0.6256	0.6287	0.6334	0
25	0.625	0.6223	0.624	0.6264	0.6298	0.6351	0
26	0.609	0.6227	0.6245	0.6271	0.6309	0.637	0
27	0.593	0.623	0.625	0.6278	0.632	0.639	0
28	0.578	0.6234	0.6255	0.6286	0.6332	0.6411	0
29	0.562	0.6238	0.626	0.6293	0.6344	0.6434	0
30	0.546	0.6241	0.6265	0.63	0.6356	0.6458	0

31	0.531	0.6245	0.627	0.6308	0.6369	0.6484	0
32	0.515	0.6248	0.6275	0.6315	0.6381	0.6512	0
33	0.499	0.6251	0.628	0.6323	0.6395	0.6542	0
34	0.484	0.6255	0.6284	0.633	0.6408	0.6575	0
35	0.468	0.6258	0.6289	0.6337	0.6422	0.6609	0
36	0.452	0.6261	0.6293	0.6344	0.6435	0.6647	0
37	0.437	0.6264	0.6298	0.6352	0.645	0.6688	0
38	0.421	0.6266	0.6302	0.6359	0.6464	0.6732	0
39	0.405	0.6269	0.6306	0.6366	0.6478	0.678	0
40	0.390	0.6272	0.631	0.6372	0.6493	0.6832	0
41	0.374	0.6274	0.6314	0.6379	0.6507	0.6889	0
42	0.359	0.6277	0.6318	0.6386	0.6522	0.6952	0
43	0.343	0.6279	0.6321	0.6392	0.6537	0.702	0
44	0.327	0.6281	0.6325	0.6398	0.6551	0.7096	0
45	0.312	0.6283	0.6328	0.6404	0.6565	0.718	0
46	0.296	0.6285	0.6331	0.641	0.6579	0.7272	0
47	0.280	0.6287	0.6334	0.6415	0.6593	0.7376	0
48	0.265	0.6289	0.6337	0.642	0.6606	0.7492	1
49	0.249	0.6289	0.6337	0.642	0.6606	0.7492	1
50	0.233	0.6289	0.6337	0.642	0.6606	0.7492	1

APPENDIX E

Staggered Labyrinth Model Results

EES model results for staggered labyrinths are shown in this section. The results are discussed and graphically presented in Chapter 4. Highlighted table sections indicate seal is functioning under choked conditions.

E.1 Five Constriction Staggered Results

Results 5 Constriction Staggered Geometry as discussed in Paragraph 4.6.1

Notes: Staggered EES Code

#	P_{in} kPa	P_{out} kPa	PR	Leakage kg/s	P_0 kPa	P_1 kPa	P_2 kPa	P_3 kPa	P_4 kPa	P_5 kPa	Choke
1	300	300	1.0000	0.00000	300	300.0	300.0	300.0	300.0	300.0	0
2	300	295.31	0.9844	0.00505	300	299.1	298.1	297.2	296.3	295.3	0
3	300	290.61	0.9687	0.00711	300	298.1	296.3	294.4	292.5	290.6	0
4	300	285.92	0.9531	0.00867	300	297.2	294.4	291.6	288.8	285.9	0
5	300	281.22	0.9374	0.00997	300	296.3	292.6	288.9	285.1	281.2	0
6	300	276.53	0.9218	0.01110	300	295.5	290.8	286.2	281.4	276.5	0
7	300	271.84	0.9061	0.01211	300	294.6	289.1	283.4	277.7	271.8	0
8	300	267.14	0.8905	0.01303	300	293.7	287.3	280.7	274.0	267.1	0
9	300	262.45	0.8748	0.01387	300	292.9	285.6	278.1	270.4	262.4	0
10	300	257.76	0.8592	0.01465	300	292.0	283.9	275.4	266.7	257.8	0
11	300	253.06	0.8435	0.01538	300	291.2	282.2	272.8	263.1	253.1	0
12	300	248.37	0.8279	0.01606	300	290.4	280.5	270.2	259.5	248.4	0
13	300	243.67	0.8122	0.01670	300	289.6	278.8	267.6	255.9	243.7	0
14	300	238.98	0.7966	0.01731	300	288.8	277.2	265.1	252.4	239.0	0
15	300	234.29	0.7810	0.01788	300	288.1	275.6	262.6	248.8	234.3	0
16	300	229.59	0.7653	0.01843	300	287.3	274.0	260.1	245.3	229.6	0
17	300	224.9	0.7497	0.01895	300	286.6	272.5	257.6	241.8	224.9	0
18	300	220.2	0.7340	0.01944	300	285.8	270.9	255.1	238.3	220.2	0
19	300	215.51	0.7184	0.01991	300	285.1	269.4	252.7	234.9	215.5	0
20	300	210.82	0.7027	0.02036	300	284.4	267.9	250.3	231.4	210.8	0
21	300	206.12	0.6871	0.02080	300	283.7	266.5	248.0	228.0	206.1	0
22	300	201.43	0.6714	0.02121	300	283.1	265.0	245.7	224.6	201.4	0
23	300	196.74	0.6558	0.02160	300	282.4	263.6	243.4	221.3	196.7	0
24	300	192.04	0.6401	0.02198	300	281.8	262.2	241.1	218.0	192.0	0
25	300	187.35	0.6245	0.02235	300	281.1	260.9	238.9	214.7	187.3	0
26	300	182.65	0.6088	0.02270	300	280.5	259.5	236.7	211.4	182.7	0
27	300	177.96	0.5932	0.02303	300	279.9	258.2	234.6	208.2	178.0	0
28	300	173.27	0.5776	0.02335	300	279.3	257.0	232.5	205.0	173.3	0
29	300	168.57	0.5619	0.02366	300	278.7	255.7	230.4	201.9	168.6	0
30	300	163.88	0.5463	0.02396	300	278.2	254.5	228.4	198.8	163.9	0

31	300	159.18	0.5306	0.02424	300	277.6	253.3	226.4	195.7	159.2	0
32	300	154.49	0.5150	0.02451	300	277.1	252.2	224.4	192.7	154.5	0
33	300	149.8	0.4993	0.02477	300	276.6	251.0	222.5	189.7	149.8	0
34	300	145.1	0.4837	0.02502	300	276.1	250.0	220.7	186.8	145.1	0
35	300	140.41	0.4680	0.02526	300	275.6	248.9	218.9	184.0	140.4	0
36	300	135.71	0.4524	0.02549	300	275.2	247.9	217.1	181.1	135.7	0
37	300	131.02	0.4367	0.02570	300	274.7	246.9	215.4	178.4	131.0	0
38	300	126.33	0.4211	0.02591	300	274.3	245.9	213.8	175.7	126.3	0
39	300	121.63	0.4054	0.02611	300	273.9	245.0	212.1	173.1	121.6	0
40	300	116.94	0.3898	0.02630	300	273.5	244.1	210.6	170.5	116.9	0
41	300	112.25	0.3741	0.02648	300	273.1	243.2	209.1	168.1	112.2	0
42	300	107.55	0.3585	0.02665	300	272.7	242.4	207.7	165.7	107.6	0
43	300	102.86	0.3429	0.02681	300	272.4	241.6	206.3	163.3	102.9	0
44	300	98.163	0.3272	0.02696	300	272.1	240.9	205.0	161.1	98.2	0
45	300	93.469	0.3116	0.02710	300	271.8	240.2	203.8	159.0	93.5	0
46	300	88.776	0.2959	0.02723	300	271.5	239.5	202.6	157.0	88.8	0
47	300	84.082	0.2803	0.02735	300	271.2	238.9	201.5	155.1	84.1	0
48	300	79.388	0.2646	0.02747	300	270.9	238.3	200.5	153.2	79.4	1
49	300	74.694	0.2490	0.02747	300	270.7	237.7	199.4	151.3	74.7	1
50	300	70	0.2333	0.02747	300	270.4	237.1	198.2	149.3	70.0	1

APPENDIX F

ECLS Results

Computational fluid dynamic results for the electro magnetically controlled labyrinth seal of the PBMR is shown. The results show pressure and temperature contours as well as velocity vector charts of the fluid flow through the labyrinth.

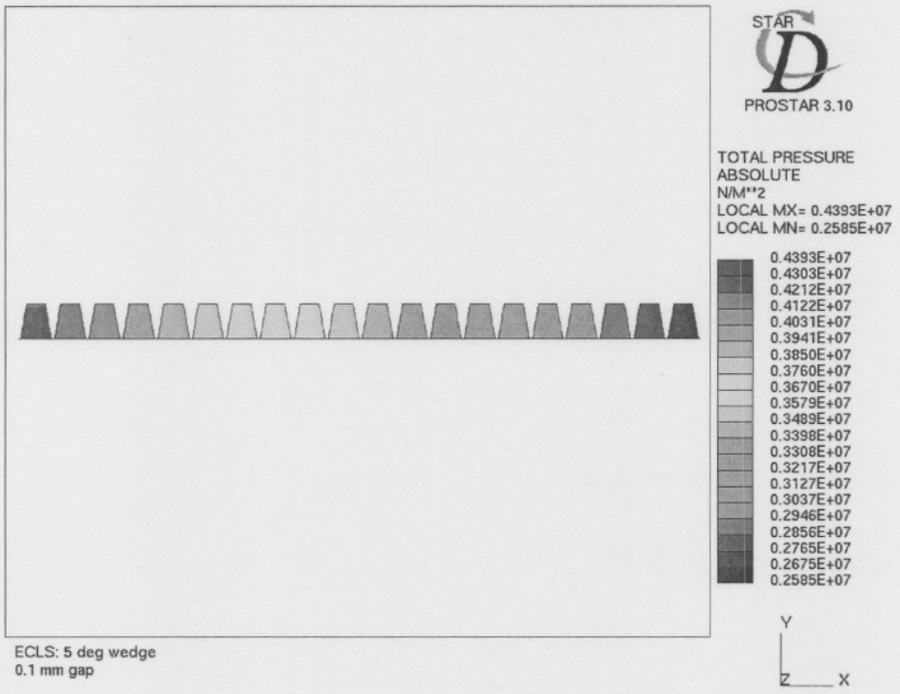

Figure F.1: Total pressure contours in a plane 0.1mm tip clearance

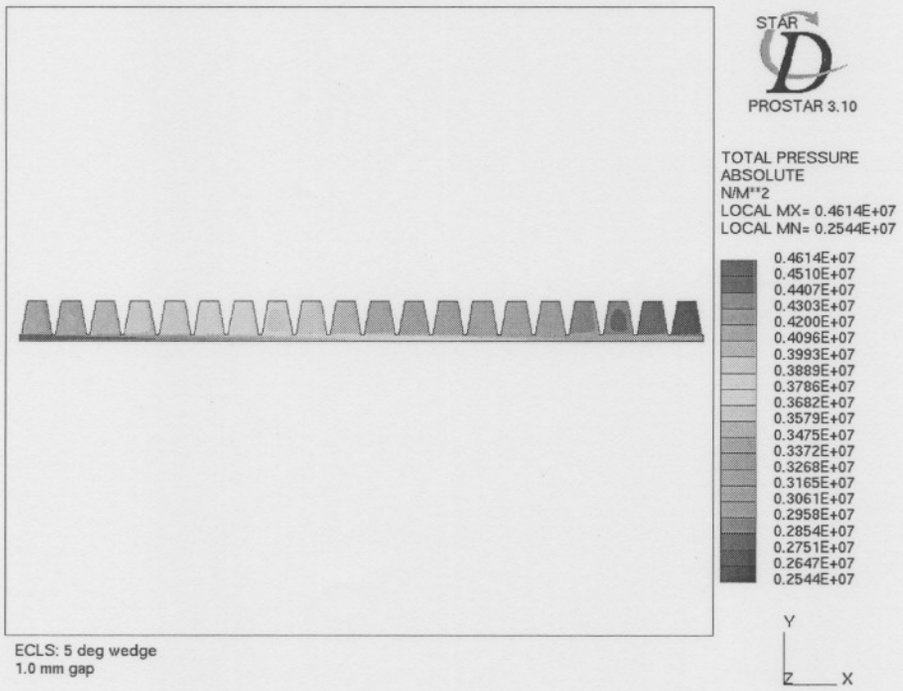

Figure F.2: Total pressure contours in a plane 1.0mm tip clearance

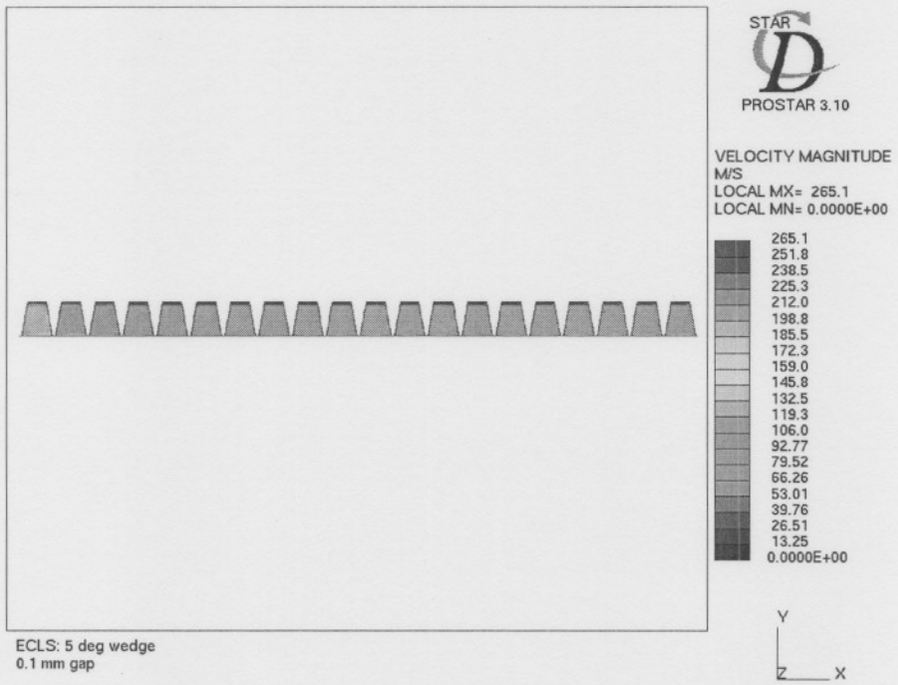

Figure F.3: Velocity magnitude contours in a plane 0.1mm tip clearance

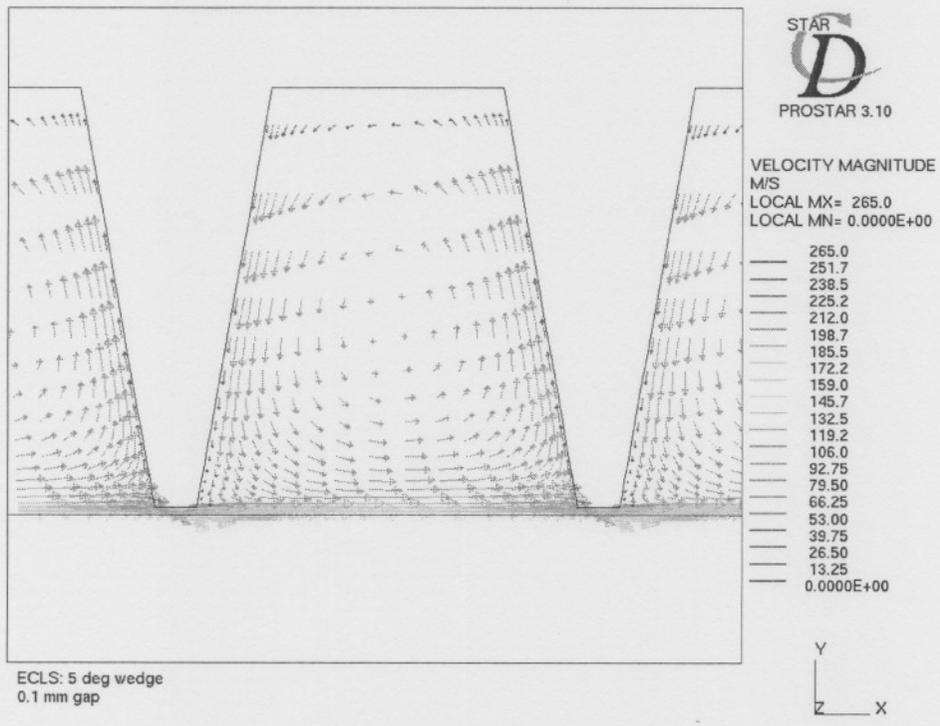

Figure F.4: Velocity vectors in a plane 0.1mm tip clearance

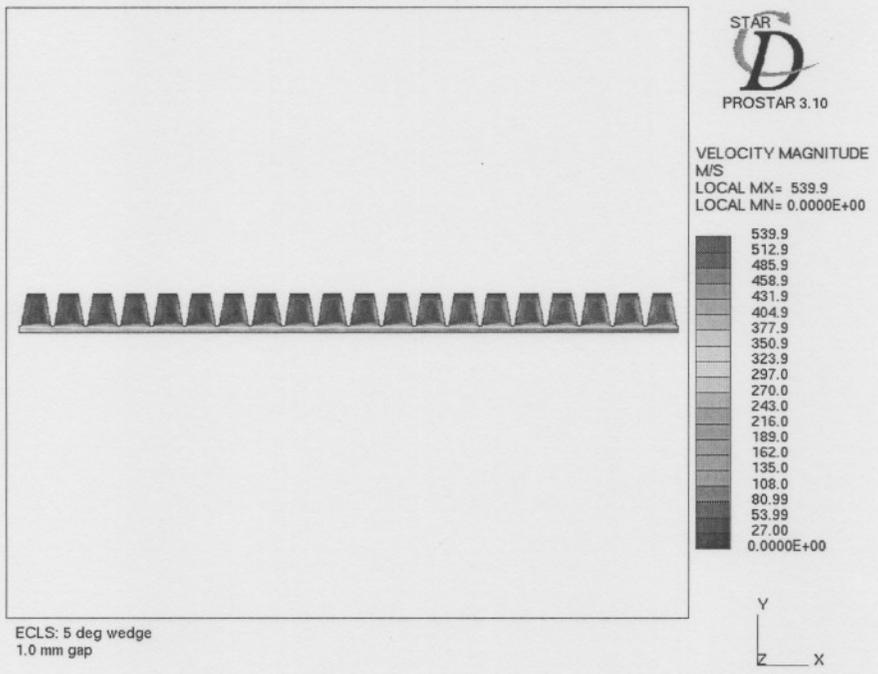

Figure F.5: Velocity magnitude contours in a plane 1.0mm tip clearance

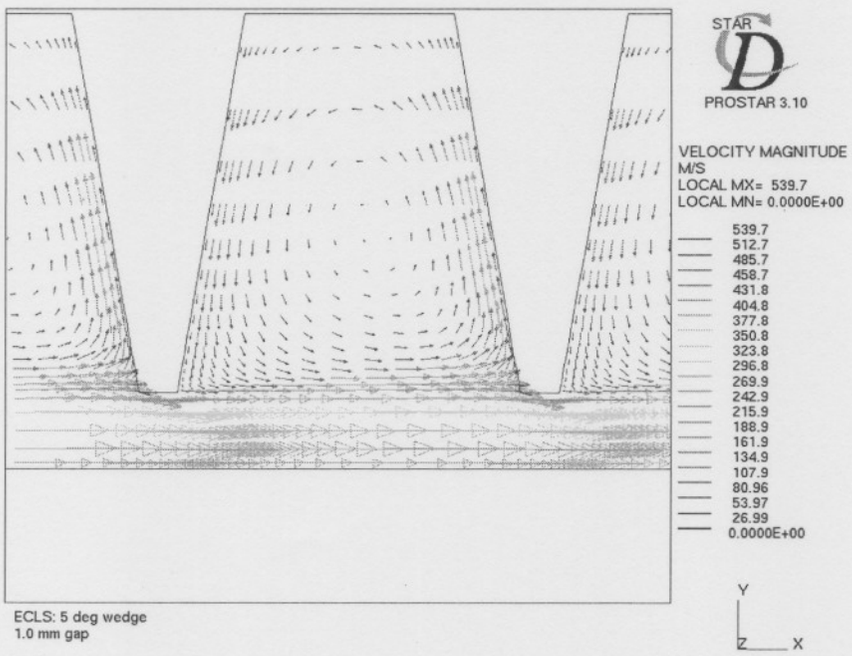

Figure F.6: Velocity vectors in a plane 1.0mm tip clearance

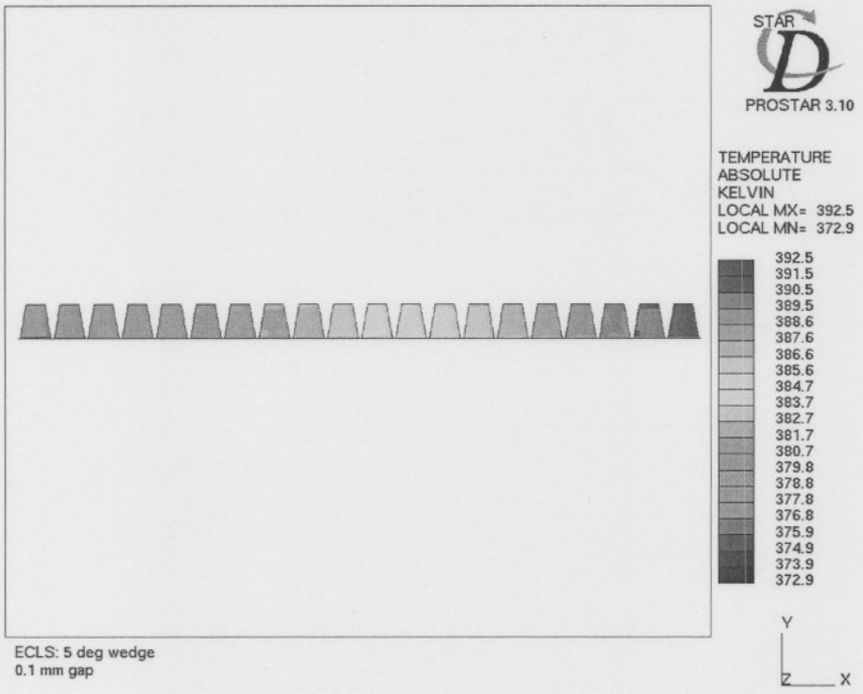

Figure F.7: Temperature contours in a plane 0.1mm tip clearance

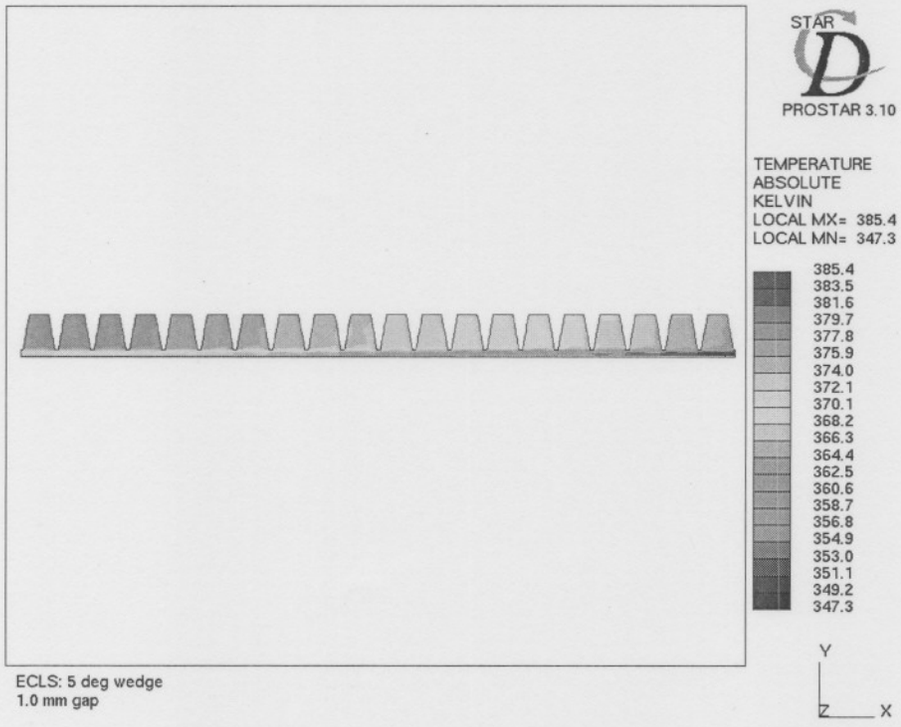

Figure F.8: Temperature contours in a plane 1.0mm tip clearance

APPENDIX G

CFD Results

APPENDIX G shows CFD results for the five constriction straight and staggered geometries that have been used in the validation process in Chapter 5. The geometries of the seals are discussed in Paragraph 4.6.

Contents

G.1 Straight Type CFD Results

Straight Labyrinth geometry was solved using Fluent 6.1.18 with standard k-ε turbulence models. The inlet and outlet boundaries was set as pressure boundaries and a pressure ratio was set up by specifying the total pressure at the inlet and static pressure at the outlet. The outlet pressure was measured upstream of the model pressure outlet.

Seal geometry was divided into 7925 cells for the standard model. The setup was tested for stability by further dividing cells to 8414, 9608 and 16112 cells. Results obtained with the refined meshes where consistent with those obtained by using 7925 cells.

G.2 Staggered Type CFD Results

A staggered labyrinth equivalent to that solved in paragraph 4.6 was also solved using Fluent 6.1.18. The model was solved using standard k-ε models and pressure boundaries were specified in a similar way as described with straight type seals.

Seal geometry was divided into 10325 cells for the base model. The model was also tested for stability by refining cells to 11078 and 13031 cells. Refined mesh results compared favorably with that of the base mesh.

APPENDIX G.1: Straight Labyrinth CFD Results

The straight labyrinth geometry as discussed in Paragraph 5.5 was solved with the use of both the engineering tool and Fluent software. Leakage flow results of both models are compared in Table G.1 followed by pressure contour plots and velocity vector charts.

Table G.1: *CFD and EES Comparison for Straight Type Labyrinth*

Total pressure			CFD Flow Rate	EES Flow Rate	% Error
Inlet [Pa]	Outlet [Pa]	p_r	[kg/s]	[kg/s]	
300000	199661.213	0.6655	0.027	0.02544	5.77
300000	189621.170	0.6321	0.028	0.02639	5.75
300000	179574.980	0.5986	0.029	0.02726	6.00
300000	169525.780	0.5651	0.030	0.02804	6.53
300000	158847.890	0.5295	0.030	0.02879	4.03
300000	149409.873	0.4980	0.031	0.02939	5.19
300000	139354.200	0.4645	0.032	0.02995	6.41
300000	129286.320	0.4310	0.032	0.03045	4.84
300000	119211.260	0.3974	0.032	0.03088	3.50
300000	99024.153	0.3301	0.033	0.03167	4.03
300000	88922.928	0.2964	0.033	0.03166	4.06
300000	78821.241	0.2627	0.033	0.03171	3.90
300000	68722.427	0.2291	0.033	0.03171	3.90
300000	58637.883	0.1955	0.033	0.03171	3.90
300000	48577.669	0.1619	0.033	0.03171	3.90

Pr = 0.667

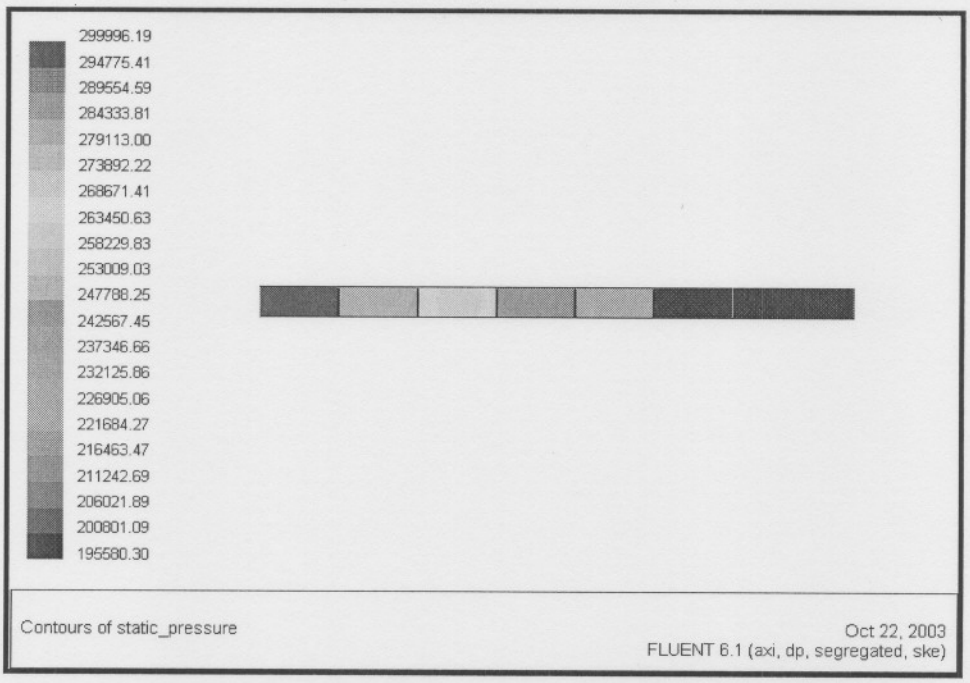

Figure G.1: Contours of static pressure for Pr=0.667.

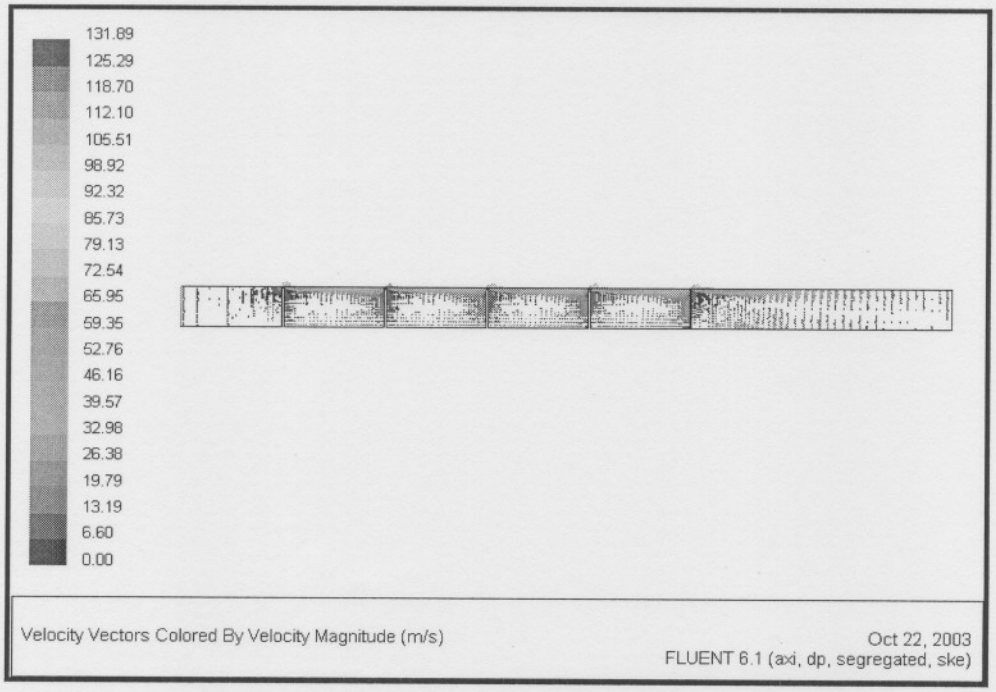

Figure G.2: Velocity vector diagram for Pr=0.667.

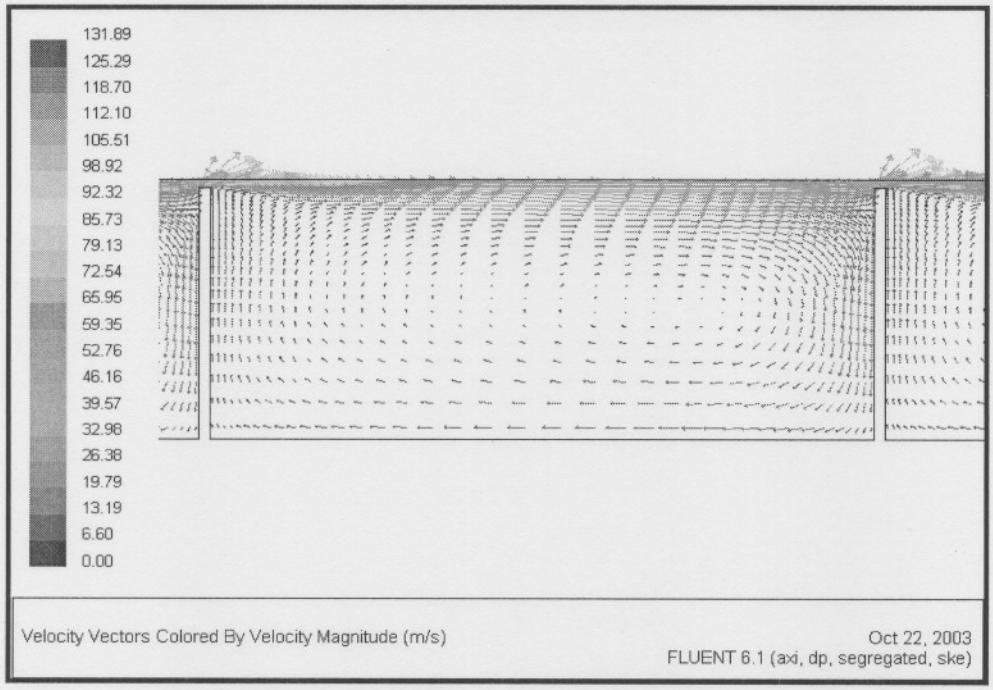

Figure G.3: Velocity vector diagram for last two constrictions with Pr=0.667.

Pr = 0.167

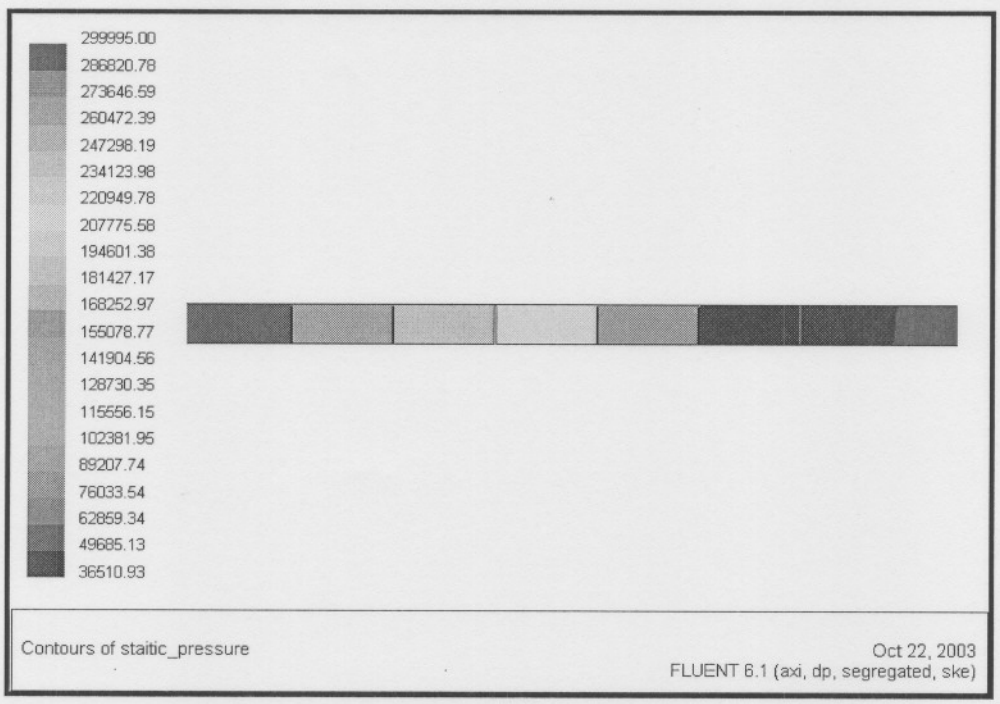

Figure G.4: Pressure contour plot for Pr=0.167.

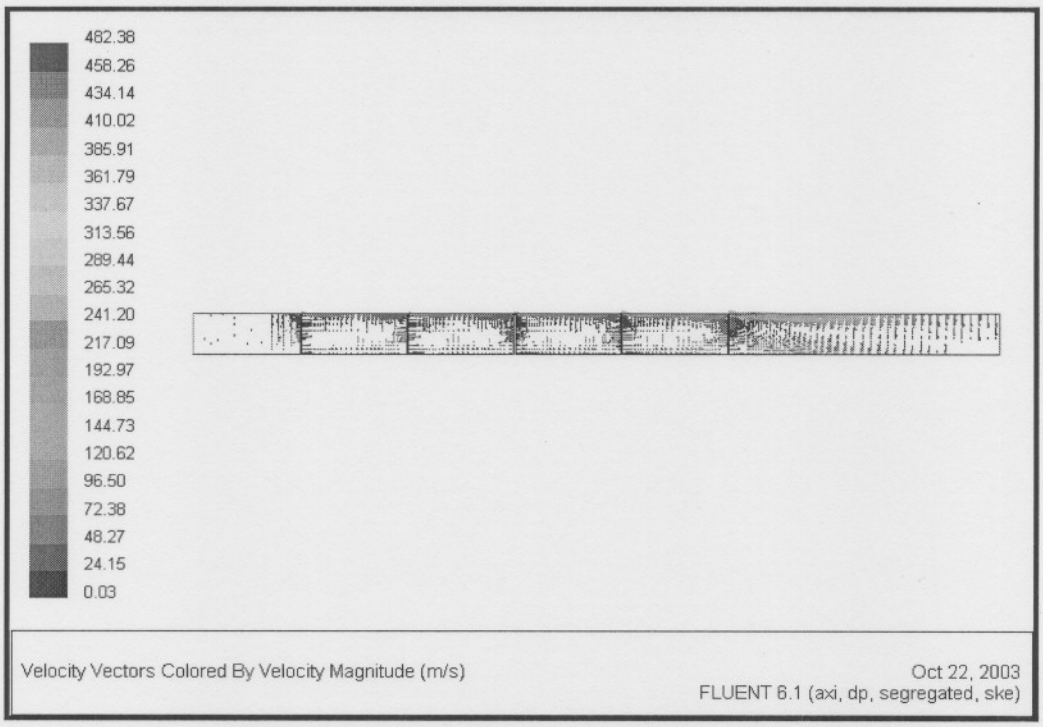

Figure G.5: Velocity vector plot for Pr=0.167.

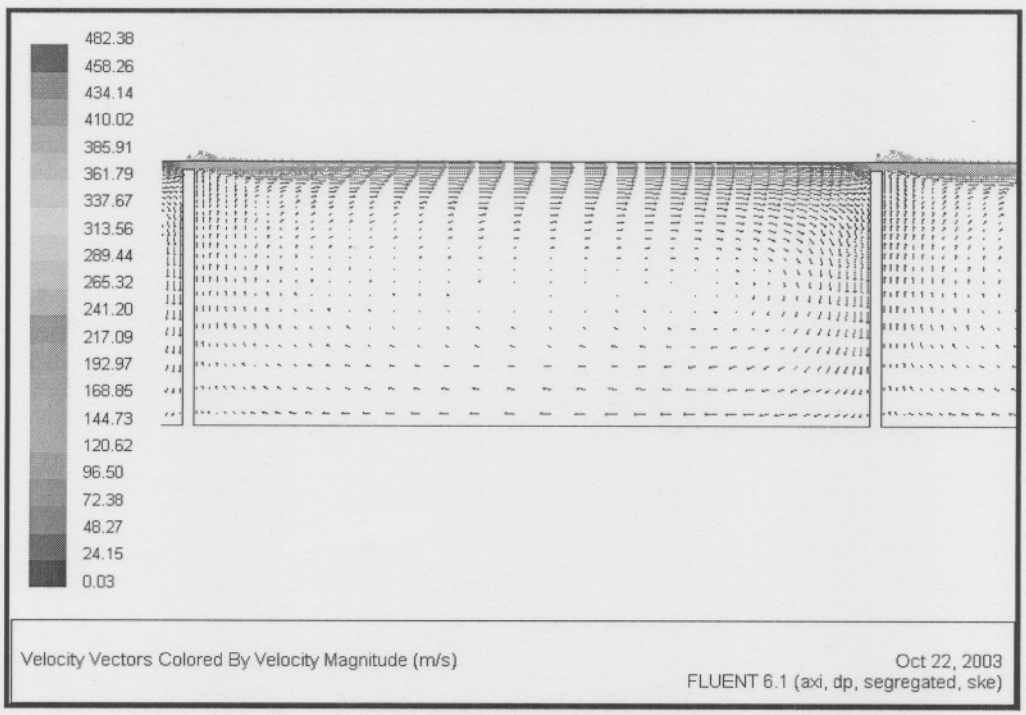

Figure G.6: Velocity vector plot for last two constrictions with Pr=0.167.

APPENDIX G.2: Staggered Labyrinth CFD Results

The staggered labyrinth geometry as discussed in Paragraph 5.6 was solved with the use of both the engineering tool and Fluent software. Leakage flow results of both models are compared in Table G.2 followed by pressure contour plots and velocity vector charts.

Table G.2: *CFD and EES comparison for staggered labyrinth seals.*

Total pressure			CFD Flow Rate	EES Flow Rate	% Error
Inlet [Pa]	Outlet [Pa]	p_r	[kg/s]	[kg/s]	
300000	199673.33	0.666	0.025	0.02203	11.63
300000	189628.89	0.632	0.026	0.02286	11.47
300000	179581.72	0.599	0.027	0.02361	11.33
300000	169531.47	0.565	0.027	0.02429	11.19
300000	159477.58	0.532	0.028	0.0249	11.07
300000	149419.48	0.498	0.029	0.02545	10.94
300000	139356.47	0.465	0.029	0.02595	10.79
300000	129287.48	0.431	0.030	0.02638	10.68
300000	119211.41	0.397	0.030	0.02675	10.57
300000	99032.47	0.330	0.030	0.02728	10.45
300000	88927.25	0.296	0.031	0.02743	10.44
300000	78829.57	0.263	0.031	0.02747	10.57
300000	68763.06	0.229	0.031	0.02747	10.70
300000	58757.49	0.196	0.031	0.02747	10.76
300000	48820.53	0.163	0.031	0.02747	10.80

Pr = 0.667

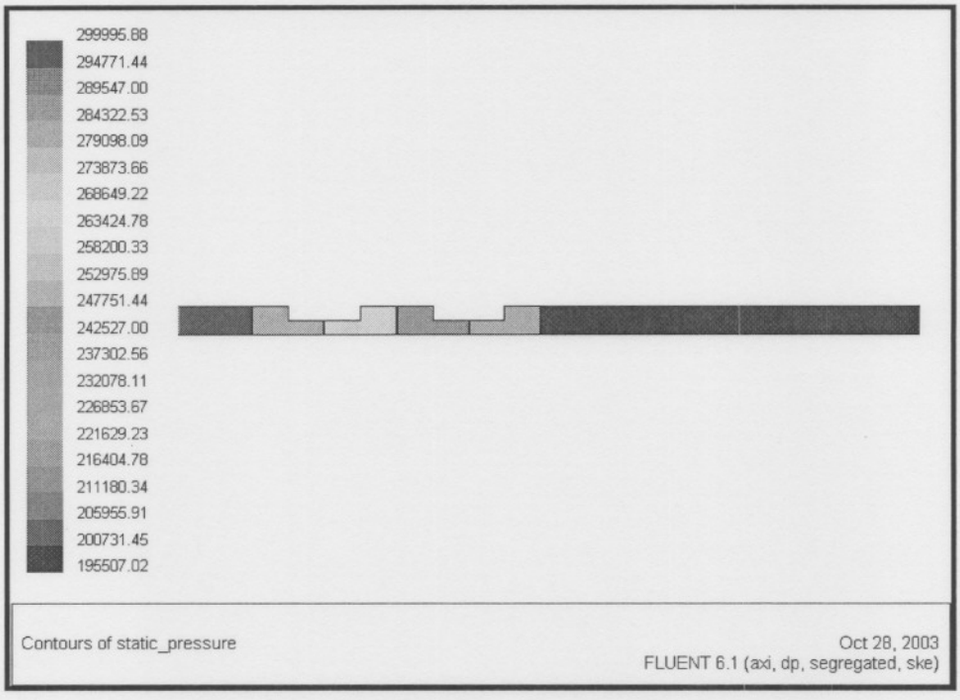

Figure G.7: Contours of static pressure for Pr=0.667.

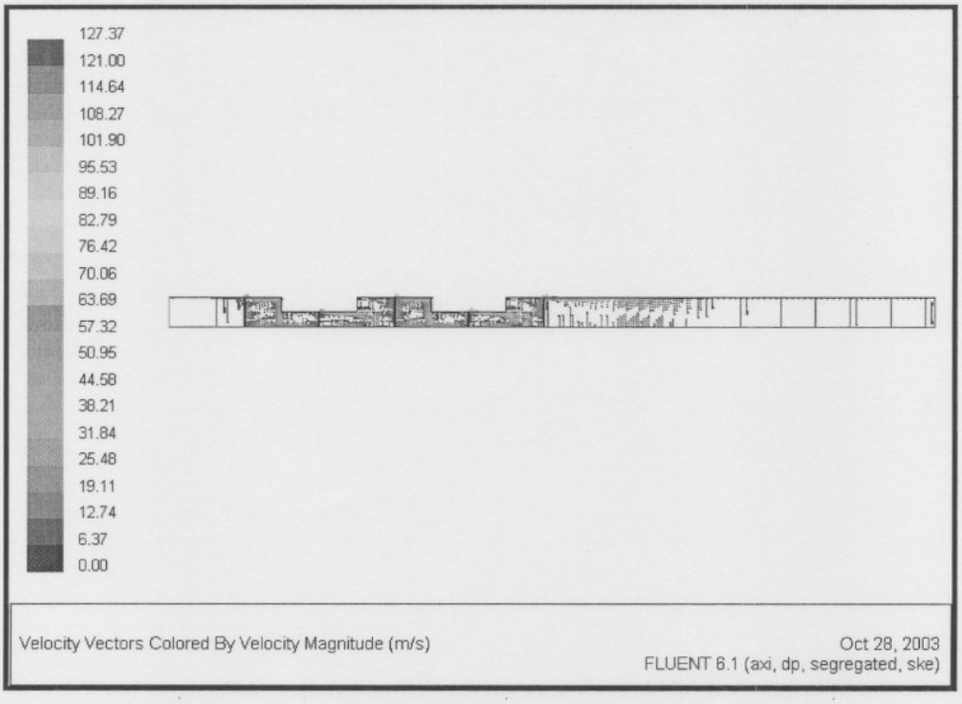

Figure G.8: Velocity vector diagram for Pr=0.667.

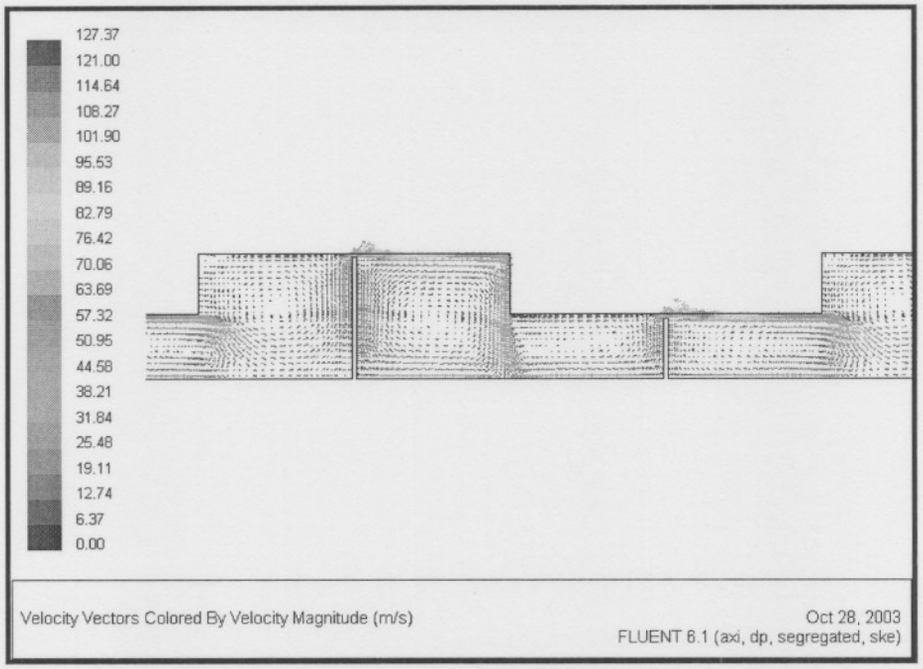

Figure G.9: Velocity vector diagram for last two constrictions with Pr=0.667.

Pr = 0.167

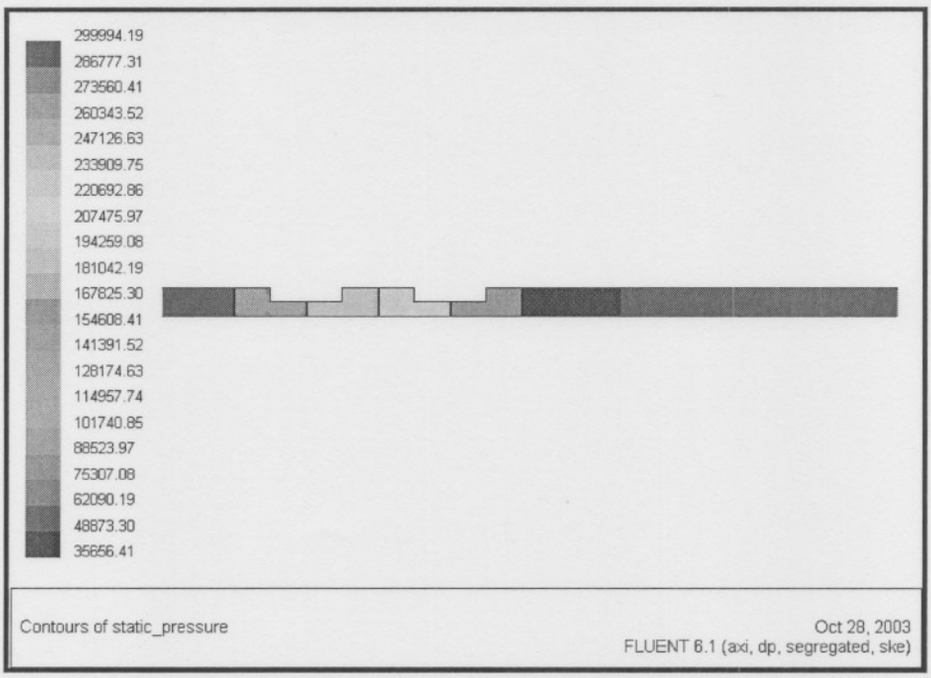

Figure G.10: Pressure contour plot for Pr=0.167.

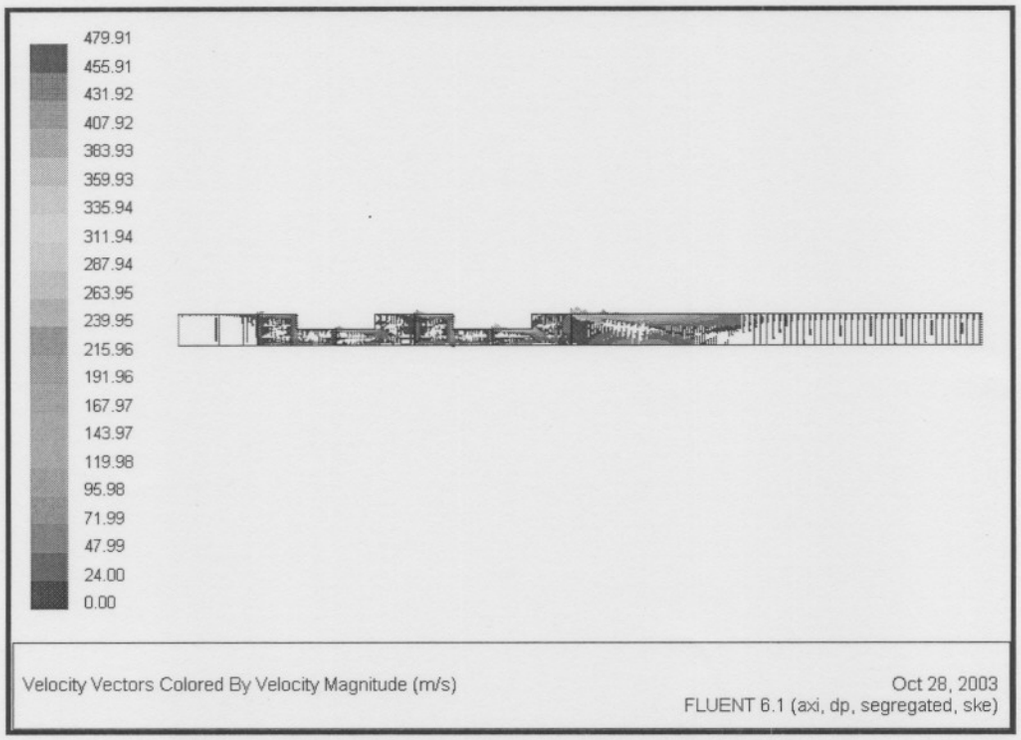

Figure G.11: Velocity vector plot for Pr=0.167.

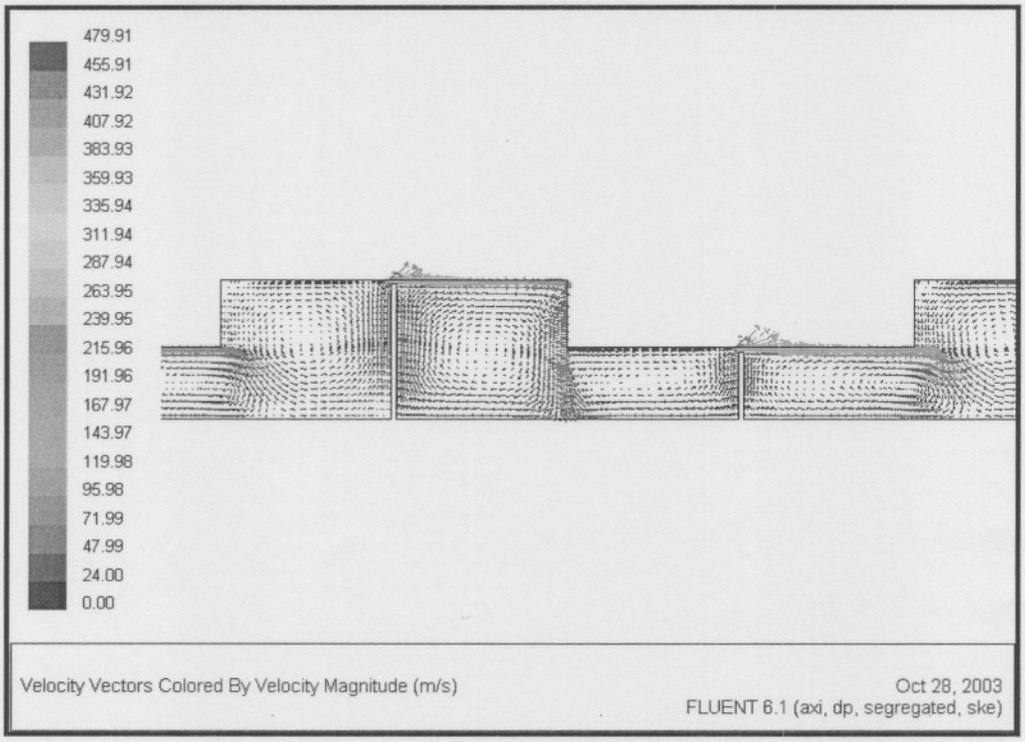

Figure G.12: Velocity vector plot for last two constrictions with Pr=0.167.